Cryptosporidium parvum: ENHANCING OUR UNDERSTANDING OF ITS UNIQUE FATTY ACID METABOLISM AND THE ELUCIDATION OF PUTATIVE NEW INHIBITORS

A Dissertation

by

JASON MICHAEL FRITZLER

Submitted to the Office of Graduate Studies of
Texas A&M University
in partial fulfillment of the requirements for the degree of

DOCTOR OF PHILOSOPHY

May 2008

Major Subject: Veterinary Microbiology

Cryptosporidium parvum: ENHANCING OUR UNDERSTANDING OF ITS UNIQUE FATTY ACID METABOLISM AND THE ELUCIDATION OF PUTATIVE NEW INHIBITORS

A Dissertation

by

JASON MICHAEL FRITZLER

Submitted to the Office of Graduate Studies of
Texas A&M University
in partial fulfillment of the requirements for the degree of

DOCTOR OF PHILOSOPHY

Approved by:

Chair of Committee,	Guan Zhu
Committee Members,	James Derr
	Karen Snowden
	Yanan Tian
Head of Department,	Gerald Bratton

May 2008

Major Subject: Veterinary Microbiology

ABSTRACT

Cryptosporidium parvum: Enhancing Our Understanding of Its Unique Fatty Acid Metabolism and the Elucidation of Putative New Inhibitors. (May 2008)

Jason Michael Fritzler, B.S., Texas A&M University

Chair of Advisory Committee: Dr. Guan Zhu

Cryptosporidium parvum is widely known for outbreaks within the immunocompetent population, as well its sometimes excruciating effects as an opportunistic agent in AIDS patients. Our understanding of the biology and host-parasite interactions of this parasitic protist is increasing at a rapid rate due to recent molecular and genetic advances. The topic of our research is in the area of *C. parvum* fatty acid metabolism, which is highly streamlined in this parasite.

In addition to a type I fatty acid synthase (CpFAS1), *C. parvum* also possesses an enormous type I polyketide synthase (CpPKS1). Because of the size of this megasynthase, functional characterization of the complete enzyme is not possible. We have isolated and characterized the loading unit of CpPKS1 which contains an acyl-[acyl carrier protein (ACP)] ligase (AL) and an ACP. This unit is responsible for the overall substrate selection and initiation of polyketide production. Our data show that CpPKS1 prefers long-chain fatty acids with the highest specificity for arachidic acid (C20). Thus, the final polyketide product could contain as many as 34 carbons.

Additionally, *C. parvum* possesses only a single fatty acid elongase. This family of enzymes serves a mechanism similar to FAS, and many have been found to be involved in de novo fatty acid synthesis in other organisms. After expressing this membrane protein in human cells, we have determined that it too prefers long-chain fatty acyl-CoAs which undergo only one round of elongation. This is in contrast to members of this enzyme family in other organisms that can initiate de novo synthesis from two- or four-carbon fatty acids via several rounds of elongation.

Our lab has previously characterized the unique acyl-CoA binding protein (CpACBP1) from *C. parvum*. Molecular and biochemical data suggested that this enzyme may serve as a viable drug target. We have screened a library of known (and somewhat common) compounds against CpACBP1, and have isolated several potential compounds to be further examined for their ability to inhibit the growth of *C. parvum*.

DEDICATION

To my wife, Lindsay, for your never ending love, support, and encouragement.

ACKNOWLEDGEMENTS

I am truly thankful to have had Dr. Guan Zhu as my mentor, and certainly appreciate his encouragement, support, guidance and friendship. I would also like to thank my committee members, Dr. Yanan Tian, Dr. James Derr, and Dr. Karen Snowden, for their invaluable advice and assistance during my graduate career. To the past and present Zhu Lab members, Dr. Dean Rider, Xiaomin Cai, Bin Zeng, Xuelin Bian and Xicheng Ding, thanks for the friendship and support. I am grateful to have had my wife Lindsay with me throughout my graduate career, and thank her for her support, enthusiasm, love and understanding. Lastly, I would like to thank my family, especially my parents, Jim and Joan Fritzler, and my grandmother, Emma Maciula, for their support and encouragement.

TABLE OF CONTENTS

CHAPTER Page

CHAPTER Page

LIST OF FIGURES

FIGURE Page

LIST OF TABLES

NOMENCLATURE

ACBP	Acyl-CoA Binding Protein
ACL	Acyl-CoA Ligase
ACP	Acyl Carrier Protein
ACS	Acyl-CoA Synthetase
AIDS	Acquired Immune Deficiency Syndrome
AL/AAL	Acyl-[Acyl Carrier Protein] Ligase
AMP	Adenosine Monophosphate
ATP	Adenosine Triphosphate
BI	Bayesian Inference
BLAST	Basic Local Alignment and Search Tool
BSA	Bovine Serum Albumin
CDC	Centers for Disease Control and Prevention
CDS	Coding Sequence
CoA	Coenzyme A
COWP	*Cryptosporidium* Oocyst Wall Protein
DAPI	*4',6'*-Diamidino-2-Phenyl Indole
DIC	Differential Interference Contrast
DMEM	Dulbecco's Modified Eagle Medium
DMSO	Dimethyl Sulfoxide
DNA	Deoxyribonucleic Acid

DTT	Dithiothreitol
EDTA	Ethylenediaminetetraacetic Acid
ELO	Elongase
FAME	Fatty Acid Methyl Ester
FAS	Fatty Acid Synthase
FBS	Fetal Bovine Serum
FDA	Food and Drug Administration
FITC	Fluorescein Iso-Thiocyanate
gDNA	Genomic Deoxyribonucleic Acid
GTP	Guanosine Triphosphate
HEK	Human Embryonic Kidney
HIV	Human Immunodeficiency Virus
HPLC	High Phase Liquid Chromatography
HSP70	70-kDa Heat Shock Protein
IgG	Immunoglobulin G
IPTG	Isopropyl-1-Thio-β-D-galactopyranoside
IUBMB	International Union of Biochemistry and Molecular Biology
JTT	Jones-Taylor-Thornton
KCS	β-Ketoacyl-CoA Synthase
LB	Luria-Bertani
LCE	Long Chain Elongase
LCFA	Long Chain Fatty Acid

MBP	Maltose Binding Protein
MCMC	Markov Chain Monte Carlo
ML	Maximum Likelihood
Mr	Molecular Weight
NAD(H)	Nicotinamide Adenine Dinucleotide
NADP(H)	Nicotinamide Adenine Dinucleotide Phosphate
NBD	N-[(7-nitro-2-1,3-benzoxadiazol-4-yl)-methyl]amino
NCBI	National Center for Biotechnology Information
NIH	National Institutes of Health
NTZ	Nitazoxanide
ORP	Oxysterol Binding Protein-Related Protein
OSBP	Oxysterol Binding Protein
PAGE	Polyacrylamide Gel Electrophoresis
PBS	Phosphate Buffered Saline
PCR	Polymerase Chain Reaction
PDB	Protein Database
PI	Post-Infection
PIR	Protein Information Resource
PKS	Polyketide Synthase
PNO	Pyruvate:$NADP^+$ Oxidoreductase
PP	Posterior Probability
PPT	Phosphopantetheinyl Transferase

PRF	Protein Research Foundation
PUFA	Polyunsaturated Fatty Acid
PV	Parasitophorous Vacuole
PVM	Parasitophorous Vacuolar Membrane
qRT-PCR	Quantitative Reverse Transcriptase Polymerase Chain Reaction
RNA	Ribonucleic Acid
rRNA	Ribosomal Ribonucleic Acid
RT-PCR	Reverse Transcriptase Polymerase Chain Reaction
SDS	Sodium Dodecyl Sulfate
SFP	Surfactin Production Element
SSU rRNA	Small Subunit Ribosomal Ribonucleic Acid
TAMU	Texas A&M University
TLC	Thin Layer Chromatography
TMP	Total Membrane Protein
TRITC	Tetramethyl Rhodamine Iso-Thiocyanate
tRNA	Transfer Ribonucleic Acid
UTP	Uridine Triphosphate

CHAPTER I

INTRODUCTION

GENERAL DISCUSSION

This past year, 2007, marked the 100-year anniversary (1907-2007) of the first description of *Cryptosporidium,* by E. E. Tyzzer. It was not until 1976 that the first human case of cryptosporidiosis was reported described as an acute, self-limiting enterocolitis in an otherwise healthy 3-year old child (118). The first report of cryptosporidiosis in immunocompromised patients came less than two months later (107). It was at this time, roughly 70 years after the first description of *Cryptosporidium*, that physicians began to fully recognize its significance as an opportunistic pathogen causing chronic and life-threatening diarrhea in AIDS patients. In 1993, more than 400,000 people were affected and approximately 100 deaths occurred among the elderly and immunocompromised populations due to contamination of the Milwaukee, Wisconsin water supply system with this parasite. This massive outbreak quickly escalated *Cryptosporidium* to headline news in the United States and around the world. The majority of cryptosporidiosis outbreaks in humans are associated with contaminated drinking and/or recreational water. This parasite can also be transmitted through direct contact both between and among humans and animals, or by food contamination. However, it is the difficulty in controlling *Cryptosporidium* contamination in water

This dissertation follows the style of Eukaryotic Cell.

(the oocysts are resistant to chlorine), the potential devastation to communities, and talk of bioterrorism agents that have caused this parasite to be listed as one of the water-borne, category B priority agents in the NIH and CDC biodefense research programs in the United States.

As in humans, newborn or young and sometimes immunocompromised animals suffer from cryptosporidiosis. Although all animals are believed to be susceptible to infection, *Cryptosporidium* infection in cattle has received the most attention. This is largely due to the high prevalence of infection in this livestock species, especially among the dairy cattle population, its economic importance, and the great potential of cattle to serve as a reservoir for human infections. Acute diarrhea is the most common clinical sign that presents in many animals such as calves, foals, piglets, deer, and goat kids, but only a mild or no diarrhea occurs in other hosts such as rodents. The major problem in animals suffering from infection with *Cryptosporidium* is reduced weight gain and chronic wasting, sometimes leading to death. For example, the commonly used laboratory strain of *C. parvum* (TAMU strain) originated from a foal that died from severe diarrhea. Not only are livestock species at risk for infection with this parasite, but companion animals such as dogs and cats also suffer from cryptosporidiosis. Although their contribution to the transmission of *Cryptosporidium* to humans is largely unknown at this time, it should never be ruled out.

Due in part to its importance in public health (both human and animal associated), as well as successful propagation in mice and calves, *C. parvum* is the most widely studied species within the *Cryptosporidium* genus. The closely related and

morphologically indistinguishable species *C. hominis* was previously considered as the human genotype of *C. parvum* (or Type 1, vs. zoonotic Type 2). However, *C. hominis* was renamed as a separate species in 2002 based on molecular divergence from Type 2 *C. parvum* as well as it being predominantly a parasite of humans (116). Although the change in names from *C. parvum* Type 1 to *C. hominis* has greatly promoted the awareness of cryptosporidiosis, the validity of *C. hominis* as a separate and distinct species is still highly debated. There has been no evidence that the two species are reproductively separate, and some have actually observed recombination between *C. parvum* and *C. hominis* in both experimental and natural conditions (189). Furthermore, complete genome sequencing projects of both *C. parvum* (2) and *C. hominis* (192) and metabolic comparisons have not identified any significant findings that would support a clear species distinction of the two pathogens.

TAXONOMIC POSITION

Cryptosporidium belongs to the Phylum Apicomplexa, which gets its name due to the morphological criteria of an apical complex that is unique to this group of protozoans. The parasite is further described within the Class Conoidasida (also known as Coccidia), Order Eucoccidiorida, Suborder Eimeriorina, and family Cryptosporiidiae (18, 98, 177). For the last several years, especially since the surge of genomic and molecular investigations, the taxonomic status of *Cryptosporidium* has been the subject of great debate. Recent molecular phylogeny consistently places this genus as an early branch at the base of the Apicomplexa, and some even suggest as a sister clade to the

Gregarines (12, 19, 25, 68, 197). Upon completion of the genome sequencing projects for both *C. parvum* and *C. hominis* it was revealed that the metabolic machinery in this genus differs from other apicomplexans (2, 192, 200). The most notable of these features are the complete lack of apicoplast and mitochondrial genomes in *Cryptosporidium* which further supports the idea that this parasite is highly divergent from the other coccidians.

The *Cryptosporidium* type species is *C. muris*, and was first described by Tyzzer when he established the genus *Cryptosporidium* (175). Roughly five years later a new species, *C. parvum*, was described based on differences in morphological size and location of infection as compared to *C. muris* (175, 176). During this early period of species discovery, many apicomplexan organisms were largely assigned to the *Cryptosporidium* genus based on similarities in life cycles. Thus, some apicomplexan organisms, such as *Sarcocystis*, were wrongly assigned to this genus (7, 13, 40, 41, 124, 174, 191). *Cryptosporidium* was found to have a unique attachment organelle in the late-1960s (61, 76, 183), which has since become the defining taxonomic unit of the genus and family (95, 97, 181, 191). However, once this structural organelle was confirmed, the basis of naming species soon turned to rely upon host specificity. This was quickly considered useless once cross-transmission studies showed that most isolates could readily transmit across host species. At that time species could not be classified further than the general group *C. parvum* (191). Only three species (*C. meleagridis, C. wrairi,* and *C. felis*) that were biologically different from *C. parvum* and *C. muris* were agreed upon as new species.

Although controversy in *Cryptosporidium* taxonomy has been present for decades, current issues remain largely due to a difficulty in defining the criteria that define a biological species (43, 191). For over a decade, mixtures of methods have been employed in order to try to more accurately define species and genotypes. Some of these methods rely solely on molecular data, but others have relied upon both molecular and biologic methods. The three most common genes used in molecular phylogenetic reconstructions are the small subunit ribosomal RNA (SSU rRNA), the 70-kDa heat shock protein (HSP70), and *Cryptosporidium* oocyst wall protein (COWP). Phylogenetic reconstructions using these three genes have consistently and clearly demonstrated genetic variability within the genus (42, 43). Not only is the correct identification of a parasite and a clear understanding of the genetic variation within the parasite group important in taxonomic classification, but it is crucial to the understanding and development of new vaccines, drugs, and diagnostics (105). It is currently suggested that a polyphasic approach be used to characterize the *Cryptosporidium* species – one that is supported by morphologic, biologic, and genetic data (43, 191). Although there is still some debate on *Cryptosporidium* taxonomy, and likely always will be, current molecular advances have aided in clearing some of the confusion. Currently, there are 15 named valid *Cryptosporidium* species (Table 1.1).

LIFE CYCLE

The apicomplexans as a group differ greatly in their life cycles. Some members of this genus have a dioxenous (two hosts) life cycle such as *Toxoplasma*, *Babesia* and

TABLE 1.1. The 15 currently recognized *Cryptosporidium* species along with their respective oocyst dimensions, primary host(s), and site(s) of infection.*

Species (Reference)	Oocyst sizes (µm)	Primary Host	Primary Site of Infection
C. parvum (176)	4.5 x 5.5	Mammals	Small intestine
C. hominis (116)	4.5 x 5.5	Humans	Small intestine
C. andersoni (99)	5.5 x 7.4	Cattle	Abomasum
C. muris (175)	5.6 x 7.4	Rodents§	Stomach
C. wrairi (183)	4.4 x 5.3	Guinea pigs	Small intestine
C. felis (74)	4.5 x 5.0	Cats	Small intestine
C. canis (48)	5.0 x 4.7	Dogs	Small intestine
C. suis (153)	5.1 x 4.4	Pigs	Small, large intestine
C. meleagridis (159)	4.3 x 4.9	Turkeys§	Small intestine
C. baileyi (37)	4.6 x 6.2	Chickens§	Large intestine, bursa, respiratory system
C. galli (154)	8.3 x 6.3	Birds	Proventriculus
C. serpentis (96)	5.3 x 6.1	Snakes	Stomach
C. saurophilum (89)	4.7 x 5.0	Lizards	Stomach, small intestine
C. molnari (4)	4.7 x 4.5	Fish	Stomach, small intestine
C. bovis (47)	4.8 x 4.6	Cattle	Abomasum†

* Data obtained from Xiao et al. 2004 (191), and other listed references. (§) indicates species that have also been found in humans, mainly immunocompromised individuals. (†) indicates speculative data.

Plasmodium, and have tissue and/or blood stages. Others such as *Eimeria*, *Isospora*, *Cyclospora* and *Cryptosporidium* undergo a monoxenous (single host) life cycle, and all stages occur in the intestine. The somewhat complex life cycle, which contains both sexual and asexual cycles, as well as six major developmental stages have been detailed for *C. parvum* (Fig 1.1) (36, 49, 173). Ingestion of the sporulated oocyst, the only exogenous stage, is the start of the endogenous life cycle. Ingestion most commonly occurs through the fecal-oral route via direct or indirect person-to-person contact, animal-to-animal contact, animal-to-human contact, or water- and food-borne ingestion, and possibly air-borne transmission (46).

The *Cryptosporidium* oocyst wall is similar to other coccidia as it is comprised of two distinct layers, but is unique because it contains a suture at one end that dissolves during excystation allowing the ejection of sporozoites. Each sporulated oocyst contains four free floating haploid sporozoites, which is in contrast to all other coccidia which have one or more sporocysts that surround the sporozoites (164). Excystation of the ingested oocyst results in the release of these four sporozoites. These are the infective stage of the life cycle, and invade and parasitize small intestinal or colon epithelial cells (141). Like other apicomplexan sporozoites, those of *Cryptosporidium* possess organelles such as the rhoptries, micronemes, and electron-dense granules. Further, they possess apical rings, but lack some features characteristic of most other coccidia such as the polar rings, micropores, and the conoid (45). All of these are present at the anterior pole of the sporozoite housed in the apical complex. It is this region of the sporozoite that invades the host cells, and this process involves the release of several materials that

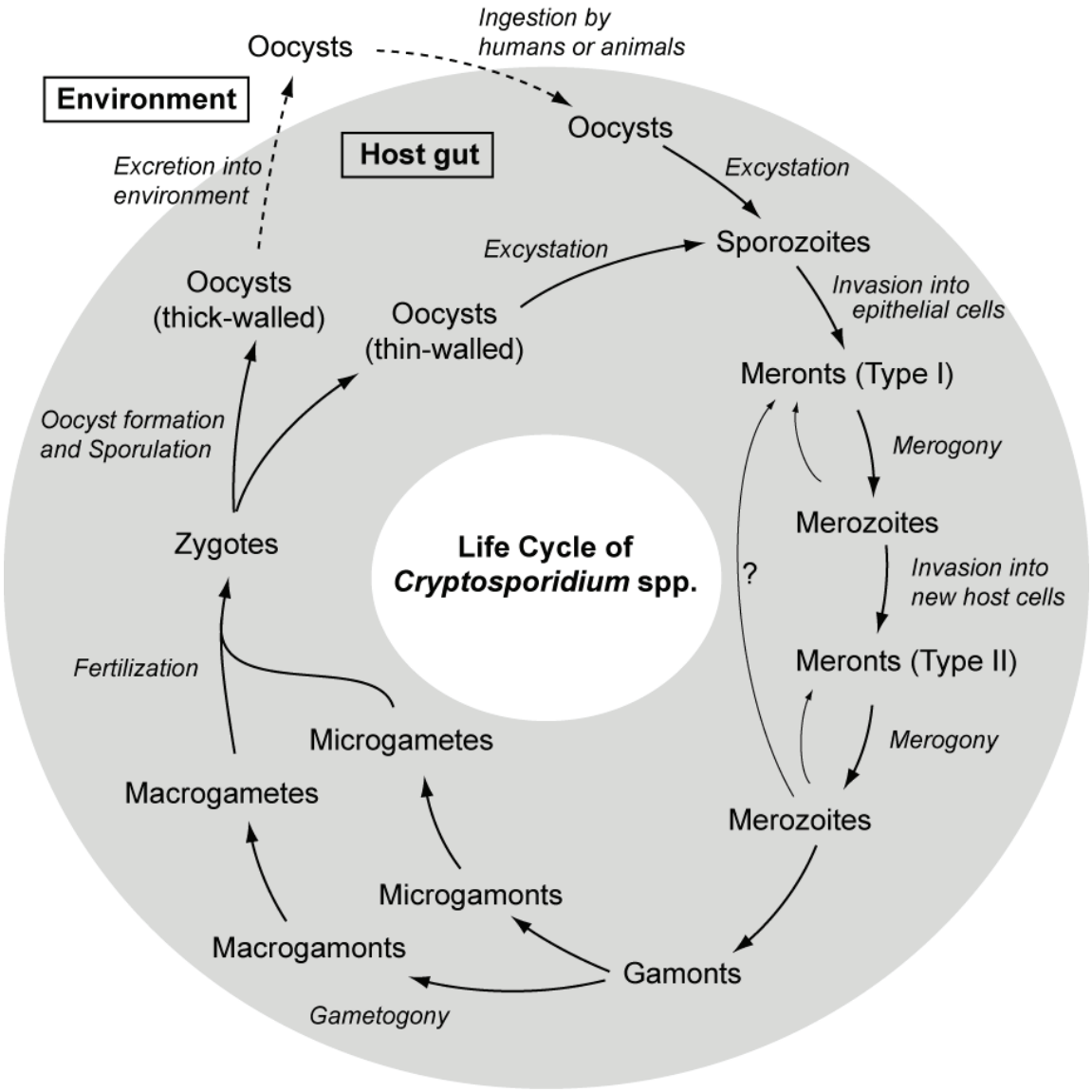

FIG. 1.1. The *Cryptosporidium* life cycle. The life cycle begins with the ingestion of sporulated oocysts. Two cycles of merogony occur, followed by gamogony. After the formation of the gametes, fertilization occurs and is the only sexual stage in the life cycle. Fertilization results in the formation of zygotes which differentiate into oocysts. These oocysts are either excreted from the host in the feces, or excyst to begin another round of the life cycle. Reproduced from Zhu G., S. Enomoto, J. M. Fritzler, M. Abrahamsen, and T. Templeton. (In Press). *Cryptosporidium* and Cryptosporidiosis. *In* C. Kole and V. M. Nene (eds.) Genome mapping in animals and microbes, with kind permission from Springer Science and Business Media.

are suspected to play a pivotal role during the invasion process (172).

Upon invasion of the host cell, the sporozoites reside within a host cell membrane-derived parasitophorous vacuolar membrane (PVM). The parasite at this point is considered as being intracellular but extracytoplasmic as it remains in a highly polar location adjacent to the surface of the columnar host intestinal epithelial cell (102, 120, 180). Within this niche, the parasite further develops into a trophozoite. During this process, the parasitophorous vacuole (PV) invaginates at the host cell interface and forms a "feeder organelle" that is believed to be the region responsible for nutrient uptake from the host cell (45, 164, 180).

The next stage in the life cycle is by asexual multiplication, occurs within the host epithelial cells, and is referred to as type I merogony. This process of merogony results in nuclear division and forms eight haploid merozoites assembled into a single type I meront. Merozoites mature within the type I meronts and are released from the PV. At this point the type I merozoites can undergo two different cycles: they can further develop through type II merogony, or undergo another round of type I merogony. The classical persistent infection observed with *Cryptosporidium* infection is probably due to the "recycling" of type I merozoites back through type I merogony (36). Type II merogony results in a type II meront containing four haploid type II merozoites. Similar to type I merozoites, the type II merozoites can undergo another cycle of type II merogony. However, it is unknown at this time if type II merozoites are able to initiate another cycle of type I merogony.

Although capable of initiating another round of type II merogony, type II

merozoites usually develop into the sexual reproductive stages of the parasite known as gamonts. Controversial preliminary investigations suggest that extracellular gamont stages of the gregarines very closely resemble the extracellular forms of *Cryptosporidium* (67, 68, 147). These gamonts soon differentiate into the male microgamonts or female macrogamonts. Macrogamonts contain one large nucleus which does not divide, and mature macrogamonts are sometimes referred to as macrogametes. On the other hand, microgamonts become multinucleate and each nucleus is incorporated into at least 16 microgametes. The sexual stage of development occurs upon the mating of the microgamete and the macrogamete.

Sexual reproduction results in a diploid zygote that develops into sporulated oocysts containing four haploid sporozoites. These oocysts can be of two types. Approximately 80% of those produced are referred to as "thick-walled" oocysts as they are composed of two outer membranes. These oocysts are the environmentally resistant form and are passed in the feces. The other 20% are composed of a single outer membrane and are referred to as "thin-walled," and are not passed in the feces. Rather, they are suspected of releasing sporozoites and cause an auto-infection. This feature, along with recycled meronts, are probably responsible for the persistent infections that are not propagated by repeated ingestion of oocysts. This often life-threatening non-resolving state of cryptosporidiosis is often observed in AIDS patients (36, 45, 102).

TREATMENT

Treatment is rarely required for immunocompetent individuals to recover from

cryptosporidiosis. In the worst cases, antidiarrheal agents along with rehydration therapy to replace fluid and electrolyte depletion are usually sufficient. However, severe complications due to *Cryptosporidium* infection can occur in those individuals with an underlying immunosuppressed condition. It is unfortunate that there is no effective drug to treat cryptosporidiosis, and although halofuginone lactate is approved in some European countries for use in sheep and cattle, no drug is approved in the United States to treat this infection in animals. The only current approved drug to treat human cryptosporidiosis in the United States is nitazoxanide (NTZ) (51, 187). Nitazoxanide is approved by the Federal Drug Administration (FDA) under the trade name Alinia (Romark Laboratories, www.romark.com) for use in both children and adults. However, it is not approved for patients of any age that have AIDS.

Broad-spectrum parasiticidal activity of NTZ against a wide range of protozoa, nematodes, trematodes, cestodes, and some anaerobic bacteria and viruses has been reported (64, 125, 146, 151, 179). It was the anti-protozoan properties of NTZ that led to clinical trials of this drug for cryptosporidiosis. Although its mechanism of action against this parasite is not clear, it may act on the *C. parvum* encoded bifunctional pyruvate:$NADP^+$ oxidoreductase (PNO) as it does in some other organisms (34, 152).

Although complete efficacy is not achieved, NTZ appears to greatly reduce oocyst excretion in immunocompetent individuals which is associated with the resolution of diarrhea. One uncontrolled study revealed that this drug reduced oocyst excretion by ≥ 95% in 58% of the patients, and was associated with complete resolution of diarrhea in 57% of these patients (39). Another prospective randomized, placebo-

controlled, double-blind study reported that a 7-day treatment of NTZ resulted in improvement of clinical symptoms in 80% of the patients (compared to 41%, placebo) and a 67% rate of oocyst eradication (compared to 22%, placebo) (150). Further, a study involving both HIV-seropositive and HIV-seronegative children showed that NTZ treatment improved the resolution of diarrhea, resulted in oocyst eradication, and decreased mortality in those that were HIV-seronegative, but not in those that were HIV-seropositive (5). On the contrary, a different study revealed that 59% of AIDS patients showed clinical improvement and displayed eradication of oocysts (149).

An older antibiotic still in use today, FDA approved in tablet form, is paromomycin which displays significant activity against a wide array of organisms (179). Paromomycin is a protein synthesis inhibitor that was originally thought to act on the aminoacyl tRNA site of ribosomes, but more recent data indicates that it may actually inhibit the maturation of tRNA itself (171). Although its mechanism of action against *Cryptosporidium* is unknown at this time, paromomycin is widely used as a control in in vitro drug studies against this parasite (23). With regards to paromomycin treatment of cryptosporidiosis in AIDS patients, it has shown relatively little efficacy. In one study only 47% of patients treated with this drug showed signs of clinical improvement, whereas 36% of those receiving a placebo control displayed the same signs of improvement (66). No benefit in using paromomycin versus placebo in AIDS patients was shown during another prospective, double-blind, placebo controlled study (66).

Although paromomycin alone does not appear to be beneficial, this drug in

combination with azithromycin (160), or with antiretroviral drugs (69) appears to display a greater efficacy than treatment with either drug alone. Paromomycin prescribed in combination with the protein synthesis inhibitor azithromycin given to AIDS patients for four weeks, followed by paromomycin alone for eight weeks results in improvement of clinical symptoms and a decrease in oocyst excretion. AIDS patients treated with azithromycin alone did show signs of clinical improvement, however oocyst excretion remained significantly positive (78). Increasing CD4 counts to restore immune system function in AIDS patients with antiretroviral therapy sometimes leads to partial recovery from *Cryptosporidium* infection, but secondary or concomitant treatment with paromomycin is of greater benefit.

Until a highly effective treatment is discovered and approved for use, the most effective means to combat cryptosporidiosis is prevention. Other than a healthy immune system, public health measures must be actively pursued to avoid exposure to the environmentally resistant oocyst. Preventative measures for immunosuppressed individuals (if not everyone) include exhaustive hand washing, avoidance of human or animal feces, avoidance of recreational water, and insurance of a safe drinking water supply.

STREAMLINED FATTY ACID METABOLISM

Efficient random sequencing of genomic DNA during preliminary studies in the 1990s both supported and allowed a feasible complete genome sequencing project for *Cryptosporidium* (100, 166, 167). Three different projects began at the turn of the

century: a group at the University of Minnesota completed the *C. parvum* nucleotide sequence (2); a group at Virginia Commonwealth University completed the *C. hominis* sequence (192); and a third project in the United Kingdom at the Medical Research Council completed the sequence of *C. parvum* chromosome 6 (9).

Until these projects were underway and completed, it was unknown just how parasitic *Cryptosporidium* really was. Predicted proteome annotation revealed that this parasite adapted to an extreme parasitic life style by utilizing a very highly streamlined metabolism. In addition to determining that the entire apicoplast and associated pathways has been discarded, as previously reported (200), the parasite has retained only a small fraction of mitochondrial functions. Genome data, and later molecular and biochemical investigations, revealed that *Cryptosporidium* possesses no de novo synthetic pathways and relies on the host and/or environmental niche to supply all nutrients including amino acids, nucleotides, and fatty acids.

Because the overall scope of this dissertation revolves around fatty acid metabolism, we will not discuss energy, amino acid, or nucleotide metabolism, and will only focus on the fatty acid metabolism enzymes. Information on these metabolic pathways can easily be located in current literature. With the absence of an apicoplast *Cryptosporidium* lacks the enzyme typically required for de novo fatty acid syntheses, a plastid-associated type II fatty acid synthase (type II FAS). However, this parasite does harbor a 25-kb type I FAS gene (*CpFAS1*) for elongating fatty acids (199, 201). Additionally, *C. parvum* possesses a related 40-kb polyketide synthase gene (*CpPKS1*) encoding a 1,500-kDa protein consisting of 29 enzymatic domains whose overall

function is still not understood at this time (198). *Plasmodium* does not contain type I FAS or PKS, however they have been found in *Toxoplasma* and *Eimeria* (196). Dinoflagellates distantly related to *Cryptosporidium* do possess PKSs, and may have a conserved function in coccidia (92, 142, 162, 163).

Although CpFAS1 and CpPKS1 are key players in *Cryptosporidium* fatty acid metabolism, they probably require the participation of several other enzymes including a long chain fatty acid elongase (LCE) and acyl-CoA binding protein (ACBP). Most organisms contain multiple LCEs, however *C. parvum* possesses only one 38-kDa LCE homologue (CpLCE1). Although the overall function of LCEs differs from that of FASs and PKSs, it is unknown whether or not CpLCE1 acts in conjunction with CpFAS1 and/or CpPKS1 in providing them with fatty acyl-CoA precursors. Regardless of the enzyme, a fatty acid must be activated to its fatty acyl-CoA counterpart to enter subsequent metabolic pathways. In some instances the activation and entry into subsequent reactions are coupled together, but in other cases ACBP mediates the incorporation of fatty acyl-CoA into various pathways by binding and transporting them to various cellular locations (87, 88). A single ACBP gene (*CpACBP1*) is housed in the *C. parvum* genome, and has previously been characterized (194).

The research presented here focuses largely on the molecular and biochemical characterization of proteins involved in *C. parvum* lipid metabolism. Chapter II concentrates on the characterization of the most important part of CpPKS1 – the loading unit. This unit is responsible for substrate specificity for the entire enzyme, thus largely responsible for the type and chain length of the final product(s). Characterization of the

sole LCE in *C. parvum* (CpLCE1) is the topic of Chapter III. It is interesting that *C. parvum* contains only one homologue of this gene, and our data supports the inability of this parasite to complete de novo fatty acid synthesis. We have previously found that CpACBP1 localizes to the PVM during intracellular development. We suspect that this enzyme could serve as a potential therapeutic target because of its location in addition to its function which is the focus of Chapter IV. Overall, we have furthered our understanding of not only these enzymes, but we have greatly deepened our understanding of *C. parvum* biochemistry and lipid metabolism.

CHAPTER II

FUNCTIONAL CHARACTERIZATION OF THE ACYL-[ACYL CARRIER PROTEIN] LIGASE IN THE *Cryptosporidium parvum* GIANT POLYKETIDE SYNTHASE*

OVERVIEW

Polyketides are a large class of structurally diverse natural secondary metabolites produced by bacteria, fungi, sponges, insects, and plants. Along with their semi-synthetic derivatives they now play a vital role as human and veterinary medicine therapeutic agents and agricultural agents including antibiotic, anticancer, antiparasitic, immunosuppressant, and insecticide compounds (70, 121, 128, 129). Other functions include serving as defensive molecules in microbes as well as having a role in organism-to-organism signaling (132, 139, 165). Polyketide biosynthesis mechanistically resembles that of fatty acids. Both fatty acid synthases (FASs) and polyketide synthases (PKSs) serve as biochemical assembly lines composed of a series of catalytic domains or discrete enzymes involved in the sequential assembly and modification of acyl groups on the growing chain (82). They both catalyze repetitive Claisen-type decarboxylative condensations between an acyl thioester and a fatty acid, and both use acyl carrier protein (ACP) as an attachment site for the growing carbon chain. However, polyketides

* Part of this chapter is reprinted from Fritzler, J. M., and G. Zhu. 2007. Functional characterization of the acyl-[acyl carrier protein] ligase in the *Cryptosporidium parvum* giant polyketide synthase. Int. J. Parasitol. 37: 307-316, with permission from Elsevier.

are far more diverse in their final product structures than the free fatty acids typically produced by FAS. The wide variety of polyketide products is mainly due to PKSs being more diverse in the reactions they catalyze as well as in the wide variety of both starter and chain extender units they use, carbon chain length, degree of reduction and/or dehydration, and folding of the final product (21, 24, 70, 81, 84, 85, 115). The complete cycle of ketoacyl reduction, dehydration, and enoyl reduction producing a saturated carbon chain that is observed in FAS may be shortened in PKSs so that a saturated or poly-unsaturated carbon chain is produced containing many keto and hydroxyl groups (71, 108). Post-PKS modifications add to the diversity of polyketides as the extended linear carbon chain products are then often glycosylated, acylated, alkylated, oxidated, and/or cyclized to form the complex biochemicals that can be used as medical and veterinary therapeutics.

Cryptosporidium parvum is a parasitic protist that infects both humans and animals. It belongs to the Phylum Apicomplexa that contains many important parasites including *Plasmodium, Toxoplasma, Babesia, Eimeria* and *Cyclospora* (197). This parasite possesses two unusual genes that encode giant polypeptides: a 25-kb fatty acid synthase (*CpFAS1*) and a 40-kb polyketide synthase (*CpPKS1*). Both genes have been previously sequenced and reported (197-199) (Sequence Information for the *CpPKS1* Gene is available in the GenBank database under accession no. AF405554). CpFAS1 has been recently expressed as recombinant individual proteins (as multifunctional units or modules). The activities of most CpFAS1 enzymatic domains have been detected using recombinant proteins, although the endogenous product of CpFAS1 remains to be

elucidated (199). On the other hand, *CpPKS1*, the first PKS identified from a protist, has yet to be expressed and functionally characterized (198).

CpPKS1 can be conceptually translated into a single 1,516-kDa polypeptide, in which the predicted 29 enzymatic domains are organized into an N-terminal loading unit, 7 internal elongation modules, and a C-terminal reductase terminating domain (198). Because of its large size, heterologous expression of the entire *CpPKS1* gene would be impractical. To overcome this problem we have decided to use a "divide and conquer" strategy, in which the giant CpPKS1 is expressed as individual, but multifunctional units or modules for biochemical analysis. Here, we report the expression and biochemical analysis of the CpPKS1 N-terminal loading unit that contains two enzymatic domains: an acyl-[ACP] ligase (AL) domain for activating and loading substrate, and an ACP domain for the attachment of acyl substrates. Although there are few PKSs with a loading unit containing the same domain organization, this study is the first to fully characterize the AL domain contained in this relatively rare loading unit. The detailed substrate preference and catalytic features of the AL domain were determined. We have also demonstrated that the ACP domain can be activated by a surfactin production element (SFP)-type phosphopantetheinyl transferase in *C. parvum* (CpSFP-PPT), and the AL domain is able to catalyze the attachment of long chain fatty acids to the activated ACP domain.

MATERIALS AND METHODS

Enzyme nomenclature. We will follow Nomenclature Committee of IUNMB (NC-IUBMB) recommendations to use "ligase" to replace "synthetase" that catalyzes "synthetic reactions with concomitant hydrolysis of a nucleoside triphosphate" (see NC-IUBMB Newsletter (http://www.chem.qmul.ac.uk/iubmb/newsletter/misc/synthase.html#1). The acyl ligase (AL) may represent either a discrete acyl-CoA ligase (ACL) or the acyl-[ACP] ligase domain (AAL) in FAS/PKS, in which ACL and acyl-CoA synthetase (ACS) are in fact interchangeable.

Protein motif analysis. The CpPKS1 loading unit AL and ACP domains were separately used as queries to search protein databases including all nonredundant GenBank Coding Sequence (CDS) translations, RefSeq Proteins, Protein Data Bank (PDB), SwissProt, Protein Information Resource (PIR), and Protein Research Foundation (PRF) at the National Center for Biotechnology Information using PSI-BLAST program (http://www.ncbi.nlm.nih.gov/BLAST) (3). Four iterative PSI-BLAST searches were performed for both the AL and ACP domains with the BLOSUM62 matrix (penalties for existence and extension = 11 and 1, respectively). Only those sequences with E-values less than 1×10^{-4} were used for multiple sequence alignments with the ClustalW algorithm using MacVector v9.0 (Accelrys Software Inc.), and observable mistakes in alignments were corrected upon visual inspection. Conserved motifs from each domain were determined from the alignments and blocks logos were obtained from position-specific scoring matrices (PSSM) from the BLOCKS server (http://blocks.fhcrc.org/blocks) (65).

Amplification and cloning of DNA construct. The 2,545-bp CpPKS1 loading unit (CpPKS1-AL-ACP) was amplified from *C. parvum* (Iowa strain) genomic DNA (gDNA) with high-fidelity *Pfu* Turbo DNA polymerase (Stratagene) using primers CpPKS1-Load-F (5' aga gga tcc ATG AAT AGT AGT AAA CCT GAG TAT G 3') and CpPKS1-Load-R (5' aga gga tcc TTA GTG AGC ATT TAT TCC AGA AAT AAC 3') (lower cases represent artificial *Bam*HI linkers). The amplified product was purified from a 1% agarose gel using a MinElute gel extraction kit (Qiagen) and first cloned into the pCR-XL-TOPO vector (Invitrogen). Plasmids were isolated from positive colonies, followed by restriction digestion analysis and sequencing to confirm their identities. Plasmids containing correct inserts were then digested with *Bam*HI to release the CpPKS1-AL-ACP insert, purified from agarose gel, ligated into the pMAL-c2X expression vector (New England Biolabs), and transformed into *Escherichia coli* Mach1 cells (Invitrogen). Positive colonies were selected via PCR using CpPKS1-Load-F and LacZ-R (5' CGC CAG GGT TTT CCC AGT CAC GAC 3', an antisense primer downstream to the multiple cloning site), as well as multi-restriction enzyme digestions to determine appropriate orientation.

Expression and purification of protein. Plasmid DNA containing the correctly oriented insert (pMAL-c2X-CpPKS1-AL-ACP) was transformed into chemically competent *E. coli* Rosetta cells (Novagen) and plated onto solid Luria-Bertani (LB) medium containing ampicillin (50 μg/ml), chloramphenicol (34 μg/ml), and glucose (2 mM). After incubation overnight at 37 °C, a single colony of transformed bacteria was first inoculated into 25 ml LB media containing the appropriate antibiotics and glucose,

and grown overnight at 30 °C in a shaking incubator. The overnight cultures were diluted 1:10 with fresh medium and allowed to grow for approximately 5 h at 25 °C until the OD_{600} reached ~ 0.5. At this time, isopropyl-1-thio-β-D galactopyranoside (IPTG) was added to a final concentration of 0.5 mM to induce protein expression, and cells were grown an additional 12 h at 16 °C. The bacteria were collected by centrifugation, resuspended in 50 ml TNE buffer (20 mM Tris.HCl pH 7.4, 200 mM NaCl, 1mM EDTA) containing a protease inhibitor cocktail optimized for bacteria (Sigma), and subjected to mild sonication on ice. Insoluble debris was removed by centrifugation. The MBP-CpPKS1-AL-ACP fusion protein was purified using amylose resin-based affinity chromatography according the manufacturer's standard protocol (New England Biolabs).

SDS-PAGE analysis of the purified protein revealed two distinct bands; one corresponding to full-length MBP-fused CpPKS1-AL-ACP (~138-kDa) and another at approximately 80-kDa. The full length fusion protein was then extracted from a glycine-based, 6% native-PAGE gel using a previously reported protocol with minor modifications (33). Briefly, the affinity-purified protein was first concentrated using a membrane based VivaSpin concentrator with a 100-kDa cut-off (VivaScience) and fractionated with a 6% native-PAGE gel. The protein bands were visualized using a zinc stain kit (Bio-Rad), individually cut from the gel, and destained in 1.5 mL microtubes for a total of 30 min, and then washed with PBS. The gel slices were thoroughly crushed, mixed with PBS (pH 7.2) that slightly covered the crushed gel, centrifuged at 20,000 g for 30 min at 4 °C, and the supernatant retrieved. This was repeated three times, and after pooling the sample a small aliquot was allocated for SDS-PAGE analysis. The full

length MBP-CpPKS1-AL-ACP fusion protein was then extensively dialyzed in PBS (pH 7.2), and concentrated using the VivaSpin concentrator. Protein concentrations were determined by a Bradford colorimetric method using bovine serum albumin (BSA) as a standard.

Acyl-[ACP] ligase (AL) activity. The AL domain is proposed to catalyze the thioesterification between a fatty acid and the adjacent ACP domain. However, we have previously shown that the AL domain from evolutionarily related CpFAS1 is able to use Co-enzyme A (CoA) as a receiver, which permits the detailed enzyme kinetic analysis for the AL domain (199). In this study, we found that the CpPKS1-AL domain was also able to catalyze the thioesterification of palmitic acid with CoA. A typical reaction (100 μl) was composed of 100 mM Tris-HCl (pH 8.0), 10 mM $MgCl_2$, 2 mM DTT, 2 mM EDTA, 5 mM ATP, 300 μM CoA, 2 mM Triton X-100, 1 mM potassium fluoride (KF), 20 μM [9,10-^{3}H(N)]palmitic acid, and 20 ng MBP-CpPKS1-AL-ACP fusion protein. After incubation at 37 °C for 10 min, reactions were stopped with the addition of 125 μl of Dole's solution (40:10:1 = isopropanol/heptane/1 M H_2SO_4) and 50 μl of water, followed by a strong vortex to thoroughly mix. A heptane extraction method was then used by the addition of 500 μl of heptane immediately followed by vigorous mixing and centrifugation at 10,000 g for 2 min. The upper organic phase was removed, while the lower aqueous phase containing the radiolabeled palmitoyl-CoA was washed three more times with heptane containing 4 mg/ml unlabeled (cold) palmitic acid (to chase out radioactive palmitic acid), and once more with heptane only. Next, 75 μl of the washed aqueous phase was mixed with 5 ml of scintillation fluid and the radioactivity was

counted in a Beckman Coulter LS 6000SE counter. Enzyme kinetics values for this reaction were calculated from a Lineweaver-Burk plot with substrate concentrations ranging from 0.39 to 400 μM. Each reaction was assayed in at least duplicates. The MBP-tag was used to replace MBP-CpPKS1-AL-ACP for background subtraction as a control at each concentration.

The kinetics for the AL domain were also similarly assayed using varying amounts of CoA (0.39 – 100 μM), ATP (0.78 – 1000 μM), and $MgCl_2$ (0.032 – 10 mM). We also tested whether the CpPKS1-AL domain could use guanosine triphosphate (GTP) or uridine triphosphate (UTP) (each at 5 mM) to replace ATP as alternate energy sources. Additionally, the inhibitory effects of triacsin C (2 – 40 μM) on the AL domain were analyzed under the same reaction conditions.

Substrate specificity of the AL domain. A substrate competition assay was employed to determine substrate specificity as previously described (199). Briefly, 20 μM of various unlabeled (cold) even carbon saturated fatty acids from C2:0 to C30:0 were added to the reaction mixture to compete with the same molar amount of [^{3}H]palmitic acid under the same conditions for the typical assay. The same heptane extraction method was performed to measure the resulting amount of radiolabeled palmitoyl-CoA in the aqueous phase. The resulting data were plotted as the percent radioactivity in each assay compared to the reactions containing only [^{3}H]palmitic acid. Controls in all experiments included reactions with no protein present and 20 ng MBP only for background subtractions. At least three independent assays were performed with at least three replicates for each reaction.

Phosphopantetheinylation of the ACP domain. Because recombinant ACP domains from CpFAS1 could only be expressed in the inactive apo form (22, 199), we suspected that the bacterial host cells were also unable to phosphopantetheinylate the ACP domain in the CpPKS1 loading unit. Therefore, we wanted to test the ability of recombinant *C. parvum* SFP-type phosphopantetheinyl transferase (CpSFP-PPT) to activate the apo-ACP domain of the CpPKS1 loading unit. CpSFP-PPT has been previously expressed as an S-tag-fused protein from an artificially synthesized DNA fragment, and its capacity in activating the ACP domains from CpFAS1 has been studied in detail (22). In this assay, a 40 μl reaction consisting of 75 mM Tris-HCl (pH 7.0), 10 mM $MgCl_2$, 4 μg MBP-CpPKS1-AL-ACP, 400 ng CpSFP-PPT, and 40 μM [1-^{14}C]acetyl-CoA was used so that the attachment of the phosphopantetheinyl group could be visualized by autoradiography. Reactions were started with the addition of the radioactive acetyl-CoA, and incubated at 37 °C for 45 minutes. The entire reaction was then subjected to 6% SDS-PAGE, and visualized from dried gels using a FUJI BAS 1800 II PhosphorImager. As a control, reactions also included no protein, MBP only, or no CpSFP-PPT to ensure that the MBP fusion tag has no activity and that the ACP domain cannot be activated in the absence of CpSFP-PPT.

AL domain mediated transfer of long chain fatty acid to holo-ACP. After determining that CpSFP-PPT was able to activate the apo-ACP domain in the recombinant CpPKS1-AL-ACP protein, we next tested whether the AL domain was able to transfer palmitic acid to the adjacent activated holo-ACP by two sequential reactions. First, the ACP domain was activated by CpSFP-PPT using the same reaction conditions

as above, except unlabeled CoA (40 μM) was used to replace radioactive acetyl-CoA, so that only the phosphopantetheinyl moiety (rather than the acetylated moiety) would be transferred to the ACP. After free CoA was removed from the reaction using a Zeba desalting spin column (Pierce), 40 μl sample was then used in a second reaction (65 μl) containing 100 mM Tris-HCl (pH 7.0), 10 mM $MgCl_2$, 2 mM EDTA, 2 mM DTT, 5 mM ATP, 2 mM Triton X-100, 1 mM KF, and 20 μM [^{3}H]palmitic acid. The reaction was incubated at 37 °C for 45 minutes, fractionated by 6% SDS-PAGE, and visualized with autoradiography as before. Similar controls were included as described for the phosphopantetheinylation of the ACP domain section.

RESULTS

The CpPKS1 loading unit contains motifs characteristic to the ACL family and ACPs. Of the 13,414-amino acid CpPKS1, the loading unit comprises only 845 amino acids (Fig. 2.1). The AL domain shares sequence similarities to many other adenylate-forming enzymes, particularly the AMP-forming, long chain fatty acyl-CoA ligases (also termed as fatty acyl-CoA synthetase, EC 6.2.1.3) (16). Like the AL domain in some PKSs, the CpPKS1-AL domain contains both adenylation and ATPase motifs (197, 198) (Fig. 2.1). The AL domain adenylation core sequence slightly differs by only a few amino acids from that of the typical AMP-binding motif (m*XX*TSGtTG*X*PK) (170), but still shares a substantial degree of similarity as determined by PSSM analysis of 242 sequences. The second motif that appears to be more restricted to the ACL family is the ATPase motif. The ATPase motif's core sequence (TGD) is highly conserved

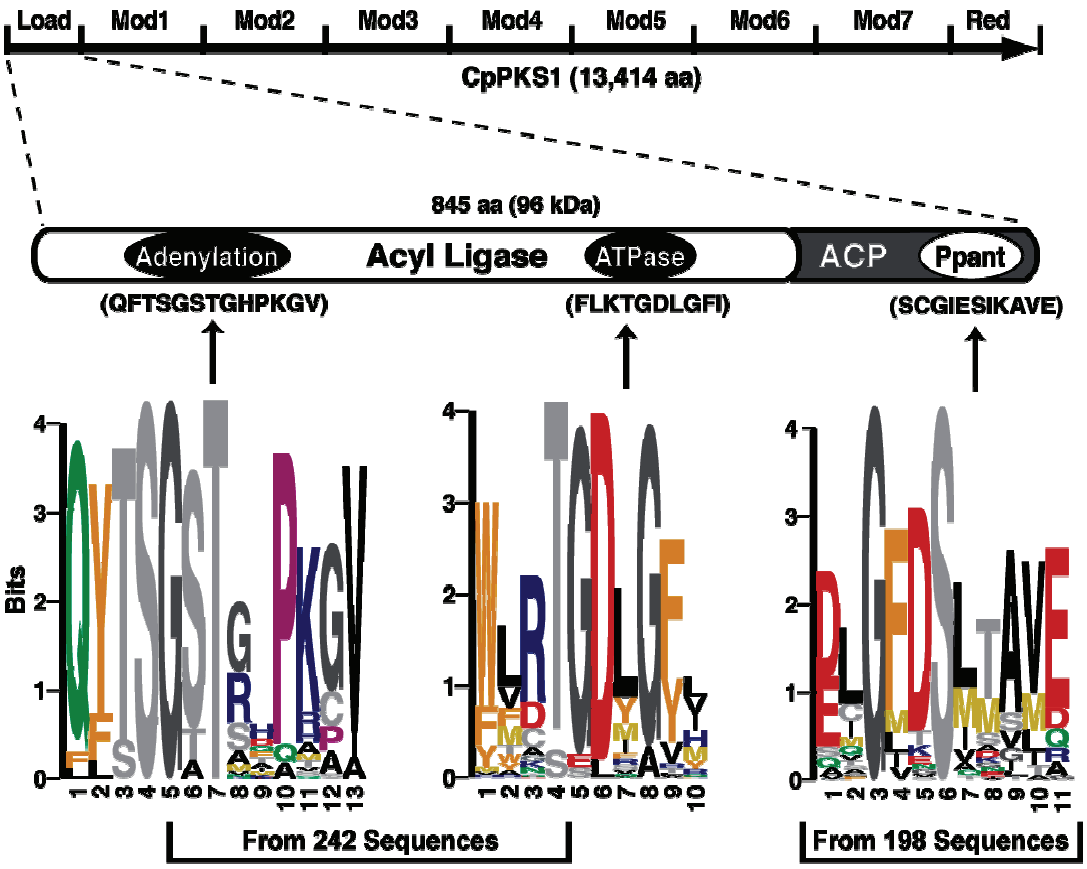

FIG. 2.1. The CpPKS1 loading unit consists of acyl ligase (AL) and acyl carrier protein (ACP) domains. The AL domain contains two highly conserved motifs responsible for the adenylation and the ATPase activities. The ACP domain contains the phosphopantetheinyl binding domain (Ppant) for the attachment of a phosphopantetheinyl moiety to the conserved serine reside. PSSM logos for the three domains were generated from the specified numbers of sequences retrieved from the GenBank protein database. Within each logo, the letter(s) represent the respective amino acid position in each motif, whereas the size of each letter represents the relative abundance of the respective amino acid within the sequences used for comparison. Motifs for the three conserved domains in the CpPKS1 loading unit are provided in parentheses for comparison to the PSSM logos. Load = loading unit, Mod = elongation modules, Red = reductase domain.

among all enzymes of this type as can be observed by the PSSM analysis of the same 242 sequences. The diversity of the 242 analyzed sequences is as follows: bacteria, 93%; fungi, 2.5%; plants, 2.1%; protists and insects, each 1.2%.

Similar to all other ACPs, the ACP domain in the CpPKS1 loading unit contains the 4'-phosphopantetheinyl-binding cofactor box (GxDS[I/L]) as defined by the PSSM analysis of 198 ACP sequences (bacteria, 92.9%; fungi, 5.6%; protists, 1.5%). However, this ACP domain appears to be one of very few ACP sequences analyzed where a glutamate (E) replaces the aspartate (D) in the core sequence. Although the function of the ACP domain is not expected to differ, it is interesting that this is one of few ACPs with this set of amino acids surrounding the conserved serine residue.

Expression and purification of recombinant CpPKS1-AL-ACP. The CpPKS1 loading unit was strategically engineered into and expressed in the pMAL-c2X expression vector as a 138-kDa MBP-fusion protein. The affinity of MBP for maltose allows for an easy amylose resin-based affinity chromatography purification method which usually provides for a rapid one-step purification of the fusion protein (83). However, regardless of the expression parameters used (i.e. growth/induction time, temperature, and IPTG concentration) for CpPKS1-AL-ACP, we always observed two major bands when purified using amylose resin-based affinity chromatography. We observed a band at the size of the predicted Mr (138-kDa), but we also observed a stronger band at ~80-kDa (Fig. 2.2, lane 2) that may represent premature termination of translation or degradation of the protein of interest. For better characterization of enzyme kinetics, the 138-kDa protein was isolated to homogeneity using a modified method for

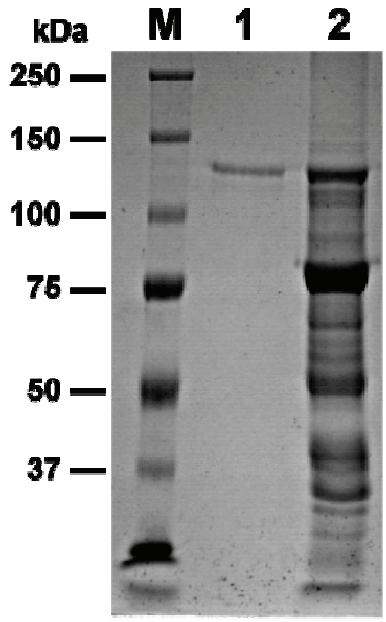

FIG. 2.2. SDS-PAGE analysis of the MBP-CpPKS1-AL-ACP fusion protein purified by a two-step approach (amylose resin-based affinity chromatography and PAGE gel extraction). The full-length fusion protein (138-kDa) was used in all enzymatic assays. M = protein marker, lane 1 = full length fusion protein from gel purification, lane 2 = amylose resin-based affinity purified protein.

eluting proteins from PAGE gels (33) (Fig. 2.2, lane 1), and used in subsequent analyses. For each one-liter culture used for protein expression, we obtained an average of ~4 mg/L of protein when purified utilizing affinity resin-based chromatography. Due to the presence of protein bands other than the protein of interest being visualized using SDS-PAGE, we estimated that the 138-kDa fusion protein was approximately 7.71% (0.316 mg/L) of the total protein purified from affinity chromatography. After gel extraction of the concentrated affinity purified protein sample, we obtained an average of 0.241 mg/L of the single-banded full length fusion protein shown in Figure 2.2, lane 1. This corresponds to a ~76% recovery of the full length 138-kDa fusion protein.

Enzyme kinetics of the AL domain. The ACL family catalyzes the formation of a fatty acyl-CoA from a fatty acid substrate, ATP, and CoA in a Mg^{2+}-dependent two-step reaction (10, 11, 16) (Fig. 2.3). A fatty acyl-adenylate intermediate is formed with the release of pyrophosphate in the first reaction, followed by conversion of the fatty acyl-adenylate to fatty acyl-ACP or acyl-CoA with the release of AMP. Like the AL domain in CpFAS1, the CpPKS1-AL domain was able to use CoA to replace holo-ACP to receive the C16 palmitic acyl chain. Using a heptane extraction-based radioactive assay, we observed that the AL activity towards palmitic acid in general followed Michaelis-Menten kinetics (K_m and V_{max} values at 1.178 μM and 2.744 μmol mg^{-1} min^{-1}, respectively) (Fig. 2.4A, dashed curve labeled with *h* [Hill coefficient] = 1). However, further analysis indicated that the AL kinetics actually fit better to a sigmoidal curve; coefficient of determination (R^2) = 0.9906 compared to 0.9829 for Michaelis-Menten kinetics (Fig. 2.4A, solid curve labeled with *h* = 1.46), indicating the presence of positive

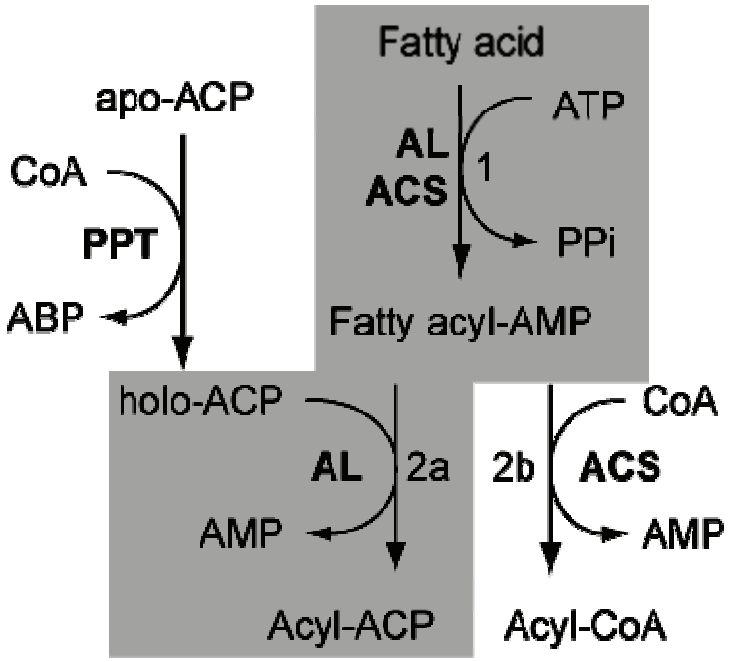

FIG. 2.3. Acyl ligase (AL) catalyzes a two-step reaction to activate fatty acids. The first step forms fatty acyl-AMP (reaction 1). In second step, AL catalyzes the formation of acyl-ACP (reaction 2a), while acyl-CoA ligase (ACL) catalyzes the formation of acyl-CoA ester (reaction 2b). However, when HSCoA is present, AAL may also catalyze the formation of acyl-CoA, thus allowing the detection of its activity by a simple heptane extraction assay. The synthesis of holo-ACP from apo-ACP is catalyzed by phosphopantetheinyl transferase (PPT). ABP = Adenosine 3',5'-bisphosphate.

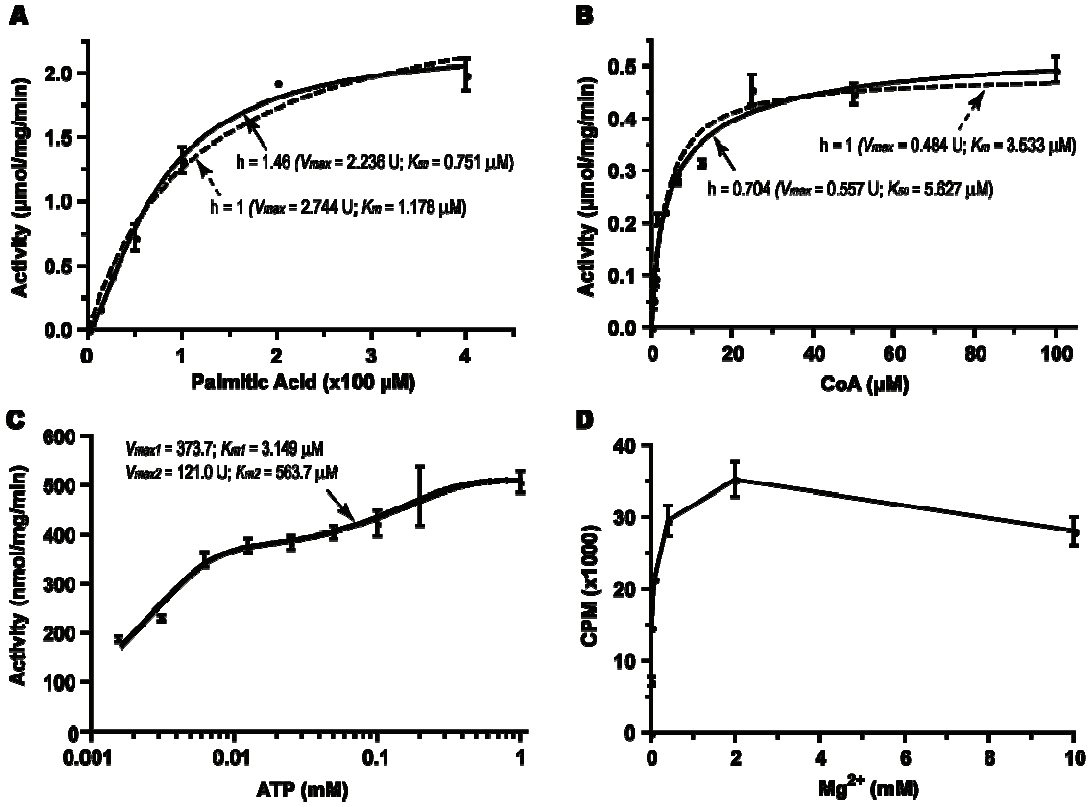

FIG. 2.4. The activity of the CpPKS1-AL domain for catalyzing the formation of palmitoyl-CoA as determined by a heptane extraction assay. (A) Allosteric kinetics assayed with various concentrations of palmitic acid indicates the presence of a positive cooperativity in the reaction (Hill coefficient, h = 1.46). (B) Allosteric kinetics assayed with various CoA indicates the presence of a small negative cooperativity (h = 0.704). (C) Binding kinetics assayed with various concentrations of ATP. The AL domain displayed two-site binding kinetics suggesting the presence of possible overall biphasic kinetics. (D) The AL domain activity is Mg^{2+}-dependent with an optimal concentration at ~2 mM. In all samples, bars represent the standard deviation derived from duplicate or triplicate reactions. U = µmol mg^{-1} min^{-1}.

cooperativity between the two steps of the overall reaction [i.e., formations of palmitoyl-AMP and palmitoyl-CoA, respectively]. Under the consideration of cooperativity, the values for K_{50} (equivalent to K_m) and V_{max} were determined at 0.751 μM and 2.236 μmol mg^{-1} min^{-1}, respectively.

The kinetic values of the CpPKS1-AL domain using CoA and ATP as substrates were also studied in detail. Using CoA as a substrate, the AL domain displayed close to typical Michaelis-Menten kinetics (K_m and V_{max} were 3.533 μM and 0.484 μmol mg^{-1} min^{-1}, respectively) (Fig. 2.4B, dashed curve). Nonlinear curve fit using an allosteric enzyme model was able to give a slightly better fit curve (R^2 = 0.9701 vs. 0.957), suggesting the presence of weak negative cooperativity (Fig. 2.4B, solid curve, h = 0.704). Under the consideration of cooperativity, the K_{50} and V_{max} values were determined at 5.627 μM and 0.557 μmol mg^{-1} min^{-1}, respectively. The AL domain appeared to have relatively strong affinity towards ATP. At ATP concentrations from 0.78 μM to 1 mM, the AL domain fit well with a biphasic kinetics model. Using this model (i.e. Observed Total Velocity (v) = $v1$ + $v2$ = V_{max1}*X/(K_{m1}+X) + V_{max2}*X/(K_{m2}+X)), the AL kinetic values for ATP were determined as K_{m1} = 3.149 μM, V_{max1} = 373.7 nmol mg^{-1} min-1, K_{m2} = 563.7 μM, V_{max2} = 121.0 nmol mg^{-1} min^{-1} (Fig. 2.4C). The AL domain also fit to the Michaelis-Menten model, although not as strong (R^2 = 0.9472 vs. 0.9664 for the biphasic model), and displayed kinetics similar to the first phase (K_m = 3.916 μM, V_{max} = 543.8 nmol mg^{-1} min^{-1}).

Like the AL domain in the loading unit of CpFAS1 (199), as well as other ALs and ACLs (16, 103), the activity of CpPKS1-AL can be inhibited by 5 mM AMP when

assayed with 5 μM ATP (Fig. 2.5). In contrast to one ACL in *Plasmodium falciparum* which can actually utilize GTP or UTP (103), CpPKS1-AL cannot (Fig. 2.5). Assay results using GTP and UTP showed very similar inhibition to the AL of CpFAS1 (199). Negative data for both of these reactions suggests that, compared to negative controls, these two co-factors might increase the efficiency during the heptane extraction method when extracting palmitic acid (199). The CpPKS1-AL domain is also Mg^{2+}-dependent with an optimal concentration at ~ 2 mM (Fig. 2.4D).

The CpPKS1 activity could be specifically inhibited by triacsin C (1-hydroxy-3-(E,E,E-2',4',7'-undecatrienylidine) (Fig. 2.6). Triacsin C is a fungal metabolite that resembles polyunsaturated fatty acids and can differentially inhibit various ACLs (Fig. 2.6, inset) (62, 86, 122). The observed IC_{50} for triacsin C to inhibit the thioesterification of palmitic acid with CoA by CpPKS1-AL was 6.64 μM (Fig. 2.6).

CpPKS1-AL prefers long chain fatty acids. The substrate specificity for CpPKS1-AL was determined using a wide range of even carbon saturated fatty acids (C2:0 – C30:0) to compete with the same molar amount of [^{3}H]palmitic acid. In this competition assay, the CpPKS1-AL domain displayed the highest affinity for arachidic acid (C20:0), with gradually reduced activities for other fatty acids with chain lengths shorter or longer than C20 (Fig. 2.7). Although long chain fatty acids (C14 to C24) are favorite substrates, it appears that CpPKS1-AL may also utilize a wide range of other fatty acids from short to very long chain fatty acids, since all tested fatty acids showed

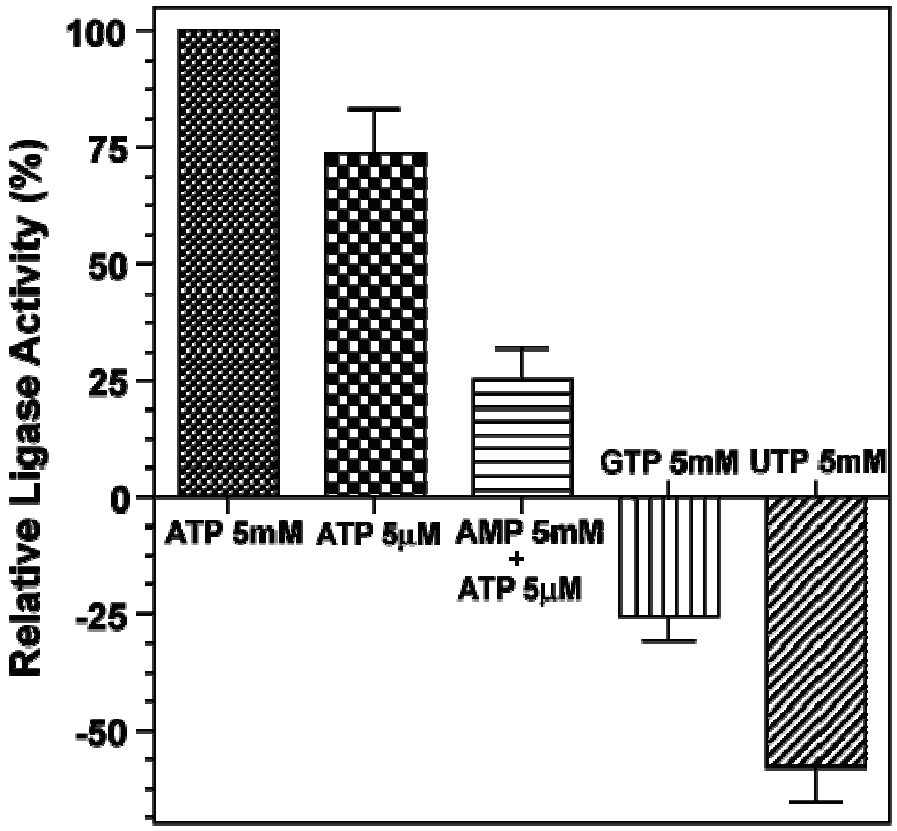

FIG. 2.5. Heptane extraction assays indicate that the activity of the CpPKS1-AL domain is ATP-dependent and can be inhibited by the product AMP. It cannot use GTP or UTP as an alternative energy source to activate palmitic acid. Bars represent the standard deviation derived from duplicate reactions.

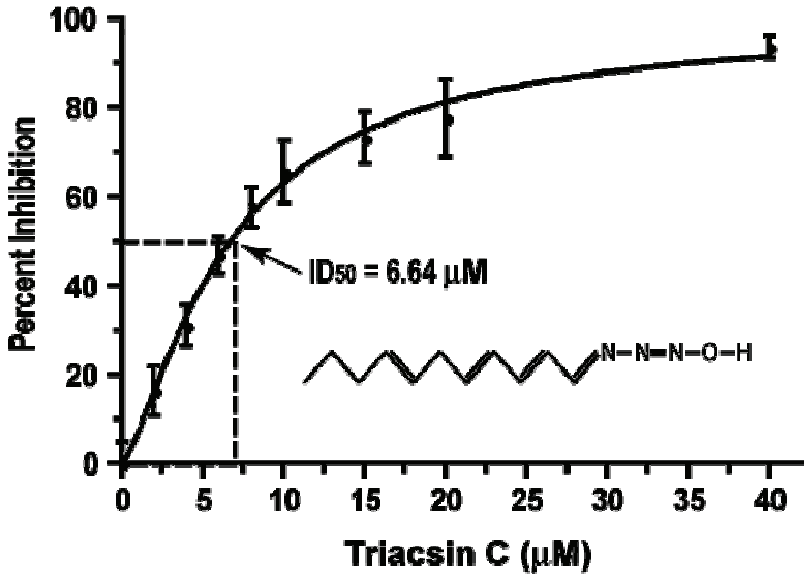

FIG. 2.6. Inhibitory effect of Triacsin C (structure depicted in the inset) on the activity of the CpPKS1-AL domain as measured by the incorporation of [^{3}H]palmitic acid into palmitoyl-CoA. Bars represent the standard deviation derived from duplicate reactions.

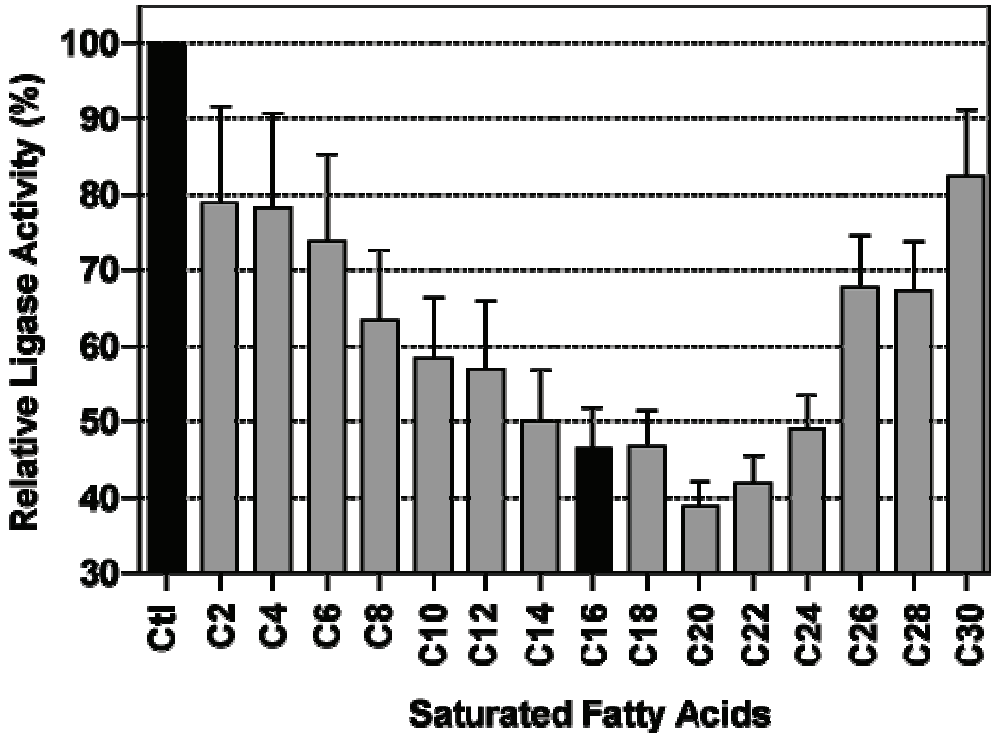

FIG. 2.7. Substrate competition assay using the same molar amount (20 μM) of unlabeled fatty acids from C2:0 to C30:0 to compete with [^{3}H]palmitic acid. Values indicate the percent activity of the formation of [^{3}H]palmitoyl-CoA relative to the positive control containing radioactive palmitic acid only (Ctl). The value obtained for C16 (indicated in black) indicates that the formation of [^{3}H]palmitoyl-CoA was formed by approximately equal amounts of both radiolabeled and non-radiolabeled palmitic acid. Bars represent the standard deviation derived from triplicate reactions.

some degree of displacement of activity towards to palmitic acid (Fig. 2.7). However, it remains to be determined whether the short chain (C2 and C4) or very long chain (C30) fatty acids may truly serve as endogenous substrates for CpPKS1-AL as these fatty acids could only displace ~20% of the activity while competing with palmitic acid.

CpPKS1-AL is capable of transferring fatty acid to the adjacent ACP domain in vitro. A two-step approach was employed to investigate the transfer of fatty acid to the ACP domain. In step one, the apo-ACP domain within the recombinant CpPKS1 loading unit was activated by CpSFP-PPT. We first confirmed that CpSFP-PPT was able to transfer the phosphopantetheinyl moiety from [^{14}C]acetyl-CoA to the ACP domain within the loading unit by autoradiography (Fig. 2.8A, lane 2). The transfer of the radioactive moiety from [^{14}C]acetyl-CoA to ACP could be chased out when same amount of cold acetyl-CoA was included in the reaction (Fig. 2.8A, lane 4), which indicates that the radioactive signal was not due to the potential non-specific binding of recombinant proteins to acetyl-CoA. We then used CpSFP-PPT to synthesize the holo-ACP domain using unlabeled HSCoA as a donor for the phosphopantetheinyl moiety. In step two, the CpPKS1-AL domain-mediated attachment of [^{3}H]palmitic acid to the holo-ACP domain was demonstrated by autoradiography (Fig. 2.8B). No radioactivity was observed in all negative controls (e.g. CpSFP-PPT only, CpPKS1 loading unit only, and PPT + MBP), indicating that only the activated ACP domain within the loading unit received palmitic acid and both CpSFP-PPT and the AL domain were required for this activity (Fig. 2.8B).

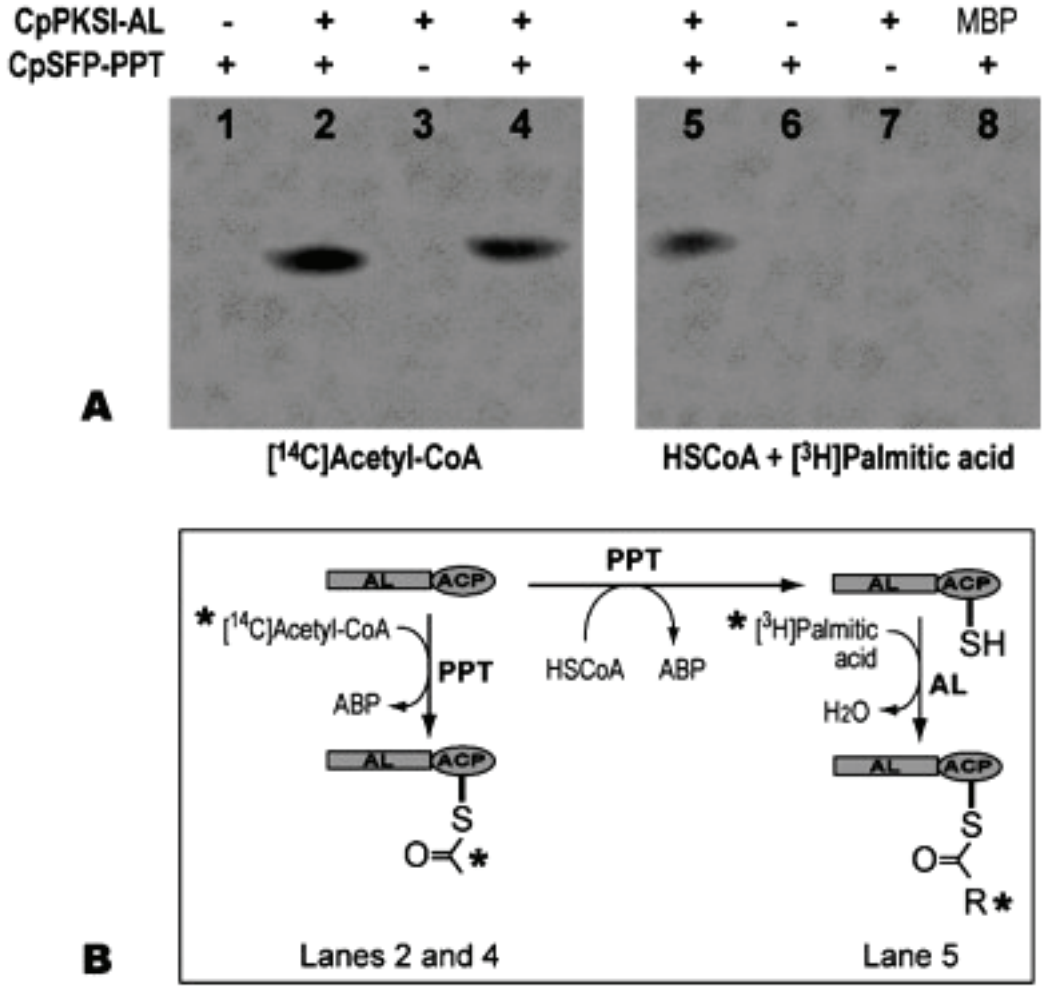

FIG. 2.8. Activation of the ACP domain by CpSFP-PPT, and the CpPKS1-AL-mediated transfer of palmitic acid to the activated ACP. (A) Autoradiography showing the CpSFP-PPT catalyzed activation of the ACP domain within the loading unit (CpPKS1-AL-ACP) by receiving a radioactive phosphopantetheinyl moiety from [^{14}C]acetyl-CoA (lanes 2 and 4). Reactions in lane 2 received all radioactive acetyl-CoA, while lane 4 received a mixture of same amount of radioactive and non-radioactive substrate. No radioactivity was detected in lanes 1 and 3 that contained only CpSFP-PPT or the loading unit, respectively. (B) Autoradiography showing the transfer of the [^{3}H]palmitoyl chain to the activated ACP domain (lane 5). Unlabeled HSCoA was used here for activating the ACP domain by CpSFP-PPT. No radioactivity was detected in reactions containing only CpSFP-PPT (lane 6), the loading unit (lane 7), or when MBP was used to replace loading unit (lane 8). (C) Diagram showing the reactions detected by autoradiography in A and B. Asterisks indicate the radioactive molecules.

DISCUSSION

CpPKS1 is the first PKS identified from a protist (protozoan) (198). It appears to share the same evolutionary ancestor with CpFAS1 based on the overall sequence similarities and phylogenetic evidence inferred from the AT and KS domains (196, 198). Among other apicomplexans that possess a plastid and associated Type II FAS, *P. falciparum* lacks Type I FAS or PKS, whereas *T. gondii* and *E. tenella* have both Type I FAS and PKS present in their genomes (data not shown, but they can be easily identified by BLAST-searching the two parasite genome databases using CpFAS1 and CpPKS1 as queries at http://ToxoDB.org and http://www.sanger.ac.uk/Projects/E_tenella). More recently, PKS genes closely related to CpPKS1 have been reported from the dinoflagellates (162, 163), suggesting that Type I FAS or PKS might have been present before the species expansion of Alveolata.

Among these two *C. parvum* megasynthases, preliminary biochemical analysis using recombinant proteins has indicated that CpFAS1 may be involved in the elongation, rather than the de novo synthesis, of fatty acids (196, 199). However, nothing was previously known about the biochemical features of CpPKS1. Furthermore, no previous studies have clearly evaluated the biochemical features of this type of loading domain among various other PKSs. The CpPKS1 product(s) and biological roles remain to be elucidated. The present study focuses on delineating the biochemical features and substrate preference for the CpPKS1 loading unit, which serves as a first, but essential step for elucidating the functional role(s) of this megasynthase.

We first expressed the loading unit containing AL and ACP domains as an MBP-fused protein and purified the fusion protein to homogeneity. Like the CpFAS1-AL domain, the CpPKS1-AL domain was able to utilize HSCoA to replace ACP for receiving the fatty acyl chain, thus allowing the detailed analysis of enzyme kinetics. It is interesting that the CpPKS1-AL domain displayed allosteric kinetics when using palmitic acid as a substrate (h = 1.46 [Fig. 2.4A]). This feature has yet to be reported among other ACLs, probably due to the fact that the enzyme kinetics might also be well analyzed by a simple Michaelis-Menten algorithm. Although a detailed mechanism behind the allosteric kinetics remains to be elucidated, it implies the presence of positive cooperativity between the two reactions catalyzed by AL (i.e., the formations of palmitoyl-AMP and palmitoyl-CoA). The kinetics for the AL domain to use ATP is also intriguing. It follows both Michaelis-Menten kinetics, and also, to a greater extent, two-site binding kinetics suggesting possible biphasic kinetics, for which the mechanism has yet to be determined. It is possible that two forms of recombinant CpPKS1 loading unit were present in purified proteins, which have different affinities for ATP.

Substrate competition assays have shown that the CpPKS1-AL domain has a general preference for long chain fatty acids, particularly to arachidic acid. This implies that CpPKS1 may be able to add a polyketide chain (likely 14 carbons due to the presence of 7 elongation modules) to a fatty acyl precursor. Although the CpPKS1-AL domain may effectively use various fatty acids, its true substrate(s) may be limited by the availability of fatty acids in the parasite cells. Due to the lack of Type II FAS in *C. parvum,* together with the fact that CpFAS1 prefers palmitic acid as its substrate, this

protist is probably incapable of synthesizing fatty acids de novo, thus it may have to rely on the uptake of fatty acids (both saturated and unsaturated) from host cells or the intestinal lumen to supply substrates for CpPKS1 and CpFAS1. On the other hand, it is possible that other types of substrates, such as polyketides, may be used by CpPKS1. However, this is less likely since this parasite lacks any other PKS genes to make precursors for CpPKS1 and the host cells or intestinal lumen are not reliable sources for polyketides. Nonetheless, the profile of substrate preference provides us important information in selecting substrates for the reconstitution of entire reactions catalyzed by CpPKS1 in the future.

CpPKS1 contains eight ACP domains (one in the loading unit and seven at the end of each elongation module), while CpFAS1 contains four ACP domains. It appears that all of these ACP domains need to be activated by the addition of a prosthetic phosphopantetheinyl moiety, which is catalyzed by PPT. *Cryptosporidium* possesses only one single SFP-type PPT (CpSFP-PPT) that was able to activate the ACP domains in CpFAS1 (22). Here we have shown that CpSFP-PPT was able to activate the ACP domain in CpPKS1 (Fig. 2.8A), indicating that this single parasite PPT may be responsible for activating the ACP domains in both CpFAS1 and CpPKS1.

Upon the activation of the ACP domain within the CpPKS1 loading unit, the function of the AL domain to transfer an acyl chain to the ACP was ultimately validated by autoradiography (Fig. 2.8B). This demonstrates that the ACP domains in all CpPKS1 modules may also be activated after they are expressed as fusion proteins, thus

permitting the future reconstitution of polyketide chain elongation and release in vitro using recombinant CpPKS1 modules and units.

CHAPTER III

Cryptosporidium parvum LONG CHAIN FATTY ACID ELONGASE*

OVERVIEW

As one of the vital compounds for all organisms, fatty acids of 14 to 18 carbons in length comprise the bulk of cellular fatty acids that serve structural and biological functions and are usually the major products of de novo synthesis in most cells. These long chain fatty acids (LCFAs) play important roles in many biological functions such as energy metabolism and membrane structure. There are several metabolic pathways that produce LCFAs, most notably the type I and type II fatty acid synthases (FASs). The type I enzymes of mammals and fungi are typically cytosolic and composed of multiple enzymes arranged into domains of one or two large polypeptide(s) (161). In contrast, the enzymes of the type II FASs are all located on separate domains and are found in prokaryotes or eukaryotic organelles of prokaryotic origin (188).

Relatively common among eukaryotic organisms are the fatty acid elongase-based systems, These elongase-based systems directly elongate a fatty acyl chain esterfied with CoA (fatty acyl-CoA), which is in contrast to the type I and type II FAS systems that elongate a fatty acyl chain attached to an acyl carrier protein (ACP). The elongase system is comprised of at least four enzymes that are responsible for adding two carbon units to the fatty acyl carboxyl end. The chemistry of this pathway is similar

* Part of this chapter is reprinted from Fritzler, J. M., and G. Zhu. 2007. *Cryptosporidium parvum* long chain fatty acid elongase. Eukaryot. Cell 6: 2018-2028, with permission from American Society for Microbiology.

to that used by type I and type II FASs. Fatty acyl elongation begins with the condensation of malonyl-CoA with a fatty acyl-CoA catalyzed by the condensing enzyme LCE (= β-ketoacyl-CoA synthase) (Fig. 3.1, step 1). The resulting β-ketoacyl-CoA is now two carbons longer and is then reduced to β-hydroxyacyl-CoA in a NAD(P)H-dependent reaction by β-ketoacyl-CoA reductase (Fig. 3.1, step 2). Dehydration occurs through the action of β-hydroxyacyl-CoA dehydratase to yield enoyl-CoA (Fig. 3.1, step 3), which is further reduced by enoyl-CoA reductase in a NAD(P)H-dependent manner (Fig. 3.1, step 4) to yield the elongated fatty acyl-CoA. Whether or not the elongated product is released for use elsewhere in the cell or is retained to undergo another round of elongation largely depends on the specific needs of the organism.

Although purification and biochemical characterization of these four enzymes is difficult due to their membrane-bound nature, it appears that the condensing enzyme is the rate-limiting enzyme of the elongase system and is commonly referred to as "elongase" (15, 32, 119). Thus, it is responsible for the fatty acid substrate specificity regarding chain length and pattern of double bonds, whereas the other three components of the elongase system display little or no particular substrate specificity (32). Comparative protein sequence analysis has classified the condensing enzymes into two distinct groups: the KCS/fatty acid elongation (FAE) group present mainly in plants, and the elongase (ELO) group present in protozoa, mammals and fungi (93). It is not uncommon for a cell or organism to contain multiple condensing enzymes that share the

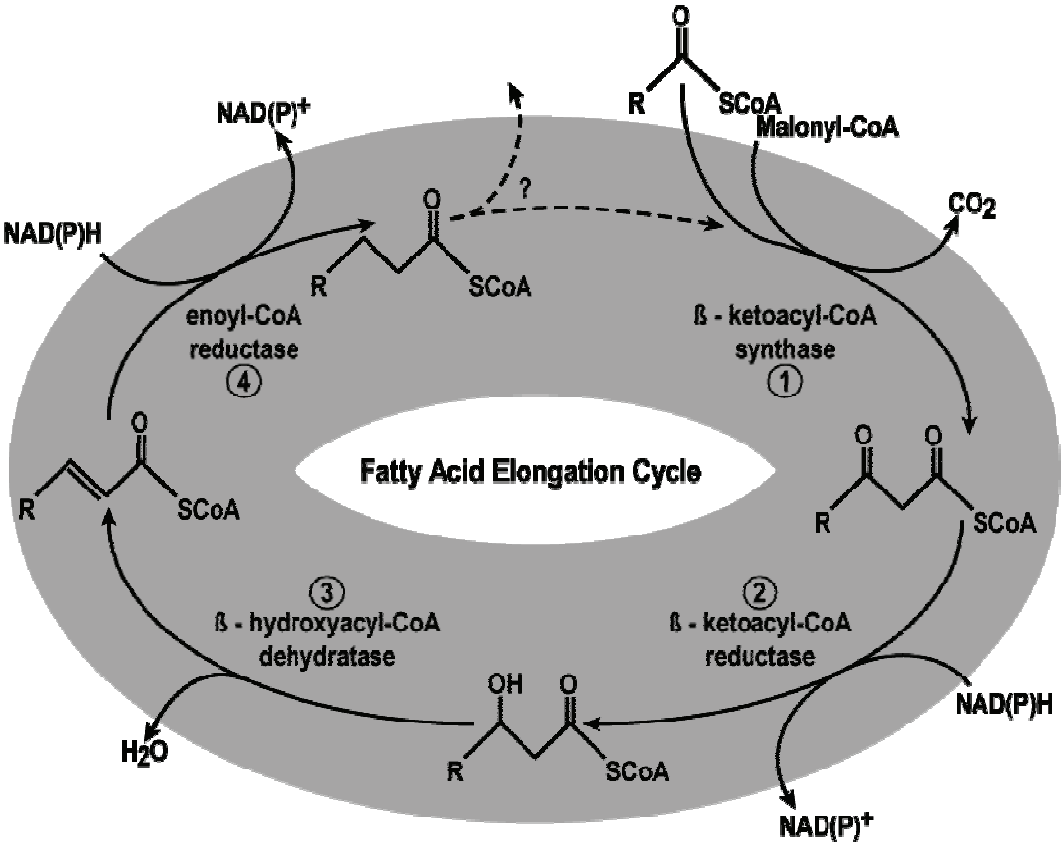

FIG. 3.1. The fatty acid elongation system. The diagram displays the four enzymes and fatty acyl-CoA intermediates involved in the two-carbon elongation of fatty acyl-CoAs. The first step is a condensation reaction catalyzed by the "elongase" enzyme (CpLCE1). This is the enzyme that determines chain length and degree of unsaturation of the substrate, and is the rate-limiting step of the system. The product of the condensation reaction then undergoes reduction by a β-ketoacyl-CoA reductase (step 2), dehydration by β-hydroxyacyl-CoA dehydratase (step 3), and a final reduction by enoyl-CoA reductase (step 4). Whether or not the elongated product is utilized elsewhere in the cell or organism or undergoes an additional round(s) of elongation largely depends on the needs of the specific cell/organism at that time.

same reductase-dehydratase-reductase enzymes. Furthermore, each system within a cell or organism may exhibit a broad range of substrate specificities (sometimes overlapping) for fatty acid chain length as well as saturated or unsaturated fatty acids (93). For example, *Saccharomyces cerevisiae* contains three elongases termed ELO1, ELO2, and ELO3, in which ELO1 has a preference for elongating C12 to C16 fatty acids, whereas ELO2 and ELO3 elongate C16 saturated and monounsaturated fatty acids to C24 and C26, respectively (133). This study aims to characterize the sole long chain elongase from *Cryptosporidium parvum* (CpLCE1), the first such study among the apicomplexan parasitic protozoa.

MATERIALS AND METHODS

Identification of CpLCE1 and phylogenetic reconstructions. The *CpLCE1* gene was originally identified from a *C. parvum* genome contig by homolog searches, which was then cloned and sequenced to confirm its identity (GenBank accession No. AAO34582). It was later annotated in the genome sequencing projects as a "7 pass integral membrane protein with FLHWFHH motif shared with fatty-acyl elongase" for *C. parvum* (XP_627348) and "fatty-acyl elongase" for *C. hominis* (XP_666343).

To determine the evolutionary relationship of CpLCE1 among elongases from other organisms we performed maximum likelihood (ML)-based phylogenetic analyses. The CpLCE1 amino acid sequence was used as a query to search protein databases including all nonredundant GenBank CDS translations, RefSeq Proteins, PDB, SwissProt, PIR and PRF at the National Center for Biotechnology Information (NCBI)

using the PSI-BLAST program (http://www.ncbi.nlm.nih.gov/BLAST) (3). Elongase sequences from other apicomplexans were also obtained from http://PlasmoDB.org (*Plasmodium*) and http://ToxoDB.org (*Toxoplasma gondii*). Four iterative BLAST searches were performed and only sequences with E-values better than 1×10^4 were selected for phylogenetic analysis.

Multiple sequence alignments were performed on 75 sequences using the ClustalW algorithm housed in the MacVector v9.5.2 program (MacVector, Inc.) and apparent mistakes in alignment were corrected upon visual inspection. A dataset containing 91 unambiguously aligned amino acid positions were used in subsequent analysis. The MrBayes v3.1.2 program (http://mrbayes.csit.fsu.edu/) was used to reconstruct trees using a Bayesian inference (BI) method (73). The program was allowed to "jump" among all available amino acid substitution models, and to consider among-site rate heterogeneity using a fraction of invariance (*Inv*) plus a four-rate Γ-distribution model during Markov chain Monte Carlo (MCMC) analysis. A total of 5×10^6 generations of searches were performed with two independent runs, each containing four chains simultaneously running. The current trees were saved every 1000 generations. Posterior probability (PP) values at tree nodes were obtained by calculating consensus trees from the last 3,000 BI trees that were obtained after the runs converged. In addition, ML analysis was also performed using the PROML program included in the PHYLIP package (http://evolution.gs.washington.edu/phylip.html). The Jones-Taylor-Thornton (*JTT*) model (77), with the consideration of *Inv* and four-rate Γ- that were estimated using TREE-PUZZLE v.5.2 program (http://www.tree-puzzle.de).

Transcript analysis for CpLCE1 at various developmental stages. Freshly isolated *C. parvum* oocysts (Iowa strain) purified by Percoll gradient centrifugation and stored in water at 4 °C (8) were used to analyze the relative transcript levels for *CpLCE1* gene. Oocysts were excysted in PBS containing 0.1% trypsin and 0.5% taurodeoxycholic acid for 90 min at 37 °C to release free sporozoites which were further purified using a Percoll gradient centrifugation method (145). Intracellular stages of *C. parvum* were obtained by infecting human HCT-8 cells with oocysts for various times (6-72 h). Total RNA was isolated from oocysts, free sporozoites, and intracellular stages using an RNeasy kit (Qiagen) following the manufacturer's recommended protocol for animal cells. The only addition to RNA isolation using this method was that oocysts were suspended in the recommended lysis buffer and underwent 10 freeze/thaw cycles (liquid nitrogen/37 °C) to disrupt the oocyst wall prior to RNA isolation.

A SYBR-green-based real time quantitative RT-PCR method was used to determine the transcript levels of *CpLCE1* at the various developmental stages. The primer pair CpLCE1-F07 (5' TCA CTT TAT CAG AAC CAA CGG TG 3') and CpLCE1-R07 (5' GGC AGT TAC CCA TTC AGC AAG 3') was used to amplify *CpLCE1* transcripts. To amplify *C. parvum* 18S rRNA as a control for normalization we used the previously reported primers 995F (5' TAG AGA TTG GAG GTT GTT CCT 3') and 1206R (5' CTC CAC CAA CTA AGA ACG GCC 3') (1). The relative level of *CpLCE1* transcripts expressed relative to those of 18S rRNA and values are reported based on at least three replicates as previously described (22, 144).

Production of antibodies. A short peptide corresponding to a unique internal sequence of CpLCE1 (^{76}FGPKIMEKRKPFKLEKPLKYW) was synthesized by the Peptide Core Facility at the Department of Veterinary Pathobiology, Texas A&M University. This short peptide is unique to CpLCE1 and is reasonably antigenic as determined by various antigenicity indexes using the MacVector v9.5.2 program (MacVector, Inc.). Initially, sera from six pathogen-free rats were collected prior to the immunization protocol, of which pre-immune sera from two of the six showed no reactivity to dot blot tests using parasite protein extracts. The synthetic peptide was freshly cross-linked to Keyhole Limpet Haemocyanin prior to each immunization. Polyclonal antibodies to CpLCE1 were raised in two pathogen-free rats that were initially immunized with 200 μg of antigen emulsified in an equal volume of Freunds complete adjuvant. Booster immunizations (100 μg) were performed at 30 and 60 days, respectively, after the primary immunization. Rat sera were then collected after the immunization protocol and specificity of the rat polyclonal antibodies were evaluated by dot and Western blot analyses with protein extracts of parasites and host cells.

Immunofluorescence microscopy. Sporozoites and intracellular developmental stages for immunolocalization analysis were obtained as above. Intracellular parasites were obtained by infecting human HCT-8 cells grown on glass coverslips treated with poly-L-lysine for 12, 36 or 60 h. Samples were fixed with 10% formalin, rinsed with PBS, and extracted with cold methanol (-20 °C). Free sporozoites were applied directly to poly-L-lysine-treated coverslips, air-dried, and then extracted. Cells were then blocked with 0.5% BSA-PBS for 10 min before incubation with primary antibodies for 1

h in 0.5% BSA-PBS. Free sporozoites were then labeled with anti-rat IgG secondary antibodies conjugated with FITC for 1 h in 0.5% BSA-TBS. Intracellular developmental stages were all exposed to a 1 h incubation in 0.5% BSA-PBS with anti-rat IgG-TRITC to visualize CpLCE1 localization. Co-localization of CpLCE1 with *C. parvum* fatty acyl-CoA binding protein (CpACBP1) and with total membrane proteins (TMPs) was similarly performed. The anti-TMP antibodies and FITC-conjugated secondary antibodies were incubated simultaneously with anti-CpLCE1 and corresponding secondary antibodies, respectively; whereas the CpACBP1 antibodies were directly labeled with Alexa Fluor 488 using the appropriate fluorophore labeling kit (Invitrogen). Co-localization of CpLCE1 with TMP or CpACBP1 was selected because the TMP antibodies have been shown to label the parasitophorous vacuolar membrane (PVM) and feeder organelle (28) and CpACBP1 localizes to the surface of merozoites as well as co-localizes with TMPs (194). All samples were mounted with a SlowFade Gold AntiFade reagent containing *4',6'*-diamidino-2-phenylindole (DAPI) for DNA counter-staining (Invitrogen) and examined with an Olympus BX51 Epi-Fluorescence microscope equipped with differential interference contrast and TRITC/FITC/DAPI filters.

Cloning and expression of CpLCE1. The 972-bp *CpLCE1* gene was amplified from *C. parvum* (Iowa strain) genomic DNA (gDNA) using the high-fidelity *Pfu* Ultra DNA polymerase (Stratagene) with the primer sets CpLCE1-Fwd (5' gcg aat tcA TGT TCA TAG AAA ATA ATA ATA AT 3') and CpLCE1-Rev (5' gct cta gaA TCG CGC TTA GTT GGT TTT T 3') (lower cases represent artificial *Eco*RI and *Xba*I linkers, respectively). The amplified product was directly ligated into the pcDNA3.1/HisC

mammalian expression vector (Invitrogen) and transformed into *Escherichia coli* TOP10 cells (Invitrogen).

Plasmid DNA containing the correct insert (pcDNA3.1/HisC-CpLCE1) and confirmed by sequencing was transfected into Human Embryonic Kidney (HEK)-293T cells. HEK-293T cells were plated in 100-mm tissue culture plates and grown at 37 °C in an atmosphere of 5% CO_2 in Dulbecco's Modified Eagle Medium (DMEM - high glucose) supplemented with 10% Fetal Bovine Serum (FBS). At ~90% confluency the pcDNA3.1/HisC-CpLCE1 plasmid or the empty plasmid pcDNA3.1/HisC (10 μg) was transfected into cells using Lipofectamine 2000 (Invitrogen) according to the manufacturer's protocol. After transfection, cells were grown for 48 h at 37 °C in DMEM plus 10% FBS.

Confirmation of transfection and protein expression. Forty-eight hours after transfection of HEK-293T cells, total RNA was isolated from CpLCE1 and pcDNA3.1/HisC transfected cultures, and non-transfected cultures (as a negative control) using an RNeasy Mini kit (Qiagen) following the manufacturer's protocol. The vector-specific T7-Fwd and BGH-Rev primers were used in conjunction with the One-Step RT-PCR kit (Qiagen) to confirm positive transfection.

Transfections were also performed in 24-well format to assess protein expression using immunofluorescence microscopy. Cells were first seeded onto glass coverslips treated with poly-L-lysine and transfected with CpLCE1 or pcDNA3.1/HisC using the method above while following the recommended protocol for Lipofectamine 2000 transfection in 24-well format. After incubation for 48 h cells were fixed with 10%

formalin, rinsed with PBS, extracted with -20°C methanol for 5 min and blocked in 0.5% BSA-PBS for 10 min. Cells were then labeled with anti-CpLCE1 primary antibodies for 1 h in 0.5% BSA-PBS followed by incubation with secondary antibodies conjugated with TRITC for 1 h in 0.5% BSA-PBS. The samples were washed after each incubation step three times with PBS for 5 min each. All samples were mounted using DAPI and examined using an Olympus BX51 Epi-Fluorescence microscope equipped with differential interference contrast and TRITC/DAPI filters. Cultures that were not transfected or transfected with pcDNA3.1/HisC were used as negative controls.

Total membrane preparation of transfected cells. Total membrane protein fractions were prepared in a method similar to that for preparing microsomal protein (104). Forty-eight hours post-transfection, cells were washed with PBS and scraped into 5 ml of ice-cold 250 mM sucrose, 20 mM HEPES, pH 7.5 containing a mammalian protease inhibitor (PI) cocktail (Sigma). After centrifugation at 1,000 *g* for 7 minutes at 4 °C, the cell pellet was resuspended in 3 ml of ice-cold sucrose/HEPES with PI. The sample was then dounce-homogenized and centrifuged at 1,000 *g* at 4 °C to remove large cellular debris. The supernatant was then centrifuged at 100,000 *g* for 1 h at 4 °C. The supernatant was discarded, and the resulting pellet was resuspended in 500 μl of 100 mM Tris-HCl, 0.1% Triton X-100, pH 7.4. Protein concentration was determined by a Bradford colorimetric method using BSA as a standard. Aliquots were snap-frozen in liquid nitrogen, and stored at -80 °C. Western blot analysis using the rat anti-CpLCE1 antibodies and monoclonal rabbit anti-rat IgG antibodies was also performed to test for the presence of CpLCE1 in the prepared membrane fractions of transfected cells.

Fatty acyl-CoA elongation assay. Initial activity of the elongation of fatty acyl-CoA by CpLCE1 was determined using variations of a mixture of previously described methods (104, 113, 155, 185). To optimize reaction conditions a 100 μl reaction containing 50 mM potassium phosphate, pH 6.5, 5 μM rotenone, 20 μM fatty acid-free BSA, 1 mM $MgCl_2$, 0.5 mM NADH, 0.5 mM NADPH, 60 μM palmitoyl-CoA, and 200 μM [2-^{14}C]malonyl-CoA was heated at 37°C for 2 min. The reaction was started with the addition of 30 μg of protein from CpLCE1 or pcDNA3.1/His C transfected cells, and allowed to proceed for 30 min at 37°C before the addition of 100 μl of 5N KOH in 10% methanol. The samples were then saponified at 65 °C for 1 h and cooled to room temperature when 100 μl each of 5*N* HCl and ethanol were added. Radiolabeled incorporated fatty acids were then extracted from the mixture using 1 ml of hexane followed by vigorous mixing and centrifugation at 10,000 *g* for 2 min. The upper organic phase was removed, while the lower aqueous phase was washed twice more with 1 ml of hexane. The hexane extracts were pooled and dried under vacuum, then 5 ml of scintillation fluid was added and the radioactivity was counted in a Beckman Coulter LS 6000SE counter. Activity was determined by subtracting the values obtained for the pcDNA3.1/HisC transfected samples from the values obtained for the CpLCE1 transfected samples. Reactions containing no membrane protein were also used as controls to determine additional background levels.

Dependence on NADH or NADPH was determined using the same assay, and the optimum pH for this enzyme was determined using the above reaction while including 50 mM potassium phosphate buffer at pH 5.0, 5.5, 6.0, and 6.5, and 50 mM Tris buffer

at pH 7.0, 7.5, 8.0, and 8.5. The kinetics for CpLCE1 were similarly assayed using varying amounts of palmitoyl-CoA (0.98 – 250 μM), malonyl-CoA (0.98 – 500 μM), and NADPH (3.9 μM – 1 mM).

Substrate preference. Once optimal reaction parameters were known, the substrate preference for CpLCE1 was determined. The fatty acyl-CoA elongation assay used was similar to that described above except it lacked NADH (included 500 μM NADPH) and included 125 μM of various saturated (C2:0 to C24:0) and unsaturated fatty acyl-CoAs (C18:1, C18:3, C20:4, and C22:6), and 250 μM [2-^{14}C]malonyl-CoA. Reactions consisted of protein fractions from either CpLCE1 or pcDNA3.1/HisC transfected samples. Activity was determined by subtracting values obtained for the pcDNA3.1/HisC transfected samples from the values obtained for the CpLCE1 transfected samples. Additionally, substrate preference data were used to test the inhibitory effect of cerulenin, a known inhibitor of both type I and II β-ketoacyl-CoA synthase, on CpLCE1 using the same reaction conditions as above while including 0.2 - 200 μM cerulenin.

TLC analysis of elongated fatty acids. The fatty acid elongation reaction was assayed as above using 30 μg protein from either CpLCE1 or pcDNA3.1/HisC transfected cells, 250 μM nonradiolabeled malonyl-CoA, and 125 μM of either myristoyl-CoA or palmitoyl-CoA (C14:0-CoA and C16:0-CoA, respectively). Reactions were terminated and fatty acids were extracted as above. Hexane fractions containing the elongated fatty acids were dried by evaporation under nitrogen before the addition of 3 ml methanol/toluene/sulfuric acid (88:10:2 v/v) to convert the extracted fatty acids into

their fatty acid methyl ester (FAME) derivatives (56, 155). The suspension was incubated for 1 h at 80 °C, allowed to cool to room temperature, and FAMEs were extracted two times with 2 ml hexane. The hexane fractions were once again allowed to evaporate to dryness under nitrogen, and were resuspended in 40 µl hexane for TLC analysis. Reverse phase LKC18 silica gel 60Å TLC plates (Whatman, Inc.) were washed with chloroform/methanol (1:1) followed by incubation at 110 °C for 1 h and cooled to room temperature before samples were spotted. The elongated products were separated using methanol:chloroform:water (15:5:1) using authentic FAME standards (Supelco) (126).

HPLC analysis of elongated fatty acids. The elongation assay and FAME preparation used for HPLC analysis were replicas of that used for TLC analysis except that the FAMEs were suspended in 200 µl 65% acetonitrile in water instead of 40 µl hexane. FAME derivatives of the elongation products were separated by reverse phase HPLC using a Shimadzu Prominance HPLC and a Zorbak SB-C18 semi-preparative column (5 µm, 9.4 × 250 mm, Agilent Technologies). Injection volumes were 100 µl and elution was performed using a binary gradient of 95% acetonitrile 5% water at a flow rate of 1.0 ml/min. The absorbance at 205 nm (A_{250}) was monitored using a SPD-M20A Diode Array Detector and the identity of the eluted products were compared to the retention times of known FAME standards (Supelco) originally suspended in 65% acetonitrile.

RESULTS

Sequence comparison of elongases related to CpLCE1. Contrary to many other eukaryotic organisms, *CpLCE1* is the only elongase homologue that can be identified from the *C. parvum* genome. This intronless gene encodes 324 amino acids that share several characteristics with related elongase homologues. Figure 3.2 displays the CpLCE1 amino acid sequence aligned with those of selected mammalian and protozoan elongases. The *Toxoplasma gondii* elongase sequence had the highest similarity with CpLCE1 (45% identical) while the six others were between 31% and 38% identical. The alignment shows that all the sequences share the characteristic FLHxxHH motif that is conserved among elongases and even fatty acid desaturases. Additionally, the KxxExxDT, NxxxHxxMYxYY, and TxxQxxQ motifs are present which are also characteristic among elongases and appear to be highly conserved especially among the polyunsaturated fatty acid (PUFA) elongases (109). Structural analysis of CpLCE1 aligned with these related elongases revealed several hydrophobic domains. Analysis with the TMAP algorithm (131) predicts six transmembrane domains which are clearly indicated. This is typical of elongases and confirms the suggestion that CpLCE1 is anchored to a membrane.

Phylogenetic relationships among apicomplexan and other eukaryotic elongases. Thousands of elongase homologues were identified from BLAST searching the GenBank protein databases. Because our goal was to obtain information about the evolution of apicomplexan elongases rather than a global approach to analyze the

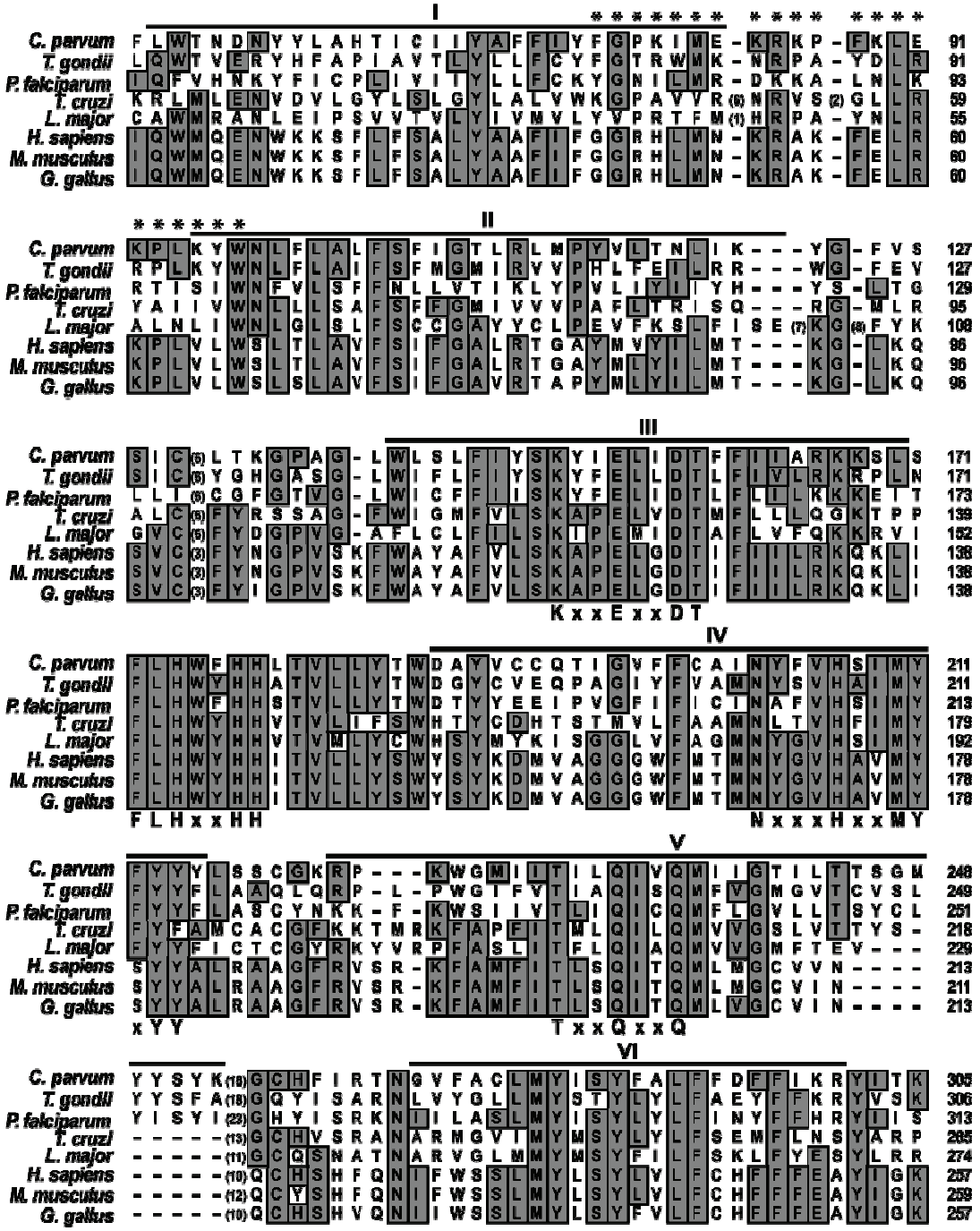

FIG. 3.2. Amino acid sequence comparison of CpLCE1 and representative eukaryotic elongase enzymes. CpLCE1 (AAO34582) is aligned with the sequences of *Toxoplasma gondii* (20.m00392), *Plasmodium falciparum* (XP_001351023), *Trypanosoma cruzi* (XP_813971), *Leishmania major* (CAJ03003), *Homo sapiens* (NP_076995), *Mus musculus* (NP_569717), and *Gallus gallus* (NP_001026710). Amino acids with at least 50% conservation between CpLCE1 and other sequences are shaded. The four highly conserved domains are indicated below the sequence, and the six transmembrane domains are labeled I-VI. (*) indicate the epitope used for antibody production.

elongase protein family, we constructed phylogenetic trees from a total of 75 taxa from a variety of other organisms. Applying a Bayesian analysis to the phylogeny resulted in distinct groups organized both by the type of elongases and to a minimal extent the taxonomy (Fig. 3.3). Although the apicomplexan elongases do not form a monophyletic clade, all of the protozoans, including both apicomplexans and the kinetoplastids (*Trypanosoma* and *Leishmania*) remain clustered together. Similar to previous phylogenetic reconstructions (101) the putative kinetoplastid elongases group together in a clade exclusive to this group of parasites. With respect to putative saturated fatty acid elongases among the apicomplexans, they form two clades, of which both appear to be closely related to the ELO-6 family of saturated fatty acid elongases.

CpLCE1 is differentially expressed and is localized to the PVM. To determine the CpLCE1 expression pattern in the complex parasite life cycle, real-time qRT-PCR and immunofluorescence detection were performed. Real-time qRT-PCR analysis indicated that the *CpLCE1* gene is differentially expressed in the *C. parvum* life cycle stages (Fig. 3.4). Relative transcript levels also increased at 36 h post-infection (PI), and to a minor extent at 60 h PI, but were detectable at all time points. The free sporozoites (a motile invasive stage of the parasite) exhibited a much higher level of *CpLCE1* transcripts compared to all other life cycle stages. The presence of CpLCE1 in protein extracts from sporozoites was clearly displayed by Western blot analysis using polyclonal rat anti-CpLCE1 antibodies (Fig. 3.4B).

Immunofluorescence microscopy indicates that CpCLE1 is present in free sporozoites, and localizes to the sporozoite membrane (Fig. 3.5A). Furthermore,

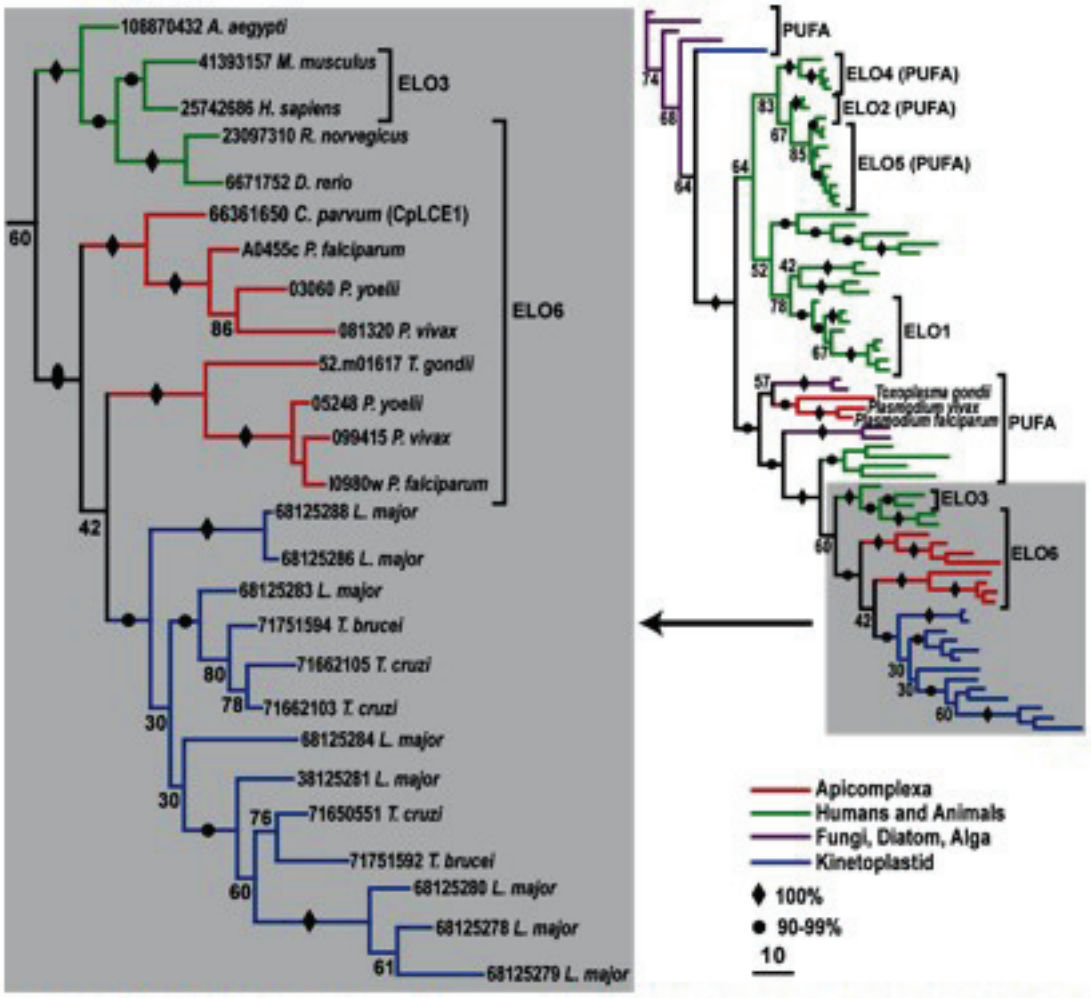

FIG. 3.3. Maximum likelihood (ML) tree derived from 75 elongase sequences (91 amino acid positions) using a Bayesian analysis of phylogeny. Posterior probability (PP) values at major nodes are indicated as either percent values, as 100% (solid diamonds), or 90 – 99% (solid circles). These PP values were derived from 3000 trees obtained after the ML values converged. In the large tree, only the elongase family of proteins are shown as references. The large tree that includes GenBank GI numbers and species names for all taxa is provided as supplementary material (figure A-1). Additional ML analysis using PROML program yielded essentially the same topology shown here.

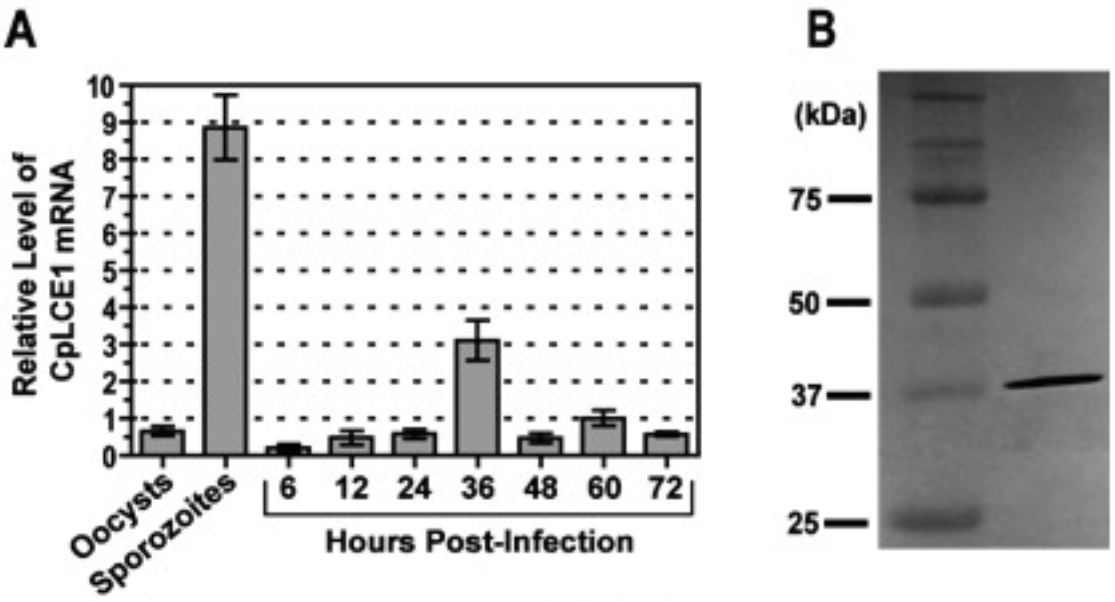

FIG. 3.4. Expression analysis of the *CpLCE1* gene in various *C. parvum* life cycle stages. (A) Relative transcript levels were determined using real-time qRT-PCR. The level of transcripts is normalized using the level of *C. parvum* 18S rRNA as a control. In all samples, bars represent the standard error-of-the-mean from triplicate reactions. (B) Western blot analysis using polyclonal rat anti-CpLCE1 antibodies of protein extracted from freshly excysted sporozoites.

Immunofluorescence microscopy indicates that CpCLE1 is present in free sporozoites, and localizes to the sporozoite membrane (Fig. 3.5A). Furthermore, CpLCE1 localizes to the parasitophorous vacuolar membrane (PVM) during intracellular development (Fig. 3.5B and 3.5C). This was determined by two separate co-localization studies. Dual-labeling experiments using a rabbit polyclonal antibody mainly against the PVM and the electron-dense feeder organelle co-localized CpLCE1 and PVM proteins (Fig. 3.5B). It has previously been shown that CpACBP1 also co-localizes with the PVM proteins (194). An additional dual-labeling experiment using rabbit polyclonal antibodies against CpACBP1 co-localized CpLCE1 and CpACBP1 proteins (Fig. 3.5C). Combined, CpLCE1 localizes to the PVM but not the merozoites within the meronts.

Cloning and expression of CpLCE1. Previous attempts in our laboratory to express and purify recombinant CpLCE1 in bacteria were unsuccessful, typically resulting in the formation of inclusion bodies. However, this is consistent of the elongase family of enzymes as they tend to have a membrane bound nature. Therefore, we expressed CpLCE1 in mammalian HEK-293T cells for characterization of this enzyme. HEK-293T cells were used as they offer several advantages. It is widely accepted that this cell line displays a very high level of transfection efficiency. This, in combination with using the pcDNA3.1/HisC expression vector allows for high-level non-replicative transient expression. Additionally, these cells also contain their own native elongase system. Thus, recombinant CpLCE1 acts in conjunction with the native HEK-293T elongase system in order to carry out the entire two-carbon fatty acid elongation cycle. However, this can sometimes be a disadvantage due to recombinant and native elongase

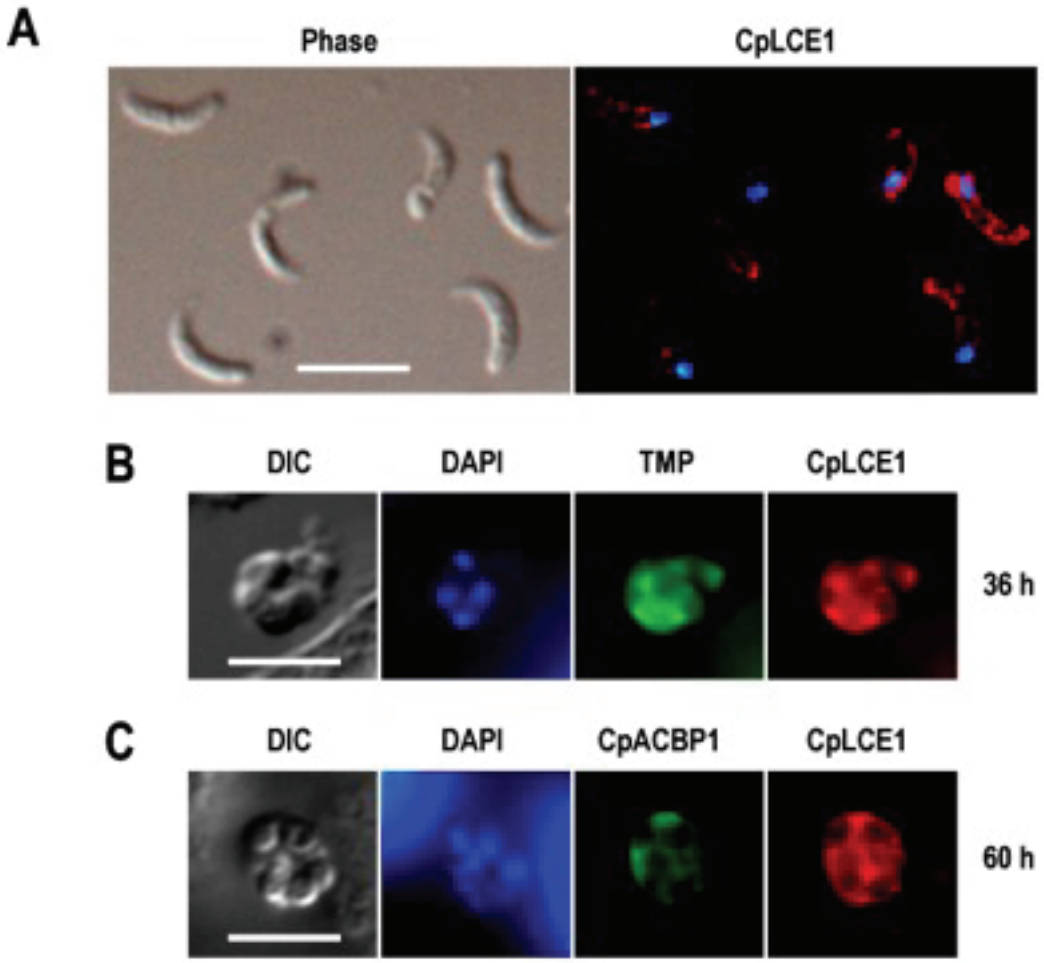

FIG. 3.5. Immunolocalization of CpLCE1 in free sporozoites and in intracellular life stages. (A) Indirect immunolabeling of freshly excysted sporozoites using rat polyclonal antibodies against CpLCE1 along with secondary antibodies conjugated with TRITC. DAPI used for counterstaining nuclei is merged with the image on the right-hand side. (B) Co-localization of CpLCE1 (TRITC) with parasite total membrane proteins (TMPs; FITC) of parasites grown for 36 h. The antibodies against parasite TMPs mainly label the PVM and the electron-dense feeder organelle. (C) Dual-labeling of intracellular parasites grown for 60 h indicating that CpLCE1 co-localizes with CpACBP1 which has previously been shown to co-localize with parasite TMPs, most likely at the PVM. Phase, phase-contrast; DIC, differential interference contrast. Bars, 5 μm.

enzymes competing for the same substrate. This often results in a relatively high degree of background activity that must be taken into consideration when interpreting data obtained from using a heterologous assay system.

Successful transfection and protein expression using this method were analyzed using RT-PCR, Western blot and immunolabeling. Total RNA was isolated from cells transfected with either CpLCE1 or pcDNA3.1/HisC (and nontransfected cells as a negative control) 48 h after transfection, and vector specific primers were used during RT-PCR to confirm positive transfection. Amplicons of the correct size corresponding to pcDNA3.1/HisC and CpLCE1 transfected cells were observed (259 bp and 1,195 bp, respectively) (Fig. 3.6A).

Western blot analysis of the membrane fractions using rat polyclonal antibodies against CpLCE1 clearly confirm that CpLCE1 is expressed, and indicate that it is contained in the purified membrane fractions (Fig. 3.6B). Immunofluorescence microscopy indicated that this protein was expressed relative to cells transfected with pcDNA3.1/HisC or nontransfected cells (Fig. 3.6C). The fluorescent signal was largely increased for the CpLCE1 transfected cells and could be observed using a relatively low exposure time (280 ms). At the same exposure there was no observed fluorescent signal from pcDNA3.1/HisC transfected or nontransfected cells. Only at an exposure time of 9.8 s did fluorescence signal begin to appear in these samples (Fig. 3.6C insets) indicating that the CpLCE1 transfected cells were indeed expressing the desired protein.

Determination of enzyme activity. It is imperative that we first clarify the elongation assay in order for the results to be appropriately understood. The membrane

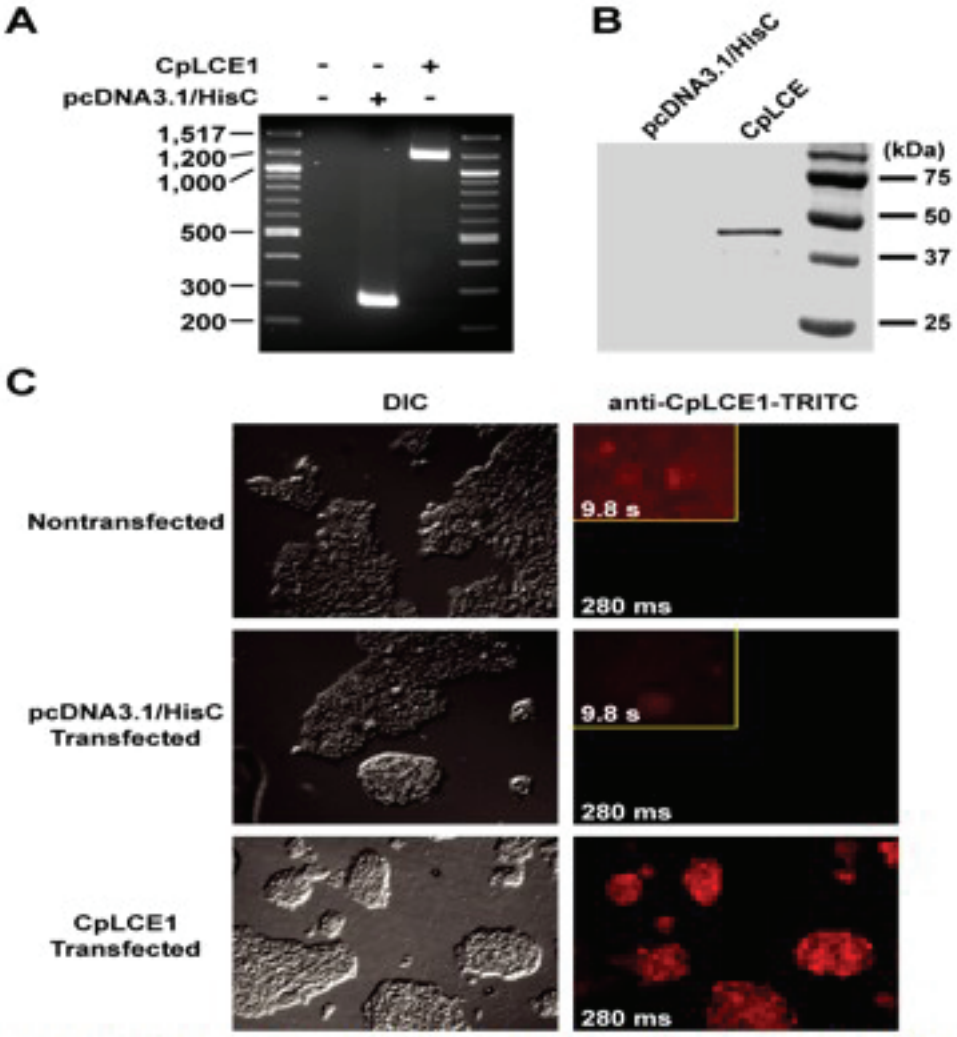

FIG. 3.6. Confirmation of successful transfection and expression of CpLCE1. (A) At 48 h post transfection total RNA was isolated from cells transfected with CpLCE1 or the empty vector, and from nontransfected cells. RT-PCR analysis viewed on a 2% agarose gel indicated that both the vector and the vector containing the CpLCE1 construct were effectively transfected. (B) Western blot analysis of the purified membrane fractions from cells transfected with CpLCE1 or pcDNA3.1/HisC. 80 μg of protein from each fraction were separated on a 10% SDS-PAGE gel, transferred to nitrocellulose, and labeled with rat polyclonal antibodies against CpLCE1. Further incubation with rabbit anti-rat antibodies conjugated to alkaline phosphatase followed with development with BCIP resulted in a single band corresponding to CpLCE1. (C) Immunofluorescence detection of CpLCE1 protein expression. Nontransfected cells were used as a negative control. Clearly, the fluorescence intensity when labeling with rat anti-CpLCE1 antibodies followed by rabbit anti rat IgG conjugated to TRITC was highest in cells transfected with CpLCE1. A 35-fold increase in exposure time (280 ms versus 9.8 s) was required to detect only minor fluorescence intensity in pcDNA3.1/HisC transfected cells (comparable to nontransfected cells, both shown as insets).

preparations of HEK-293T cells used in this study contain all four enzymes of the elongase system. Thus, in samples that have been transfected with CpLCE1 there are two sets of condensing enzymes which are responsible for the incorporation of ^{14}C from [2-^{14}C]malonyl-CoA. The products formed during the initial condensation reaction (catalyzed by the native elongase and by CpLCE1) then proceed through the subsequent three steps of the elongation system (β-ketoacyl-CoA reductase, β-hydroxyacyl-CoA dehydratase, enoyl-CoA reductase) to produce a final two-carbon extended product (refer to Fig. 3.1 for reaction details). Therefore, there is detectable background activity that is present when using this heterologous system and must be distinguished from activity produced by recombinant CpLCE1.

Total fatty acid elongation activity was measured in isolated membrane fractions of HEK-293T cells transfected with CpLCE1 and compared with HEK-293T cells transfected with the empty vector alone (pcDNA3.1/HisC). Supernatant fractions resulting from the membrane purification process were also used as controls. Palmitoyl-CoA (C16:0-CoA) was initially chosen as the fatty acid substrate for the elongation assay, which measured the incorporation of ^{14}C from [2-^{14}C]malonyl-CoA into elongated fatty acid products. Total elongation activity was increased in the membrane fractions from CpLCE1 transfected cells compared to cells transfected with the empty vector (Fig. 3.7A). The activity detected in the supernatant fractions of both CpLCE1 and pcDNA3.1/HisC transfected cells were not significantly different from each other, but were significantly higher than the activity detected in the membrane fractions (Fig. 3.7A). The activity in the supernatant fractions is expected due to the soluble enzymes

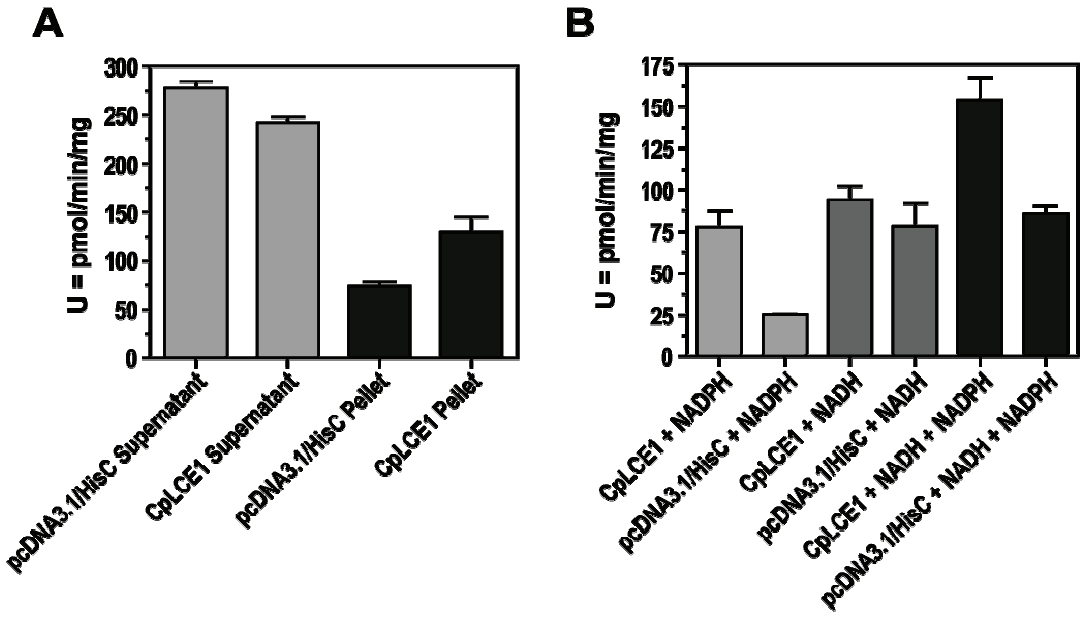

FIG. 3.7. Elongase activity determination and NADPH dependence. (A) The final pellet fraction after membrane purification of CpLCE1 transfected cells displayed higher elongase activity than that from cells transfected with the empty vector. Both NADH and NADPH were used as co-substrates. The high activity observed in the soluble fractions likely results from soluble proteins utilizing malonyl-CoA and NAD(P)H. (B) Total elongation activity as measured when including various combinations of NAD(P)H. As expected, the most significant difference among fractions containing CpLCE1 and control fractions was observed when using NADPH as the sole co-substrate. Values were obtained by subtracting the activity detected using fractions from cells transfected with the empty vector. Values are represented as U = pmol/min/mg of total membrane protein. In all samples, bars represent the standard error-of-the-mean from triplicate reactions.

that use malonyl-CoA as a co-substrate such as the soluble FAS enzymes. Thus, in agreement with western blot and immunofluorescent analysis (Fig. 3.6B and 3.6C, respectively) the CpLCE1 activity is contained in the membrane fractions of cells transfected with CpLCE1.

To further confirm that the observed activity was indeed that of the elongase complex, we separately incubated membrane fractions with or without NAD(P)H (Fig. 3.7B). When NADH was used as a co-substrate activity was detected in both the CpLCE1 and pcDNA3.1/HisC transfected samples, however they were not significantly different from each other confirming that the subsequent reduction reactions of the elongation system do not utilize NADH as a co-substrate. The activity observed here is due to partial contribution of other membrane enzymes that make use of NADH. When NADPH was used as the sole co-substrate the membrane fractions from the CpLCE1 transfected cells displayed a significantly greater elongation activity compared to the cells transfected with the vector alone. Combined, this data confirms that NADPH is the required co-substrate for the elongation system reduction reactions, and that CpLCE1 is capable of carrying out the initial reaction of the elongase system.

Optimization of CpLCE1 assay and enzyme kinetics. Because palmitoyl-CoA could serve as a substrate for CpLCE1, it was used to optimize the conditions of the elongation reaction prior to testing additional fatty acid substrates to determine substrate specificity. The highest rate of [^{14}C]malonyl-CoA incorporation into elongated fatty acid products was observed when the concentration of palmitoyl-CoA was 125 μM (Fig. 3.8A). Additionally, enzyme kinetics analysis revealed that CpLCE1 displayed typical

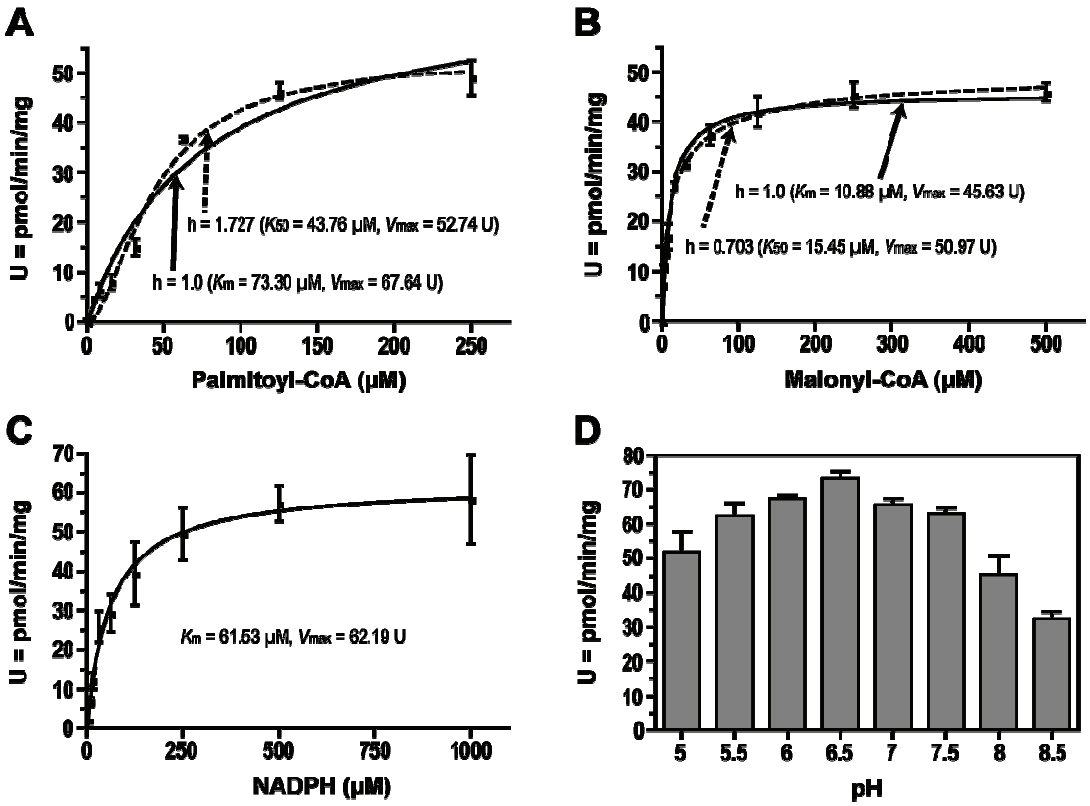

FIG. 3.8. Enzyme kinetics of the condensation reaction, and kinetics and pH optimum for the overall elongation system. (A) Allosteric kinetics assayed with various concentrations of palmitoyl-CoA indicates the presence of positive cooperativity in the condensation reaction (Hill coefficient, h = 1.727). The optimum palmitoyl-CoA concentration was 125 µM. (B) Allosteric kinetics assayed with various concentrations of malonyl-CoA indicates the presence of negative cooperativity (h = 0.703) with an optimum concentration of 250 µM. (C) Enzyme kinetics assayed with various concentrations of NADPH. As the two reduction steps of the elongation system require NADPH, results show that when using palmitoyl-CoA as a substrate and CpLCE1 as the condensing enzyme, the elongase system displays general Michaelis-Menten kinetics. (D) The optimum pH of the condensing enzyme is 6.5. Values were obtained by subtracting the activity detected using fractions from cells transfected with the empty vector. Values are represented as U = pmol/min/mg of total membrane proteins. In all samples, bars represent the standard error-of-the-mean from triplicate reactions.

Michaelis-Menten kinetics towards palmitoyl-CoA (h = 1, K_m = 73.30 μM, V_{max} = 67.64 U [1 U = pmol/min/mg of total membrane protein] (Fig. 3.8A, solid curve). However, further analysis indicated that the CpLCE1 kinetics actually fit better to a sigmoidal curve (R^2 = 0.9707 vs. 0.9577) indicating the presence of positive cooperativity (Fig. 3.8A, dashed curve labeled with h = 1.727). Under the consideration of cooperativity, the values for K_{50} (equivalent to K_m) and V_{max} were determined to be 43.76 μM and 52.74 U, respectively. Kinetics analysis of CpLCE1 towards malonyl-CoA revealed similarities to that observed towards palmitoyl-CoA. While the optimal concentration of malonyl-CoA was 250 μM, CpLCE1 displayed a slightly better fit to a sigmoidal curve (Fig. 3.8B, dashed curve labeled with h = 0.703; R^2 = 0.9387). This is a slight negative cooperativity with K_{50} = 15.45 μM and V_{max} = 50.97 U as compared to the general Michaelis-Menten kinetics (Fig. 3.8B, solid curve labeled with h = 1, K_m = 10.88 μM, V_{max} = 45.63 U; R^2 = 0.9265). When using increasing concentrations of NADPH, general Michaelis-Menten kinetics were observed (Fig. 3.8C) with K_m = 61.53 μM and V_{max} = 62.19 U, and the optimum concentration of NADPH was 500 μM. The observed NADPH kinetics are in respect to the two reduction reactions that occur as a result of activity initiated by CpLCE1 – the condensation reaction. Fatty acid elongation activity was also determined to be highest at a pH optimum of 6.5 (Fig. 3.8D).

CpLCE1 displays the highest activity towards C14:0 and C16:0. Using the optimal assay conditions found above, we determined the substrate specificity of CpLCE1 using a wide range of fatty acyl-CoAs. Figure 3.9 shows the total fatty acid elongation activity in membrane fractions from CpLCE1 transfected HEK-293T cells

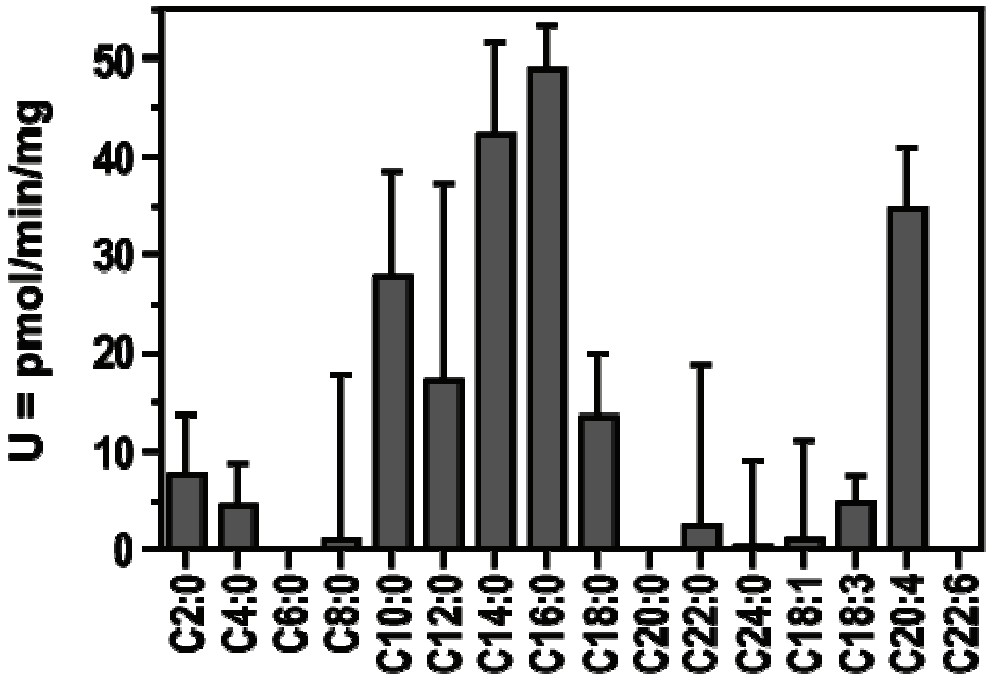

FIG. 3.9. Substrate specificity of CpLCE1. Saturated fatty acyl-CoAs from C2:0 to C24:0, and various unsaturated fatty acyl-CoAs were used to determine the substrate preference of the condensing enzyme. Values were obtained by subtracting the activity detected using fractions from cells transfected with the empty vector. Values are represented as U = pmol/min/mg of total membrane proteins. In all samples, bars represent the range of values from two sets of triplicate reactions.

using even carbon saturated fatty acyl-CoAs from C2:0 to C24:0, and the unsaturated (or polyunsaturated) fatty acyl-CoAs C18:1, C18:3, C20:4, and C22:6. When compared to membrane fractions from pcDNA3.1/HisC transfected cells, the cells expressing recombinant CpLCE1 displayed significantly higher elongase activities when assayed with the medium to long chain fatty acyl-CoAs C10:0 – C18:0, and the highest with C14:0 and C16:0. Relatively little to no activity was detected above background when short or very long chain fatty acyl-CoAs were used as substrates. Interestingly, arachidonic acid (C20:4) was the only unsaturated fatty acid that displayed a rather significant activity above background. This was not expected and is considered to be an artifact due to in vitro assay conditions.

Analysis of elongation products. The two fatty acyl-CoAs shown to display the highest elongation activity when used as substrates (myristoyl-CoA and palmitoyl-CoA) were used to analyze the elongated products using both TLC and HPLC. Upon completion of the reaction the elongation fatty acid products were methylated to their methyl ester derivatives for comparison with fatty acid methyl ester standards. When elongation products of membrane fractions from CpLCE1 transfected cells were analyzed using reverse phase TLC the major products were palmitic acid (C16:0) and stearic acid (C18:0) when incubated with myristoyl-CoA (C14:0) or palmitoyl-CoA (C16:0), respectively (Fig. 3.10A). As a background control, membrane fractions from cells transfected with pcDNA3.1/HisC were also analyzed using TLC. The major product of the control when using palmitoyl-CoA as a substrate was stearic acid.However, when incubated with myristoyl-CoA there were two products detected on

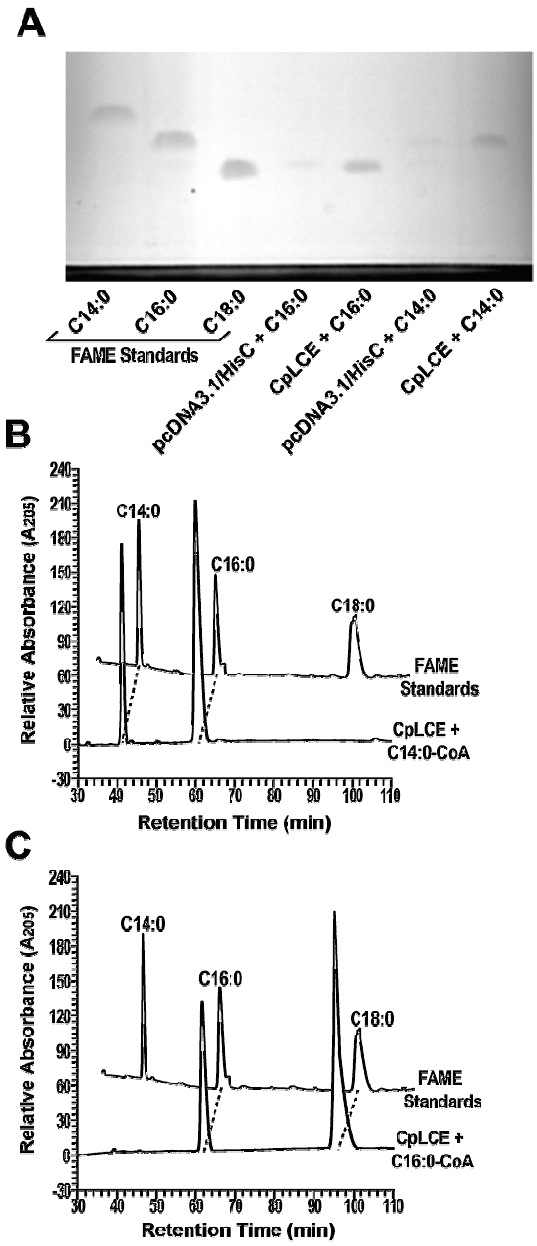

FIG. 3.10. Fatty acid elongation product analysis using TLC and HPLC. (A) The products of fatty acid elongation were converted to their methyl ester derivatives for analysis using reverse-phase TLC. Both myristoyl-CoA and palmitoyl-CoA (C14:0 and C16:0, respectively) were used as substrates based on the substrate preference data. (B) HPLC analysis of elongation products converted to methyl esters is comparable to that observed using TLC. The data shows that only one round of elongation occurs regardless of the fatty acyl substrate used. Retention times of all samples were compared to authentic fatty acid methyl standards. HPLC peaks were detected at an absorbance of 250 nm (A_{250}).

TLC: palmitic acid and stearic acid indicating that membrane fractions not transfected with CpLCE1 were capable of additional rounds of elongation. In either case, the production of a two-carbon elongated product by the CpLCE1 transfected cells resulted in a significantly larger quantity than that of the pcDNA3.1/HisC transfected samples.

To ensure that only one round of elongation was occurring in membrane fractions transfected with CpLCE1, the elongation products were also analyzed using HPLC. If additional rounds of elongation were indeed occurring, then the higher sensitivity HPLC analysis would detect multiple products. Similar to analysis with TLC the elongation reaction, fatty acid methyl esters were derived from the elongated products for comparison to methyl ester standards. Analysis by HPLC agreed with TLC analysis further indicating only one round of elongation occurs in the CpLCE1 transfected samples. When incubated with myristoyl-CoA as a substrate, palmitic acid was detected (Fig. 3.10B) and when palmitoyl-CoA was used as a substrate the addition of two carbons resulting in stearic acid was detected (Fig. 3.10C). In both instances, the substrate was also detected indicating that not all substrate was converted into an elongated product.

Inhibition of elongation by cerulenin. Cerulenin is a common eukaryotic and bacterial β-ketoacyl-[ACP] synthase inhibitor. Initially, we tested its inhibitory effects using palmitoyl-CoA as the substrate, in which cerulenin displayed a maximum inhibition of 20.5% at a concentration of 200 μM (Fig. 3.11, solid line). Because differential inhibition of cerulenin has been shown to occur depending on fatty acid chain length (117) we also tested inhibition when using myristoyl-CoA as a substrate.

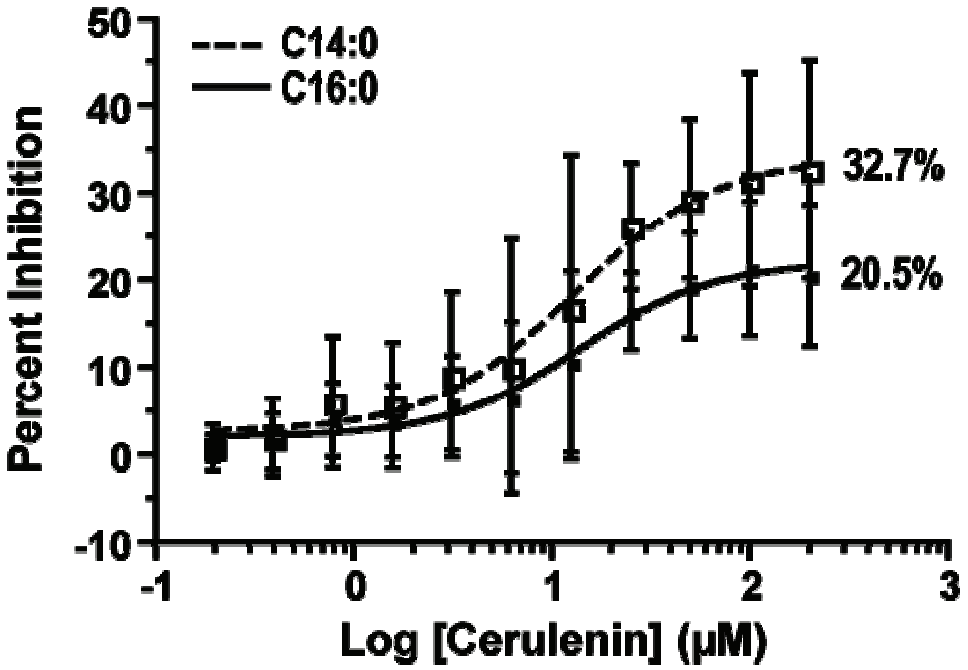

FIG. 3.11. Inhibitory effect of cerulenin on the activity of CpLCE1. The inhibition effects when using both myristoyl-CoA (C14:0) and palmitoyl-CoA (C16:0) were assayed. . Values were obtained by subtracting the activity detected using fractions from cells transfected with the empty vector. Values are represented as total [^{14}C]malonyl-CoA incorporation (pmoles) based on a total of 30 μg membrane protein. In all samples, bars represent the range of values from two sets of triplicate reactions.

However, similar to using palmitoyl-CoA as a substrate, cerulenin displayed a maximum inhibition of 32.7% at a concentration of 200 μM (Fig. 3.11, dashed line). Thus, CpLCE1 appears to be relatively insensitive to cerulenin up to 200 μM when using both myristoyl-CoA and palmitoyl-CoA as substrates.

DISCUSSION

Among the apicomplexans CpLCE1 is the first elongase to be studied, and one of very few studied among the parasitic protists. It is interesting that the *C. parvum* genome encodes only one elongase, whereas both *T. gondii* and *P. falciparum* contain three. However, differences in fatty acid metabolism (and lipid metabolism in general) among these organisms do exist. Among the apicomplexans that possess a plastid and associated type II FAS, *P. falciparum* lacks a type I FAS or PKS, but *T. gondii* and *E. tenella* both possess a type I FAS and PKS (196). Similarly, *C. parvum* contains only a type I FAS and PKS (53, 198, 199, 201). Thus, it is not a surprise that *C. parvum*, with its very streamlined metabolism, contains only one elongase.

Generally, fatty acid elongases are divided into two groups: (i) those involved or suspected to be involved in the elongation of saturated and monounsaturated fatty acids, and (ii) those that are responsible for elongation of PUFAs (75). Those of the first group are typically of the ELO1, 3 and 6 families, whereas the latter consists of the ELO2, 4 and 5 families. Molecular analyses of CpLCE1 indicated that it contains structural characteristics possessed by the elongase family including four highly conserved motifs and several predicted transmembrane domains. Furthermore, phylogenetic

reconstructions indicate that CpLCE1 is contained within the ELO6 family. This family is suggested to be involved in the elongation of C12:0 to C16:0 saturated fatty acid substrates to C18:0 products and do not have the ability to elongate beyond C18:0 (75). The majority of the kinetoplastid elongases analyzed form a clade with the ELO6-like apicomplexan elongases suggesting that all of these originated from a common ancestor. Additionally, CpLCE1 appears to be more distant from unsaturated elongase families.

Real-time qRT-PCR indicated that CpLCE1 transcript levels are expressed in all stages of the *C. parvum* life cycle, but are highest in the sporozoites followed by stages at 36 h and 60 h PI. In addition to membrane localization in sporozoites, immuno-staining has primarily localized CpLCE1 to the PVM similar to both CpACBP1 and the *C. parvum* oxysterol binding protein (OSBP)-related protein 1 (CpORP1) (194, 195). *Cryptosporidium parvum* is an intracellular parasite, but it is considered extracytoplasmic because of being covered by a PVM on the host intestinal epithelial cells (29). Although association with the feeder organelle is still undetermined, it is interesting that CpLCE1 localizes to the PVM along with CpACBP1 and CpORP1 which could possibly be involved in lipid uptake across the PVM (194, 195). Whether CpLCE1 acts in conjunction with these two in either lipid uptake or formation of the PVM is not understood at this time. Regardless, PVM proteins may serve as prime chemotherapeutic and/or immunotherapeutic targets in this parasite for which fully effective treatment is currently unavailable.

The extreme hydrophobicity of elongase proteins has caused many difficulties in the solubilization and purification of these membrane-bound condensing enzymes, and

has greatly hindered the biochemical characterization of their defined roles in fatty acid elongation. Nearly all enzymatic studies of these elongase enzymes have been carried out using membrane fractions. Thus, we expressed CpLCE1 in mammalian HEK-293T cells in order to characterize the biochemical features of this enzyme.

Substrate preference revealed that CpLCE1 displays the highest activity when myristoyl-CoA and palmitoyl-CoA (C14:0 and C16:0, respectively) are used as substrates. This is in agreement with phylogenetic reconstructions that grouped CpLCE1 with the ELO6 family of elongases which generally prefer C12:0 to C16:0 as substrates. It is interesting that CpLCE1 showed little to no preference for all other saturated and unsaturated substrates except for arachidonyl-CoA (C20:4). It is unknown if this is due to in vitro effects, or whether CpLCE1 would potentially have the ability to elongate C20:4 in vivo. Although total lipid analysis studies in *C. parvum* is lacking, one report suggests that C20:4 comprises only 0.7% of the total neutral fatty acid content in *C. parvum*, and 2.3% and 1.2% in the total phospholipid and phosphatidylcholine content, respectively (112), indicating that that C20:4 is present only in small amounts in *C. parvum.* However, the C22 product of elongation was not detected. No other enzyme involved in *C. parvum* fatty acid metabolism has displayed preference for an unsaturated substrate, which leads us to believe that elongation of arachidonyl-CoA is an assay artifact.

Analyses of the CpLCE1 catalyzed elongation products indicate that only one round of elongation occurs, thus extending the length of each substrate by only two carbons. The factors that determine exactly how many rounds of elongation occur are

unknown, and could rely on the needs of the individual cell or organism at the time in which elongation occurs. Our substrate preference data indicated that both myristoyl-CoA and palmitoyl-CoA are capable of serving as substrates. However, it is intriguing that the longest chain product observed when using C14:0 as a substrate was C16:0. It is not clear why the elongated C16:0 does not serve as a substrate itself and undergo another round of elongation. This could be an artifact due to heterologous assay conditions, however other elongase enzymes expressed and assayed using similar methods clearly demonstrate as many as three rounds of elongation (114).

Cerulenin was shown to have a minimal effect in inhibition of CpLCE1 with a maximal inhibition of 20.5% and 32.7% when using the substrates C16:0-CoA and C14:0-CoA, respectively. This is interesting due to the ability of cerulenin to efficiently inhibit both type I and type II β-ketoacyl-CoA synthases, which was the case for the control fractions transfected with pcDNA3.1/HisC. At low concentrations of cerulenin (~2.1 μM) activity was inhibited by 80% and remained constant over the tested concentrations (data not shown). The observed activity of cerulenin on CpLCE1 could be due to several of factors: (i) the alkyl chain of cerulenin is too long to bind to the active site of the enzyme (63), or (ii) the active site serving as the target of cerulenin could be somewhat inaccessible due to the extreme hydrophobicity of the enzyme (193). Elongase enzymes of other types and different families from various organisms have also shown differential inhibition by cerulenin. For example, the plant type elongases appear to be fairly resistant (50, 126), whereas ELO2 and ELO3 but not ELO1 from *Trypanosoma* is susceptible (63). Further analyses on the ELO-6 family of enzymes as

well as elongase enzymes purified to homogeneity are needed in order to fully and accurately determine the effects of cerulenin.

CHAPTER IV

THE PURSUIT OF THE *Cryptosporidium parvum* FATTY ACYL-CoA BINDING PROTEIN (ACBP) AS A DRUG TARGET

OVERVIEW

Cryptosporidium is well known to be a troublesome water-borne pathogen for immunocompetent and especially immunosuppressed individuals. A countless number of outbreaks caused by both *C. parvum* and *C. hominis* occur each year around the world. Transmission is typically via contaminated water supplies and/or recreational water by the environmentally and chlorine resistant oocysts. The vulnerability of community water supplies to this parasite, as well as increased biodefense concerns have escalated *Cryptosporidium* to one of the water-borne category B pathogens in the NIH and CDC biodefense research programs.

Despite numerous investigations, there is currently no real effective drug to treat cryptosporidiosis. Drug therapy would no doubt benefit several groups (106). Severe cases often requiring hospitalization among immunocompetent individuals usually occur in children and the elderly. Transplant recipients and those undergoing cancer chemotherapy are often immunocompromised. These patients usually have to temporarily halt their treatment regimens in order to combat cryptosporidiosis. Anti-cryptosporidials would certainly be beneficial to these patients, as well as to those who are HIV-positive and are at great risk for a devastating infection with *Cryptosporidium*.

Several suggestions have been postulated as to why this apicomplexan appears to have a natural resistance to drug therapy (106). One such factor is the apparent lack of or difference in drug targets at both molecular and structural levels, namely differences in biochemical pathways. Additionally, if drugs actually reach the parasite, they may be readily transported out via transport proteins. Perhaps the most widely discussed factor is the parasites' unique intracellular but extracytoplasmic location within the host cell (72, 106, 178). Upon initiation of infection, the infective sporozoite is enveloped by the host cell apical membrane forming a space between the parasite and host cell membrane known as the parasitophorous vacuole (PV). Because parasite basal membranes fuse with the host cell membrane, the PV extends only over the apical end and its membrane covering is termed the parasitophorous vacuolar membrane (PVM). Although it is unclear at this time, preliminary data indicate that the basal membranes modulate the transport of some drugs and do not allow drugs that enter the cytoplasm of the host cell to enter the parasite (59, 106). This appears to be the case for both geneticin, and the clinically relevant drug paromomycin as apical but not basolateral exposure of these drugs led to parasite inhibition (59).

We hypothesize that parasite proteins located in the PVM may serve as valuable drug targets. One such protein is the *C. parvum* acyl-CoA binding protein (CpACBP1). Our laboratory has previously characterized this unique protein both at the molecular and biochemical levels (194). This family of proteins is critical to lipid metabolism as their main function is as an intracellular acyl-CoA transporter and pool former (58, 88, 157). Animals, plants, protists and several pathogenic bacteria have been found to

contain this highly conserved protein (20). Although they are typically small (~10-kDa) cytosolic molecules, there have been larger (≥ 55-kDa) ACBPs found in animals and plants. The unique CpACBP1 is a long-type ACBP containing an N-terminal ACBP domain and a C-terminal ankyrin-repeat sequence. Although it differs from the typical cytosolic ACBPs, it is similar to the membrane bound ACBPs from *Arabidopsis* (31, 94). Our previous analysis indicates that CpACBP1 is also a membrane protein associated with the PVM probably via interaction of its ankyrin repeats with other proteins in the PVM. It is unlikely that CpACBP1 is involved in the early stages of PVM formation as it is not expressed during initial stages of infection, but it is widely known that *C. parvum* must import fatty acids from the host cell or the intestinal lumen. Although *C. parvum* is incapable of de novo fatty acid synthesis, it is capable of elongating and utilizing long-chain fatty acids (52, 53, 196, 199). Thus, in cooperation with an acyl-CoA synthetase, it is possible that CpACBP1 serves as a fatty acyl-CoA scavenger to facilitate fatty acid uptake at the PVM.

Here, we report improved enzyme kinetics and substrate preference for CpACBP1 through the use of a fluorescence-based binding assay. Additionally, we identified several compounds that inhibit the binding of fatty acyl-CoA to CpACBP1. This is the first report of its kind that we are aware of. To identify these inhibitors, we screened a library of 1,040 compounds, most of which are approved for use in humans for various diseases and/or ailments.

MATERIALS AND METHODS

Cloning and expression of CpACBP1. We have previously cloned and expressed CpACBP1 (194). Briefly, the entire ORF of *CpACBP1* was amplified from *C. parvum* (Iowa Strain) genomic DNA (gDNA) and cloned into the pMAL-c2x expression vector (New England Biolabs). After selecting and sequencing PCR-positive colonies, the constructs were transformed into chemically competent Rosetta 2 *Escherichia coli* cells (Novagen) and plated onto solid Luria-Bertani (LB) medium containing ampicillin (50 μg/ml), chloramphenicol (34 μg/ml), and glucose (2 mM). After incubation overnight at 37 °C, a single colony of transformed bacteria was first inoculated into 25 ml LB media containing the appropriate antibiotics and glucose, and grown overnight at 30 °C in a shaking incubator. The overnight cultures were diluted 1:10 with fresh medium and allowed to grow for approximately 5 h at 30 °C until the OD_{600} reached ~ 0.5. At this time, isopropyl-1-thio-β-D galactopyranoside (IPTG) was added to a final concentration of 0.5 mM to induce protein expression, and cells were grown an additional 5 h at 30 °C. The bacteria were collected by centrifugation, resuspended in 50 ml TNE buffer (20 mM Tris.HCl pH 7.4, 200 mM NaCl, 1mM EDTA) containing a protease inhibitor cocktail optimized for bacteria (Sigma), and subjected to mild sonication on ice. Insoluble debris was removed by centrifugation. The MBP-CpACBP1 fusion protein was purified using amylose resin-based affinity chromatography according the manufacturer's standard protocol (New England Biolabs). Purified proteins were dialyzed extensively against Dulbecco's PBS (Sigma), and stored at -80 ºC.

Fluorometry. All reactions were set up in 96-well white plates that offer a high signal reflectance and reduced background fluorescence (Thermoelectron), and all fluorescence measurements were taken using a Fluoroskan Ascent fluorometer (Thermoelectron, Inc.). The fluorometer program was set to maintain a constant temperature of 25 ºC and to shake the samples for 20 s at 120 rpm (1 mm diameter rotation) prior to fluorescence measurement. Fluorescence was measured using a set of filters (excitation – 544/7.5 nm; emission – 590/7 nm) sufficient for 16-NBD-C16:0-CoA (N-[(7-nitro-2-1,3-benzoxadiazol-4-yl)-methyl]amino palmitoyl Coenzyme A; Avanti Polar Lipids) and was set at a 20 – 60 ms integration time, normal beam. Measurements were based on the increase in fluorescence observed with binding of substrate to the enzyme. The average of 3 – 5 scans was taken for each measurement, and each experiment was replicated three times.

Enzyme kinetics and substrate preference. Previous characterization of CpACBP1 by our lab was carried out using a Lipidex 1000 assay (136, 148, 194). Because our ultimate goal in this study involved fluorescence measurements using NBD labeled palmitoyl-CoA as a substrate, we wanted to determine a relative comparison of data between the two methods. First, the pH of the reaction was optimized using PBS at pH 5.5, 6.0, 6.5, 7.0, 7.5, 8.0, and 8.5. In addition to PBS, reaction components consisted of 0.1 µM MBP-CpACBP1 and 0.25 µM NBD-C16:0-CoA in a volume of 100 µl. Enzyme kinetics assays were performed using 0.1 µM MBP-CpACBP1, NBD-C16:0-CoA (16 nM – 1 µM), and PBS pH 7.5 to a final volume of 100 µl. We also employed a susbtrate competition assay to determine substrate specificity using this assay set-up.

Assays included 0.1 μM MBP-CpACBP1, 0.25 uM NBD-C16:0-CoA, 0.25 uM unlabeled saturated (C2:0 – C26:0) or unsaturated (C18:1, C18:3, C20:4, and C22:6) fatty acyl-CoAs, and PBS pH 7.5 in a final volume of 100 μl. In addition we also assayed the binding of palmitic acid (C16:0) to CpACBP1. For each assay, the enzyme was the final reaction component added and reactions incubated at 25 ºC for 5 min to assure maximum binding before proceeding with fluorescence measurements.

Screening of compound library against CpACBP1. We were graciously given access to a drug library consisting of 1,040 compounds by Friedhelm Schroeder (Texas A&M University). This library was purchased from Microsource Discovery Systems as the National Institutes of Health and Juvenile Diabetes Research Foundation (NIH/JDRF) custom collection. Our goal was to test the compounds in this library on their effect of inhibiting binding of NBD-C16:0-CoA to CpACBP1. Each compound was provided dissolved in DMSO at a concentration of 10 mM, and was diluted to 10 μM in PBS pH 7.5 prior to the assay. Thus, the final concentration of DMSO in the assay was 0.0025%.

We first performed an initial screen of all compounds in order to determine which displayed a ≥ 50% inhibition of binding. These assays included 0.1 μM MBP-CpACBP1, 0.25 μM NBD-C16:0-CoA, 0.25 μM library compound, and PBS pH 7.5 in a final volume of 100 μl. As previously, the enzyme was the final reaction component added and reactions were incubated at 25 ºC for 5 min before proceeding with fluorescence measurements. Additionally, the absorption spectrum of selected compounds was obtained using a Multiskan Spectrum spectrophotometer

(Thermoelectron). Those compounds that exhibited an absorption spectrum in the range of 580 – 600 nm were excluded from further assays.

After determining which compounds displayed a ≥ 50% inhibition of binding of NBD-C16:0-CoA to MBP-CpACBP1, we performed inhibition kinetics measurements. Kinetics assays included 0.1 μM MBP-CpACBP1, 0.25 μM NBD-C16:0-CoA, 20 nm – 2 μM library compound, and PBS pH 7.5 to a final volume of 100 μl. After a 5 minute incubation at 25 ºC, fluorescence measurements were taken.

RESULTS

Determination of enzyme activity. Binding of fatty acyl-CoA to recombinant CpACBP1 was determined using a fluorescence-based assay. Based on prior data from our laboratory using the Lipidex 1000 assay, CpACBP1 displayed the highest binding affinity for palmitoyl-CoA (C16:0-CoA) (194). Partially due to this result, and in addition to limited fluorescent fatty acyl-CoA analogues, we chose to use NBD labeled palmitoyl-CoA as our substrate. When NBD is in a non-polar environment, it displays minimal fluorescence. However, when present in a polar environment, such as the binding pocket of an enzyme, the fluorescence signal produced greatly increases.

We first tested our assay to ensure that this fluorescent palmitoyl-CoA analogue was indeed able to bind to CpACBP1. Because we expressed CpACBP1 as a MBP-fusion protein, we also tested the interaction between MBP and NBD-C16:0-CoA. Overall results display that the fluorescence signal obtained when using MBP only as a control was virtually null, whereas that of the CpACBP1 fusion protein was much

greater affirming the basis of our assay (Fig. 4.1A). Additionally, we optimized the assay with respect to pH of the reaction. We found that binding affinity is highest with a basic pH, and was the highest at a pH of 7.5 (Fig. 4.1B).

Enzyme kinetics. Previous data also indicated that CpACBP1 kinetics when using palmitoyl-CoA resulted in a K_d value of 405 nM, a value that is comparable to other ACBPs when determined using the same assay (137, 194). We also determined enzyme kinetics using the fluorescence-based assay for three reasons: first, the Lipidex 1000 assay reflects competitive binding between ACBP and Lipidex 1000 rather than the true acyl-CoA binding affinity (137, 194); next, other assays such as fluorescence or dialyser-based assays typically give much better K_d values and are a better representation of true binding affinity (27, 54, 111, 182, 184); and finally to compute a K_d value needed to calculate IC_{50} values during enzyme inhibition studies. Our kinetics measurements revealed a K_d value of 171.2 nM (Fig. 4.2). Data are presented as the mean and standard error of triplicate experiments each measured three times. Controls included reactions with only MBP or NBD-C16:0-CoA, or both to subtract background fluorescence.

Substrate preference. Various unlabeled fatty acyl-CoAs (0.25 uM) were used in competition with an equimolar concentration of NBD-C16:0-CoA to determine the binding preference of CpACBP1. Results show that CpACBP1 prefer short-to-long-chain fatty acyl-CoAs (C4:0 – C16:0) with the highest (and similar) affinity (Fig. 4.3). Although binding affinity was decreased for all other saturated acyl-CoA esters tested (up to C26:0), there was no apparent binding to unsaturated acyl-CoA

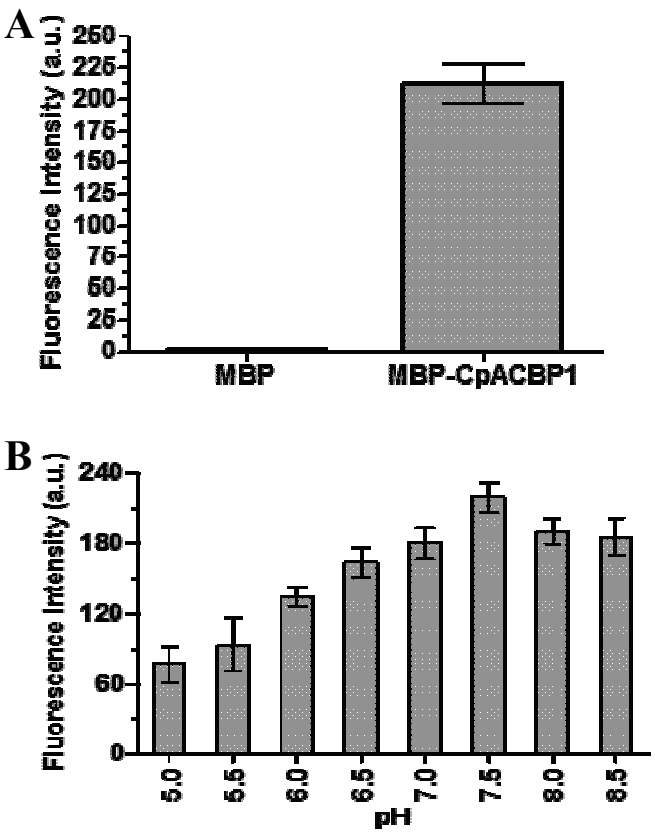

FIG. 4.1. Enzyme activity and pH optimization of the binding of C16:0-CoA to CpACBP1. (A) Specific and non-specific binding of NBD-C16:0-CoA (0.25 μM) by MBP-fused CpACBP1 (0.1 μM) and the MBP tag (0.1 μM) as determined by a fluorescent-based assay. (B) The optimum pH for the highest binding affinity was 7.5. Values were obtained by subtracting the activity detected using reactions containing only MBP or NBD-C16:0-CoA, or both. In all samples, bars represent the standard-error-of-the-mean from triplicate experiments. (a.u.) = arbitrary units.

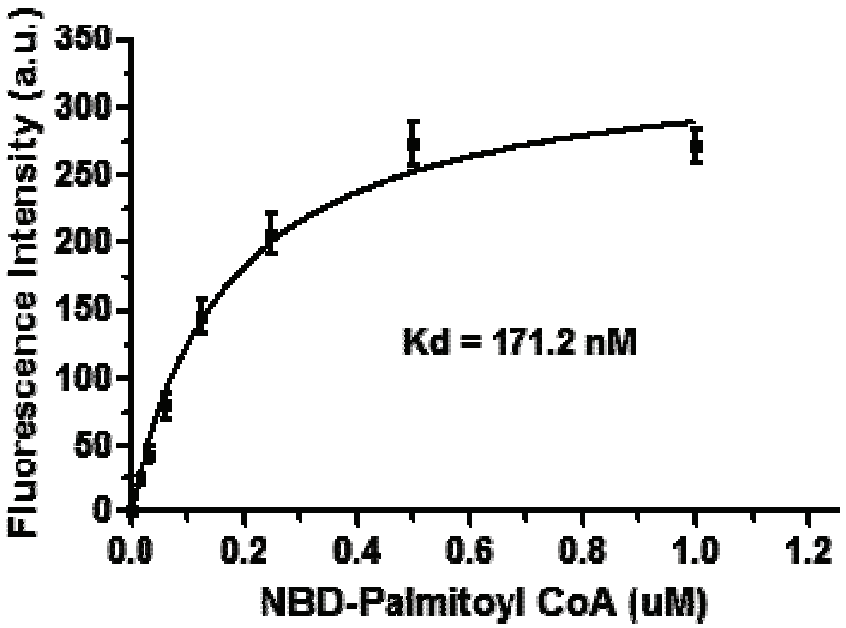

FIG. 4.2. Binding kinetics of recombinant CpACBP1 with NBD-C16:0-CoA as determined from fluorescence detection. Bars represent the standard-error-of-the-mean from triplicate experiments. (a.u.) = arbitrary units.

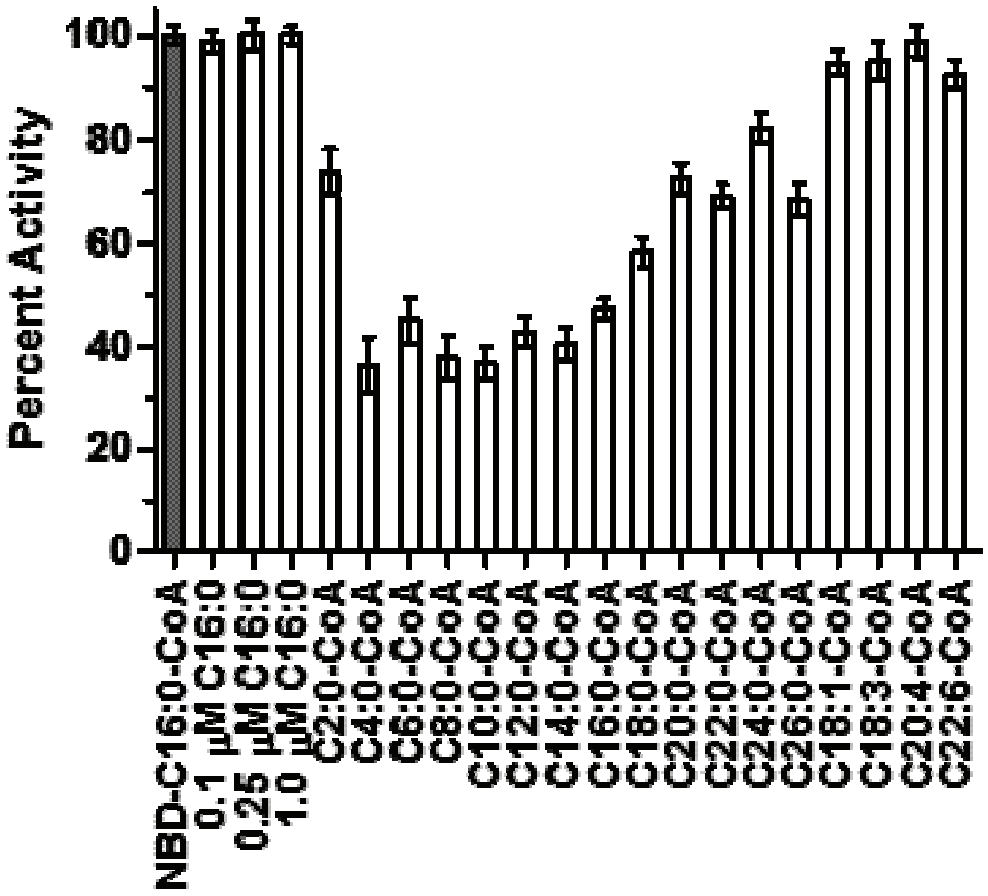

FIG. 4.3. Substrate specificity of CpACBP1. Saturated fatty acyl-CoAs from C2:0 to C26:0, and various unsaturated fatty acyl-CoAs were used to determine the substrate preference of CpACBP1 using a competition assay. Additionally, three concentrations of C16:0 fatty acid was used in competition with NBD-C16:0-CoA to determine whether CpACBP1 bound to fatty acids. Values are represented as the percent activity of CpACBP1 as determined by the amount of bound NBD-C16:0-CoA. Bars represent the standard-error-of-the-mean from triplicate experiments.

esters. Similarly, no binding affinity to palmitic acid at concentrations of 0.1, 0.25, and 1.0 μM which is consistent with the ACBP protein family. Substrate preference data using the Lipidex 1000 assay were similar, except CpACBP1 was unable to bind acyl-CoA esters with acyl chains of 20 carbons or longer (194). This observation is likely due to binding competition between ACBP and Lipidex 1000 during the extraction step of the assay (137, 194). Data are presented as the mean and standard error of triplicate experiments each measured three times. Controls included reactions with only MBP or NBD-C16:0-CoA (or C16:0 fatty acid), or both to subtract background fluorescence.

Elucidation of CpACBP1 inhibitors. The ultimate goal of this study was to discover compounds that inhibit the binding properties of CpACBP1. The NIH/JDRF compound library contains 1,040 compounds of which most are approved for use in humans, and all have known bioactivities. Of the 1,040 compounds initially screened, we found that 37 (3.56%) displayed ≥ 50% inhibition. These 37 compounds were then examined to ensure that they did not have properties that interfered with our assay. Of these, nine displayed absorption spectra in the 580 – 600 nm range, thus likely serving as fluorescent quenchers in our assay. Therefore, we ended with 28/1040 (2.69%) compounds that displayed 50% or greater inhibition in the binding of NBD-C16:0-CoA to CpACBP1. Table 4.1 displays these 28 compounds along with their mean binding inhibitory effect [mean (± standard error)]. Additionally, we have listed

TABLE 4.1. Compounds that were shown to inhibit the binding affinity of CpACBP1 by ≥ 50%.

Compound[a]	% ACBP Inhibition (S.E.)[b]	IC_{50} (μM)[c]	K_i (μM)[d]	Bioactivity[e]
1S,2R-Phenylpro-panolamine HCl	51.22 (2.19)	0.202	0.082	Decongestant, Anorexic
Acetazolamide	49.89 (3.20)	0.018	0.007	Carbonic Anhydrase Inhibitor, Diuretic, Antiglaucoma
Bithionol	59.44 (0.68)	0.117	0.048	Anthelmintic, Antiseptic
Broxyquinoline	72.18 (7.82)	0.132	0.054	Antiinfectant, Disinfectant
Chlorpromazine	58.00 (2.04)	0.144	0.059	Antiemetic, Antipsychotic
Cloxacillin Sodium	55.24 (12.9)	0.123	0.05	Antibacterial
Cloxyquin	63.86 (3.11)	0.097	0.039	Antibacterial, Antifungal
Curcumin	56.32 (0.46)	0.216	0.088	Antiedemic, Antiinflammatory, Anti-bacterial, Antifungal, Lipo/cyclooxygenase Inhibitor
Gambogic Acid	50.62 (2.98)	0.207	0.084	Antiinflammatory, Cytotoxic, Inhibits HeLa Cells *In Vitro*
Homatropine Methylbromide	59.23 (18.2)	0.811	0.33	Anticholinergic (Opthalmic)
Hydralazine HCl	62.85 (11.1)	0.163	0.066	Antihypertensive
Hydrocortisone Acetate	49.17 (9.95)	0.362	0.147	Glucocorticoid, Antiinflammatory
Isoxicam	57.18 (12.6)	0.176	0.072	Antiinflammatory
Meclocycline Sulfosalicylate	56.75 (2.13)	0.153	0.062	Antibacterial
Mitoxanthrone HCl	50.96 (8.34)	0.128	0.052	Antineoplastic
Oxacillin Sodium	50.30 (1.63)	0.272	0.111	Antibacterial
Phenazopyridine HCl	67.24 (1.21)	0.144	0.059	Analgesic
Phenelzine Sulfate	51.69 (5.95)	0.199	0.081	Antidepressant
Phenothrin	73.87 (2.84)	0.14	0.057	Ectoparasiticide
Phenytoin Sodium	64.40 (5.55)	0.327	0.133	Anticonvulsant, Antieleptic
Pregnenolone	53.35 (6.29)	0.259	0.105	Glucocortcoid, Antiinflammatory
Pristimerin	53.52 (4.64)	0.168	0.068	Antineoplastic, Antiinflammatory
Quinalizarin	78.95 (3.24)	0.141	0.057	Antiviral, HIV-1 Integrase Inhibitor
Rifampin	58.73 (5.07)	0.227	0.092	Antibacterial
Rifaximin	56.14 (3.08)	0.269	0.109	Antibacterial, RNA Synthesis Inhibitor
Sodium Dehydrocholate	51.05 (7.16)	0.116	0.047	Choleretic
Streptozosin	49.75 (5.77)	0.304	0.124	Antineoplastic, Alkylating Agent
Tyrothricin	75.27 (2.24)	0.039	0.016	Topical Antibacterial

(a) Compound names as provided in the NIH/JDRF library. (b) Average percent inhibition (± standard error of five experiments) of the binding affinity by each compound (0.25 μM) of CpACBP1 (0.1 μM) to NBD-C16:0-CoA (0.25 μM). (c) Values determined from inhibition curves (supplementary figure A-2). Defined as the value that displays 50% binding inhibition. (d) See results section for formula used to calculate Ki values. (e) The bioactivities as provided in the NIH/JDRF library. These activities are not an exhaustive list.

their respective bioactivities as provided by the producers of the compound library, although we realize that some of these compounds may have activities other than those listed. Data were derived from triplicate experiments each measured five times. Controls included reactions with only MBP or NBD-C16:0-CoA, or both to subtract background fluorescence.

Inhibition kinetics. The top 28 compounds were then assayed to determine their enzyme kinetics. Using compound concentrations ranging from 20 nM – 2 μM, we analyzed each compound to elicit their respective IC_{50} values. Table 4.1 also lists these values for each compound, and inhibition plots are provided as supplementary material (Fig. A-2). From the IC50 values, we derived the Ki constants for each compound using the following formula: Ki = IC50 / (1 + (substrate / Kd)), where substrate is the concentration of NBD-C16:0-CoA (0.25 μM) and Kd is the value calculated above (171.2 nM).

DISCUSSION

Drug discovery is a very challenging and difficult endeavor, especially for *Cryptosporidium* for several reasons: first, the biochemistry and cell biology of this parasite are not completely understood. With current genomic and molecular techniques, we are quickly gaining a better perceptive of these two main barriers to efficacious drug development; second, the inability to cryopreserve this parasite which would smooth the process of establishing standard isolates in an attempt to provide consistency and lesser variability (106); third, positively identifying viable potential drug targets that are

essential to replication of the parasite are lacking. Although "best guesses" are made, and could prove to be accurate, the ability to propagate *Cryptosporidium* continuously in vitro would open many avenues of therapeutic research; and finally, as with most parasitic drug development, the majority of *Cryptosporidium* drug discovery occurs at academic and nonprofit research institutions that are not ideally suited for drug discovery.

The genome projects for both *C. parvum* (2) and *C. hominis* (192) have no doubt increased our understanding of the biochemical pathways and of host/parasite interactions. As with all organisms, lipids are essential to the growth and survival of *Cryptosporidium*. We now know that this parasite cannot synthesize fatty acids de novo, thus it must obtain them from the host cell or the intestinal lumen. Our understanding of the exact process of fatty acid transport from these locations into the parasite is lacking. However, we are gaining a better understanding of proteins that likely aid in this undertaking, as well as where these proteins are located at various stages of the parasite life cycle.

Although we remain unsure of whether or not CpACBP1 is essential to *Cryptosporidium* survival, we believe that it serves as a viable drug target. Fatty acids that enter the parasite cell must first be converted to their acyl-CoA esters before further processing through the fatty acid metabolic machinery. Because *C. parvum* contains only one ACBP it is likely that this parasite could not survive without the intracellular transfer and pooling of fatty acyl-CoA esters. Previous data has shown that CpACBP1 localizes to the PVM, which is likely in conjunction with a fatty acyl-CoA synthetase or

another unknown PVM protein (194). Thus, it appears that inhibiting binding of acyl-CoAs to CpACBP1 would result in the inability of the parasite to further process fatty acids.

Although there are very minimal investigations into halting the supply of fatty acids for their further metabolism in *Cryptosporidium*, we have proceeded with this area of exploration. We have identified several compounds which inhibit binding of fatty acyl-CoA to CpACBP1 in vitro. Whether or not these drugs have the potential to act on CpACBP1 in vivo is unknown, and will likely remain unknown for a long period of time. Of the final 28 compounds found to be viable CpACBP1 inhibitors in this study, several have been studied in greater detail in other parasitic protozoa (Table 4.2) resulting in a wide array of effects on those parasites. Only three of the drugs presented here have been previously tested as treatments for cryptosporidiosis. Bithionol was shown to be relatively inactive in in vitro studies (190). In another study, rifampin reduced the number of parasites by 17.4% when used at a concentration of 8 µg/µl, and by 74.4% when used in combination with 50 µM of ranalexin (57). Treatment with 600 mg, 3 times a day for 14 days resulted in resolution of clinical symptoms and clearing infection in HIV-infected patients (6). Further studies, which we are currently pursuing, are needed to further analyze the CpACBP1 inhibitors to determine their effect on *Cryptosporidium* itself.

TABLE 4.2. CpACBP1 inhibitors from this study that have been examined in other parasitic protozoa.

Protist	Compound (Reference)
Plasmodium spp.	Acetazolamide (90, 91, 143) Chlorpromazine (55, 79, 110, 156) Rifampin (134, 135) Tyrothricin (138) Curcumin (35, 140)
Giardia lamblia	Bithionol (169) Curcumin (130)
Trichomonas vaginalis	Bithionol (169)
Entamoeba histolytica	Bithionol (168) Chlorpromazine (123)
Trypanosoma spp.	Chlorpromazine (38, 44, 60) Hydralazine (80)
Schistosoma mansoni	Chlorpromazine (17)
Leishmania spp.	Chlorpromazine (127, 186) Rifampin (14, 30) Curcumin (26)

CHAPTER V

SUMMARY

The apicomplexan *Cryptosporidium parvum* possesses several unique features in its highly streamlined metabolism, and we are just beginning to glimpse the many secrets that this parasite holds. The scope of the research presented here encompasses the *C. parvum* fatty acid metabolism. This emerging parasite possesses a unique 1,500-kDa polyketide synthase (CpPKS1) comprised of 29 enzymes for synthesizing a yet undetermined polyketide. Our studies in Chapter I were on the biochemical characterization of the 845-aa loading unit containing acyl-[ACP] ligase (AL) and acyl carrier protein (ACP). We determined that the CpPKS1-AL domain has a substrate preference for long chain fatty acids, particularly for the C20:0 arachidic acid. When using [^{3}H]palmitic acid and CoA as co-substrates, the AL domain displayed allosteric kinetics towards palmitic acid (Hill coefficient, h = 1.46, K_{50} = 0.751 μM, V_{max} = 2.236 μmol mg^{-1} min^{-1}) and CoA (h = 0.704, K_{50} = 5.627 μM, V_{max} = 0.557 μmol mg^{-1} min^{-1}), and biphasic kinetics towards to ATP (K_{m1} = 3.149 μM, V_{max1} = 373.3 nmol mg^{-1} min^{-1}, K_{m2} = 121.0 μM, and V_{max2} = 563.7 nmol mg^{-1} min^{-1}). The AL domain is Mg^{2+}-dependent, and its activity could be inhibited by triacsin C (IC_{50} = 6.64 μM). Furthermore, the ACP domain within the loading unit could be activated by the *C. parvum* surfactin production element (SFP)-type phosphopantetheinyl transferase (CpSFP-PPT). After attachment of the fatty acid substrate to the AL domain for conversion into the fatty-acyl intermediate, the AL domain is able to transfer palmitic

acid to the activated holo-ACP in vitro. These observations ultimately validate the function of the CpPKS1-AL-ACP unit, and make it possible to further dissect the function of this megasynthase using recombinant proteins in a stepwise procedure.

In Chapter II, we reported the presence of a new fatty acyl-CoA elongation system in *Cryptosporidium* and the functional characterization of the key enzyme -- a single long chain fatty acid elongase (LCE). This enzyme contains conserved motifs and predicted transmembrane domains characteristic to the elongase family, and is placed within the ELO6 family specific for saturated substrates. *CpLCE1* gene transcripts are present at all life cycle stages, but the levels are highest in free sporozoites and stages at 36 h and 60 h post-infection that typically contain free merozoites. Immuno-staining revealed localization to the outer surface of sporozoites and to the (PVM). Recombinant CpLCE1 displayed allosteric kinetics towards malonyl-CoA and palmitoyl-CoA, and Michaelis-Menten kinetics towards NADPH. Myristoyl-CoA (C14:0) and palmitoyl-CoA (C16:0) display the highest activity when used as substrates, and only one round of elongation occurs. CpLCE1 is fairly resistant to cerulenin, an inhibitor for both type I and II fatty acid synthases (i.e., maximum inhibition of 20.5% and 32.7% when C16:0 and C14:0 were used as substrates). These observations ultimately validate the function of CpLCE1, which could serve as a possible drug target in future studies.

As with many of the fatty acid metabolism enzymes, *C. parvum* contains only one acyl-CoA binding protein (ACBP). Previous molecular and biochemical characterization of this enzyme by our laboratory resulted in some interesting findings. Most notably was its localization to the PVM in mid-to-late parasite life stages. The

localization of this protein to this region is intriguing because it is believed that many of the nutrients (including fatty acids, nucleotides, sugars, carbohydrates, etc) enter the parasite via the apically located PVM. Although it is currently unknown if CpACBP1 truly is a PVM protein, or if it is attached to another protein localized at the PVM, we hypothesized that CpACBP1 may serve as a viable drug target. Therefore, we were interested in utilizing a compound library consisting of compounds with known functions, many of which are currently used for various diseases or ailments. Using a fluorescence-based assay we identified several compounds that successfully inhibited the binding of fatty acyl-CoA to CpACBP1. Although this is a preliminary step in the drug discovery process, it has provided very beneficial data. Whether or not the compounds discussed here actually inhibit CpACBP1 in the parasite itself is unknown. Our laboratory is currently testing these compounds against *C. parvum* development using in vitro culture methods.

REFERENCES

1. **Abrahamsen, M. S., and A. A. Schroeder**. 1999. Characterization of intracellular *Cryptosporidium parvum* gene expression. Mol. Biochem. Parasitol. **104**:141-146.

2. **Abrahamsen, M. S., T. J. Templeton, S. Enomoto, J. E. Abrahante, G. Zhu, C. A. Lancto, M. Deng, C. Liu, G. Widmer, S. Tzipori, G. A. Buck, P. Xu, A. T. Bankier, P. H. Dear, B. A. Konfortov, H. F. Spriggs, L. Iyer, V. Anantharaman, L. Aravind, and V. Kapur**. 2004. Complete genome sequence of the apicomplexan, *Cryptosporidium parvum*. Science **304**:441-445.

3. **Altschul, S. F., T. L. Madden, A. A. Schaffer, J. Zhang, Z. Zhang, W. Miller, and D. J. Lipman**. 1997. Gapped BLAST and PSI-BLAST: a new generation of protein database search programs. Nucleic Acids Res **25**:3389-3402.

4. **Alvarez-Pellitero, P., and A. Sitja-Bobadilla**. 2002. *Cryptosporidium molnari* n. sp. (Apicomplexa: Cryptosporidiidae) infecting two marine fish species, *Sparus aurata* L. and *Dicentrarchus labrax* L. Int J Parasitol **32**:1007-1021.

5. **Amadi, B., M. Mwiya, J. Musuku, A. Watuka, S. Sianongo, A. Ayoub, and P. Kelly**. 2002. Effect of nitazoxanide on morbidity and mortality in Zambian children with cryptosporidiosis: a randomised controlled trial. Lancet **360**:1375-1380.

6. **Amenta, M., E. R. Dalle Nogare, C. Colomba, T. S. Prestileo, F. Di Lorenzo, S. Fundaro, A. Colomba, and A. Ferrieri**. 1999. Intestinal protozoa in HIV-infected patients: effect of rifaximin in *Cryptosporidium parvum* and *Blastocystis hominis* infections. J Chemother **11**:391-395.

7. **Anderson, D. R., D. W. Duszynski, and W. C. Marquardt**. 1968. Three new coccidia (Protozoa: Telosporea) from kingsnakes, *Lampropeltis* spp., in Illinois, with a description of *Eimeria zamensi* Phisalix, 1921. J Parasitol **54**:577-581.

8. **Arrowood, M. J., and C. R. Sterling**. 1987. Isolation of *Cryptosporidium* oocysts and sporozoites using discontinuous sucrose and isopycnic Percoll gradients. J. Parasitol. **73**:314-319.

9. **Bankier, A. T., H. F. Spriggs, B. Fartmann, B. A. Konfortov, M. Madera, C. Vogel, S. A. Teichmann, A. Ivens, and P. H. Dear**. 2003. Integrated mapping, chromosomal sequencing and sequence analysis of *Cryptosporidium parvum*. Genome Res **13**:1787-1799.

10. **Bar-Tana, J., G. Rose, R. Brandes, and B. Shapiro**. 1973. Palmitoyl-coenzyme A synthetase. Mechanism of reaction. Biochem J. **131**:199-209.

11. **Bar-Tana, J., G. Rose, and B. Shapiro**. 1973. Palmitoyl-coenzyme A synthetase. Isolation of an enzyme-bound intermediate. Biochem J. **135**:411-416.

12. **Barta, J. R., and R. C. Thompson**. 2006. What is *Cryptosporidium*? Reappraising its biology and phylogenetic affinities. Trends Parasitol **22**:463-468.

13. **Bearup, A. J.** 1954. The coccidia of carnivores of Sydney. Aust Vet J **30**:185-186.

14. **Berman, J. D., and L. S. Lee**. 1983. Activity of oral drugs against *Leishmania tropica* in human macrophages in vitro. Am J Trop Med Hyg **32**:947-951.

15. **Bernert, J. T., Jr., and H. Sprecher**. 1977. An analysis of partial reactions in the overall chain elongation of saturated and unsaturated fatty acids by rat liver microsomes. J Biol Chem. **252**:6736-6744.

16. **Black, P. N., Q. Zhang, J. D. Weimar, and C. C. DiRusso**. 1997. Mutational analysis of a fatty acyl-coenzyme A synthetase signature motif identifies seven amino acid residues that modulate fatty acid substrate specificity. J Biol Chem **272**:4896-4903.

17. **Boyle, J. P., J. V. Zaide, and T. P. Yoshino**. 2000. *Schistosoma mansoni*: effects of serotonin and serotonin receptor antagonists on motility and length of primary sporocysts in vitro. Exp Parasitol **94**:217-226.

18. **Brends, S. J.** 1989-2005. Systema Naturae 2000. The Taxonomicon. Universal Taxonomic Services, Amsterdam, The Netherlands. [http://sn2000.taxonomy.nl/].

19. **Bull, S., R. Chalmers, A. P. Sturdee, A. Curry, and J. Kennaugh**. 1998. Cross-reaction of an anti-*Cryptosporidium* monoclonal antibody with sporocysts of *Monocystis* species. Vet Parasitol **77**:195-197.

20. **Burton, M., T. M. Rose, N. J. Faergeman, and J. Knudsen**. 2005. Evolution of the acyl-CoA binding protein (ACBP). Biochem J **392**:299-307.

21. **Caffrey, P.** 2003. Conserved amino acid residues correlating with ketoreductase stereospecificity in modular polyketide synthases. Chembiochem. **4**:654-657.

22. **Cai, X., D. Herschap, and G. Zhu**. 2005. Functional characterization of an evolutionarily distinct phosphopantetheinyl transferase in the apicomplexan *Cryptosporidium parvum*. Eukaryot Cell. **4**:1211-1220.

23. **Cai, X., K. M. Woods, S. J. Upton, and G. Zhu**. 2005. Application of quantitative real-time reverse transcription-PCR in assessing drug efficacy against the intracellular pathogen *Cryptosporidium parvum* in vitro. Antimicrob Agents Chemother **49**:4437-4442.

24. **Cane, D. E., C. T. Walsh, and C. Khosla**. 1998. Harnessing the biosynthetic code: combinations, permutations, and mutations. Science. **282**:63-68.

25. **Carreno, R. A., D. S. Martin, and J. R. Barta**. 1999. *Cryptosporidium* is more closely related to the gregarines than to coccidia as shown by phylogenetic analysis of apicomplexan parasites inferred using small-subunit ribosomal RNA gene sequences. Parasitol Res **85**:899-904.

26. **Chan, M. M., N. S. Adapala, and D. Fong**. 2005. Curcumin overcomes the inhibitory effect of nitric oxide on *Leishmania*. Parasitol Res **96**:49-56.

27. **Chao, H., G. G. Martin, W. K. Russell, S. D. Waghela, D. H. Russell, F. Schroeder, and A. B. Kier**. 2002. Membrane charge and curvature determine interaction with acyl-CoA binding protein (ACBP) and fatty acyl-CoA targeting. Biochemistry **41**:10540-10553.

28. **Chen, X. M., B. Q. Huang, P. L. Splinter, H. Cao, G. Zhu, M. A. McNiven, and N. F. LaRusso**. 2003. *Cryptosporidium parvum* invasion of biliary epithelia requires host cell tyrosine phosphorylation of cortactin via c-Src. Gastroenterology **125**:216-228.

29. **Chen, X. M., J. S. Keithly, C. V. Paya, and N. F. LaRusso**. 2002. Cryptosporidiosis. N. Engl. J. Med. **346**:1723-1731.

30. **Choi, C. M., and E. A. Lerner**. 2002. Leishmaniasis: recognition and management with a focus on the immunocompromised patient. Am J Clin Dermatol **3**:91-105.

31. **Chye, M. L., B. Q. Huang, and S. Y. Zee**. 1999. Isolation of a gene encoding *Arabidopsis* membrane-associated acyl-CoA binding protein and immunolocalization of its gene product. Plant J **18**:205-214.

32. **Cinti, D. L., L. Cook, M. N. Nagi, and S. K. Suneja**. 1992. The fatty acid chain elongation system of mammalian endoplasmic reticulum. Prog. Lipid. Res. **31**:1-51.

33. **Cohen, S. L., and B. T. Chait**. 1997. Mass spectrometry of whole proteins eluted from sodium dodecyl sulfate-polyacrylamide gel electrophoresis gels. Anal. Biochem. **247**:257-267.

34. **Ctrnacta, V., J. G. Ault, F. Stejskal, and J. S. Keithly**. 2006. Localization of pyruvate:NADP+ oxidoreductase in sporozoites of *Cryptosporidium parvum*. J Eukaryot Microbiol **53**:225-231.

35. **Cui, L., and J. Miao**. 2007. Cytotoxic effect of curcumin on malaria parasite *Plasmodium falciparum*: inhibition of histone acetylation and generation of reactive oxygen species. Antimicrob Agents Chemother **51**:488-494.

36. **Current, W. L., and N. C. Reese**. 1986. A comparison of endogenous development of three isolates of *Cryptosporidium* in suckling mice. J Protozool **33**:98-108.

37. **Current, W. L., S. J. Upton, and T. B. Haynes**. 1986. The life cycle of *Cryptosporidium baileyi* n. sp. (Apicomplexa, Cryptosporidiidae) infecting chickens. J Protozool **33**:289-296.

38. **De Castro, S. L., M. N. Soeiro, and N. De Meirelles Mde**. 1992. *Trypanosoma cruzi*: effect of phenothiazines on the parasite and its interaction with host cells. Mem Inst Oswaldo Cruz **87**:209-215.

39. **Doumbo, O., J. F. Rossignol, E. Pichard, H. A. Traore, T. M. Dembele, M. Diakite, F. Traore, and D. A. Diallo**. 1997. Nitazoxanide in the treatment of cryptosporidial diarrhea and other intestinal parasitic infections associated with acquired immunodeficiency syndrome in tropical Africa. Am J Trop Med Hyg **56**:637-639.

40. **Dubey, J. P., and B. P. Pande**. 1963. Observations on the coccidian oocysts from Indian Jungle cat (*Felis chaus*). Indian JMicrobiol **3**:103-108.

41. **Duszynski, D. W.** 1969. Two new coccidia (Protozoa: Dimeriidae) from Costa Rican lizards with a review of the *Eimeria* from lizards. J Protozool **16**:581-585.

42. **Egyed, Z., T. Sreter, Z. Szell, B. Beszteri, M. Dobos-Kovacs, K. Marialigeti, A. W. Cornelissen, and I. Varga**. 2002. Polyphasic typing of *Cryptosporidium baileyi*: a suggested model for characterization of cryptosporidia. J Parasitol **88**:237-243.

43. **Egyed, Z., T. Sreter, Z. Szell, and I. Varga**. 2003. Characterization of *Cryptosporidium* spp.--recent developments and future needs. Vet Parasitol **111**:103-114.

44. **Faerman, C. H., S. N. Savvides, C. Strickland, M. A. Breidenbach, J. A. Ponasik, B. Ganem, D. Ripoll, R. L. Krauth-Siegel, and P. A. Karplus**. 1996. Charge is the major discriminating factor for glutathione reductase versus trypanothione reductase inhibitors. Bioorg Med Chem **4**:1247-1253.

45. **Fayer, R.** 1997. *Cryptosporidium* and cryptosporidiosis. CRC Press, Boca Raton, FL.

46. **Fayer, R., U. Morgan, and S. J. Upton**. 2000. Epidemiology of *Cryptosporidium*: transmission, detection and identification. Int J Parasitol **30**:1305-1322.

47. **Fayer, R., M. Santin, and L. Xiao**. 2005. *Cryptosporidium bovis* n. sp. (Apicomplexa: Cryptosporidiidae) in cattle (*Bos taurus*). J Parasitol **91**:624-629.

48. **Fayer, R., J. M. Trout, L. Xiao, U. M. Morgan, A. A. Lai, and J. P. Dubey**. 2001. *Cryptosporidium canis* n. sp. from domestic dogs. J Parasitol **87**:1415-1422.

49. **Fayer, R., and B. L. Ungar**. 1986. *Cryptosporidium* spp. and cryptosporidiosis. Microbiol Rev **50**:458-483.

50. **Fehling, E., R. Lessire, C. Cassagne, and K. D. Mukherjee**. 1992. Solubilization and partial purification of constituents of acyl-CoA elongase from *Lunaria annua*. Biochim Biophys Acta **1126**:88-94.

51. **Fox, L. M., and L. D. Saravolatz**. 2005. Nitazoxanide: a new thiazolide antiparasitic agent. Clin Infect Dis **40**:1173-1180.

52. **Fritzler, J. M., J. J. Millership, and G. Zhu**. 2007. *Cryptosporidium parvum* long-chain fatty acid elongase. Eukaryot Cell **6**:2018-2028.

53. **Fritzler, J. M., and G. Zhu**. 2007. Functional characterization of the acyl-[acyl carrier protein] ligase in the *Cryptosporidium parvum* giant polyketide synthase. Int. J. Parasitol. **37**:307-316.

54. **Frolov, A., and F. Schroeder**. 1998. Acyl coenzyme A binding protein. Conformational sensitivity to long chain fatty acyl-CoA. J Biol Chem **273**:11049-11055.

55. **Geary, T. G., A. A. Divo, and J. B. Jensen**. 1986. Effect of calmodulin inhibitors on viability and mitochondrial potential of *Plasmodium falciparum* in culture. Antimicrob Agents Chemother **30**:785-788.

56. **Ghanevati, M., and J. G. Jaworski**. 2001. Active-site residues of a plant membrane-bound fatty acid elongase beta-ketoacyl-CoA synthase, FAE1 KCS. Biochim. Biophys. Acta. **1530**:77-85.

57. **Giacometti, A., O. Cirioni, F. Barchiesi, M. Fortuna, and G. Scalise**. 1999. In vitro anticryptosporidial activity of ranalexin alone and in combination with other peptides and with hydrophobic antibiotics. Eur J Clin Microbiol Infect Dis **18**:827-829.

58. **Gossett, R. E., A. A. Frolov, J. B. Roths, W. D. Behnke, A. B. Kier, and F. Schroeder**. 1996. Acyl-CoA binding proteins: multiplicity and function. Lipids **31**:895-918.

59. **Griffiths, J. K., R. Balakrishnan, G. Widmer, and S. Tzipori**. 1998. Paromomycin and geneticin inhibit intracellular *Cryptosporidium parvum* without trafficking through the host cell cytoplasm: implications for drug delivery. Infect Immun **66**:3874-3883.

60. **Gutierrez-Correa, J., and A. O. Stoppani**. 2002. Myeloperoxidase-generated phenothiazine cation radicals inactivate *Trypanosoma cruzi* dihydrolipoamide dehydrogenase. Rev Argent Microbiol **34**:83-94.

61. **Hampton, J. C., and B. Rosario**. 1966. The attachment of protozoan parasites to intestinalepithelial cells of the mouse. J Parasitol **52**:939-949.

62. **Hartman, E. J., S. Omura, and M. Laposata**. 1989. Triacsin C: a differential inhibitor of arachidonoyl-CoA synthetase and nonspecific long chain acyl-CoA synthetase. Prostaglandins **37**:655-671.

63. **Hee Lee, S., J. L. Stephens, and P. T. Englund**. 2007. A fatty-acid synthesis mechanism specialized for parasitism. Nat. Rev. Microbiol. **5**:287-297.

64. **Hemphill, A., J. Mueller, and M. Esposito**. 2006. Nitazoxanide, a broad-spectrum thiazolide anti-infective agent for the treatment of gastrointestinal infections. Expert Opin Pharmacother **7**:953-964.

65. **Henikoff, S., J. G. Henikoff, W. J. Alford, and S. Pietrokovski**. 1995. Automated construction and graphical presentation of protein blocks from unaligned sequences. Gene **163**:GC17-26.

66. **Hewitt, R. G., C. T. Yiannoutsos, E. S. Higgs, J. T. Carey, P. J. Geiseler, R. Soave, R. Rosenberg, G. J. Vazquez, L. J. Wheat, R. J. Fass, Z. Antoninievic, A. L. Walawander, T. P. Flanigan, and J. F. Bender**. 2000. Paromomycin: no more effective than placebo for treatment of cryptosporidiosis in patients with advanced human immunodeficiency virus infection. AIDS Clinical Trial Group. Clin Infect Dis **31**:1084-1092.

67. **Hijjawi, N. S., B. P. Meloni, M. Ng'anzo, U. M. Ryan, M. E. Olson, P. T. Cox, P. T. Monis, and R. C. Thompson**. 2004. Complete development of *Cryptosporidium parvum* in host cell-free culture. Int J Parasitol **34**:769-777.

68. **Hijjawi, N. S., B. P. Meloni, U. M. Ryan, M. E. Olson, and R. C. Thompson**. 2002. Successful in vitro cultivation of *Cryptosporidium andersoni*: evidence for the existence of novel extracellular stages in the life cycle and implications for the classification of *Cryptosporidium*. Int J Parasitol **32**:1719-1726.

69. **Hommer, V., J. Eichholz, and F. Petry**. 2003. Effect of antiretroviral protease inhibitors alone, and in combination with paromomycin, on the excystation, invasion and in vitro development of *Cryptosporidium parvum*. J Antimicrob Chemother **52**:359-364.

70. **Hopwood, D. A.** 1997. Genetic contributions to understanding polyketide synthases. Chem Rev **97**:2465-2498.

71. **Hopwood, D. A., and D. H. Sherman**. 1990. Molecular genetics of polyketides and its comparison to fatty acid biosynthesis. Annu Rev Genet **24**:37-66.

72. **Huang, B. Q., X. M. Chen, and N. F. LaRusso**. 2004. *Cryptosporidium parvum* attachment to and internalization by human biliary epithelia in vitro: a morphologic study. J Parasitol **90**:212-221.

73. **Huelsenbeck, J. P., and F. Ronquist**. 2001. MRBAYES: Bayesian inference of phylogenetic trees. Bioinformatics **17**:754-755.

74. **Iseki, M.** 1979. *Cryptosporidium felis* sp. n. (Protozoa: Eimeriorina) from the domestic cat. Jpn J Parasitol **28**:285-307.

75. **Jakobsson, A., R. Westerberg, and A. Jacobsson**. 2006. Fatty acid elongases in mammals: their regulation and roles in metabolism. Prog. Lipid Res. **45**:237-249.

76. **Jervis, H. R., T. G. Merrill, and H. Sprinz**. 1966. Coccidiosis in the guinea pig small intestine due to a *Cryptosporidium*. Am J Vet Res **27**:408-414.

77. **Jones, D. T., W. R. Taylor, and J. M. Thornton**. 1992. The rapid generation of mutation data matrices from protein sequences. Comput. Appl. Biosci. **8**:275-282.

78. **Kadappu, K. K., M. V. Nagaraja, P. V. Rao, and B. A. Shastry**. 2002. Azithromycin as treatment for cryptosporidiosis in human immunodeficiency virus disease. J Postgrad Med **48**:179-181.

79. **Kalkanidis, M., N. Klonis, L. Tilley, and L. W. Deady**. 2002. Novel phenothiazine antimalarials: synthesis, antimalarial activity, and inhibition of the formation of beta-haematin. Biochem Pharmacol **63**:833-842.

80. **Kalu, A. U., and E. Haruna**. 1985. Effects of vasopressor drugs on number of *Trypanosoma congolense* in ruminant blood. Vet Parasitol **17**:287-294.

81. **Katz, L.** 1997. Manipulation of modular polyketide synthases. Chem. Rev. **97**:2557-2576.

82. **Keating, T. A., and C. T. Walsh**. 1999. Initiation, elongation, and termination strategies in polyketide and polypeptide antibiotic biosynthesis. Curr Opin Chem Biol. **3**:598-606.

83. **Kellermann, O. K., and T. Ferenci**. 1982. Maltose-binding protein from *Escherichia coli.* Methods Enzymol. **90 Pt E**:459-463.

84. **Khosla, C.** 1997. Harnessing the biosynthetic potential of modular polyketide synthases. Chem. Rev. **97**:2577-2590.

85. **Khosla, C., and R. J. Zawada**. 1996. Generation of polyketide libraries via combinatorial biosynthesis. Trends Biotechnol. **14**:335-341.

86. **Kim, J. H., T. M. Lewin, and R. A. Coleman**. 2001. Expression and characterization of recombinant rat Acyl-CoA synthetases 1, 4, and 5. Selective inhibition by triacsin C and thiazolidinediones. J Biol Chem **276**:24667-24673.

87. **Knudsen, J., M. V. Jensen, J. K. Hansen, N. J. Faergeman, T. B. Neergaard, and B. Gaigg**. 1999. Role of acylCoA binding protein in acylCoA transport, metabolism and cell signaling. Mol Cell Biochem **192**:95-103.

88. **Knudsen, J., T. B. Neergaard, B. Gaigg, M. V. Jensen, and J. K. Hansen**. 2000. Role of acyl-CoA binding protein in acyl-CoA metabolism and acyl-CoA-mediated cell signaling. J Nutr **130**:294S-298S.

89. **Koudela, B., and D. Modry**. 1998. New species of *Cryptosporidium* (Apicomplexa: Cryptosporidiidae) from lizards. Folia Parasitol **45**:93-100.

90. **Krungkrai, J., A. Scozzafava, S. Reungprapavut, S. R. Krungkrai, R. Rattanajak, S. Kamchonwongpaisan, and C. T. Supuran**. 2005. Carbonic anhydrase inhibitors. Inhibition of *Plasmodium falciparum* carbonic anhydrase with aromatic sulfonamides: towards antimalarials with a novel mechanism of action? Bioorg Med Chem **13**:483-489.

91. **Krungkrai, S. R., N. Suraveratum, S. Rochanakij, and J. Krungkrai**. 2001. Characterisation of carbonic anhydrase in *Plasmodium falciparum*. Int J Parasitol **31**:661-668.

92. **Kubota, T., Y. Iinuma, and J. Kobayashi**. 2006. Cloning of polyketide synthase genes from amphidinolide-producing dinoflagellate *Amphidinium* sp. Biol Pharm Bull **29**:1314-1318.

93. **Leonard, A. E., S. L. Pereira, H. Sprecher, and Y. S. Huang**. 2004. Elongation of long-chain fatty acids. Prog. Lipid Res. **43**:36-54.

94. **Leung, K. C., H. Y. Li, S. Xiao, M. H. Tse, and M. L. Chye**. 2006. *Arabidopsis* ACBP3 is an extracellularly targeted acyl-CoA-binding protein. Planta **223**:871-881.

95. **Levine, N. D.** 1961. Protozoan parasites of domestic animals and of man. Burgess Publishing Company, Minneapolis, MN.

96. **Levine, N. D.** 1980. Some corrections of coccidian (Apicomplexa: Protozoa) nomenclature. J Parasitol **66**:830-834.

97. **Levine, N. D.** 1984. Taxonomy and review of the coccidian genus *Cryptosporidium* (protozoa, apicomplexa). J Protozool **31**:94-98.

98. **Levine, N. D.** 1985. Phylum II. Apicomplexa Levine, 1970, p. 322-374. *In* J. J. Lee, S. H. Hunter, and E. C. Bovee (eds.), An illustrated guide to the Protozoa. Allen Press, Lawrence, KS.

99. **Lindsay, D. S., S. J. Upton, D. S. Owens, U. M. Morgan, J. R. Mead, and B. L. Blagburn**. 2000. *Cryptosporidium andersoni* n. sp. (Apicomplexa: Cryptosporiidae) from cattle, *Bos taurus*. J Eukaryot Microbiol **47**:91-95.

100. **Liu, C., V. Vigdorovich, V. Kapur, and M. S. Abrahamsen**. 1999. A random survey of the *Cryptosporidium parvum* genome. Infect Immun **67**:3960-3969.

101. **Livore, V. I., K. E. Tripodi, and A. D. Uttaro**. 2007. Elongation of polyunsaturated fatty acids in trypanosomatids. Febs J **274**:264-274.

102. **Marshall, M. M., D. Naumovitz, Y. Ortega, and C. R. Sterling**. 1997. Waterborne protozoan pathogens. Clin Microbiol Rev **10**:67-85.

103. **Matesanz, F., I. Duran-Chica, and A. Alcina**. 1999. The cloning and expression of Pfacs1, a *Plasmodium falciparum* fatty acyl coenzyme A synthetase-1 targeted to the host erythrocyte cytoplasm. J. Mol. Biol. **291**:59-70.

104. **Matsuzaka, T., H. Shimano, N. Yahagi, T. Yoshikawa, M. Amemiya-Kudo, A. H. Hasty, H. Okazaki, Y. Tamura, Y. Iizuka, K. Ohashi, J. Osuga, A. Takahashi, S. Yato, H. Sone, S. Ishibashi, and N. Yamada**. 2002. Cloning and characterization of a mammalian fatty acyl-CoA elongase as a lipogenic enzyme regulated by SREBPs. J. Lipid. Res. **43**:911-920.

105. **McManus, D. P., and J. Bowles**. 1996. Molecular genetic approaches to parasite identification: their value in diagnostic parasitology and systematics. Int J Parasitol **26**:687-704.

106. **Mead, J. R.** 2002. Cryptosporidiosis and the challenges of chemotherapy. Drug Resist Updat **5**:47-57.

107. **Meisel, J. L., D. R. Perera, C. Meligro, and C. E. Rubin**. 1976. Overwhelming watery diarrhea associated with a cryptosporidium in an immunosuppressed patient. Gastroenterology **70**:1156-1160.

108. **Metz, J. G., P. Roessler, D. Facciotti, C. Levering, F. Dittrich, M. Lassner, R. Valentine, K. Lardizabal, F. Domergue, A. Yamada, K. Yazawa, V. Knauf, and J. Browse**. 2001. Production of polyunsaturated fatty acids by polyketide synthases in both prokaryotes and eukaryotes. Science **293**:290-293.

109. **Meyer, A., H. Kirsch, F. Domergue, A. Abbadi, P. Sperling, J. Bauer, P. Cirpus, T. K. Zank, H. Moreau, T. J. Roscoe, U. Zahringer, and E. Heinz**. 2004. Novel fatty acid elongases and their use for the reconstitution of docosahexaenoic acid biosynthesis. J Lipid Res **45**:1899-1909.

110. **Miki, A., K. Tanabe, T. Nakayama, C. Kiryon, and K. Ohsawa**. 1992. *Plasmodium chabaudi*: association of reversal of chloroquine resistance with increased accumulation of chloroquine in resistant parasites. Exp Parasitol **74**:134-142.

111. **Milne, K. G., and M. A. Ferguson**. 2000. Cloning, expression, and characterization of the acyl-CoA-binding protein in African trypanosomes. J Biol Chem **275**:12503-12508.

112. **Mitschler, R. R., R. Welti, and S. J. Upton**. 1994. A comparative study of lipid compositions of *Cryptosporidium parvum* (Apicomplexa) and Madin-Darby bovine kidney cells. J Eukaryot Microbiol. **41**:8-12.

113. **Moon, Y. A., and J. D. Horton**. 2003. Identification of two mammalian reductases involved in the two-carbon fatty acyl elongation cascade. J Biol Chem. **278**:7335-7343.

114. **Moon, Y. A., N. A. Shah, S. Mohapatra, J. A. Warrington, and J. D. Horton**. 2001. Identification of a mammalian long chain fatty acyl elongase regulated by sterol regulatory element-binding proteins. J Biol Chem **276**:45358-45366.

115. **Moore, B. S., and C. Hertweck**. 2002. Biosynthesis and attachment of novel bacterial polyketide synthase starter units. Nat Prod Rep. **19**:70-99.

116. **Morgan-Ryan, U. M., A. Fall, L. A. Ward, N. Hijjawi, I. Sulaiman, R. Fayer, R. C. Thompson, M. Olson, A. Lal, and L. Xiao**. 2002. *Cryptosporidium hominis* n. sp. (Apicomplexa: Cryptosporidiidae) from *Homo sapiens*. J Eukaryot Microbiol **49**:433-440.

117. **Morita, Y. S., K. S. Paul, and P. T. Englund**. 2000. Specialized fatty acid synthesis in African trypanosomes: myristate for GPI anchors. Science **288**:140-143.

118. **Nime, F. A., J. D. Burek, D. L. Page, M. A. Holscher, and J. H. Yardley**. 1976. Acute enterocolitis in a human being infected with the protozoan *Cryptosporidium*. Gastroenterology **70**:592-598.

119. **Nugteren, D. H.** 1965. The enzymic chain elongation of fatty acids by rat-liver microsomes. Biochim Biophys Acta. **106**:280-290.

120. **O'Donoghue, P. J.** 1995. *Cryptosporidium* and cryptosporidiosis in man and animals. Int J Parasitol **25**:139-195.

121. **O'Hagan, D.** 1991. The polyketide metabolites. E. Horwood, New York.

122. **Omura, S., H. Tomoda, Q. M. Xu, Y. Takahashi, and Y. Iwai**. 1986. Triacsins, new inhibitors of acyl-CoA synthetase produced by *Streptomyces* sp. J. Antibiot. (Tokyo) **39**:1211-1218.

123. **Ondarza, R. N., E. Hernandez, A. Iturbe, and G. Hurtado**. 2000. Inhibitory and lytic effects of phenothiazine derivatives and related tricyclic neuroleptic compounds, on *Entamoeba histolytica* HK9 and HM1 trophozoites. Biotechnol Appl Biochem **32 (Pt 1)**:61-67.

124. **Pande, B. P., B. B. Bhatia, and P. P. Chauhan**. 1972. A new genus and species of cryptosporidiid Coccidia from India. Acta Vet Acad Sci Hung **22**:231-234.

125. **Pankuch, G. A., and P. C. Appelbaum**. 2006. Activities of tizoxanide and nitazoxanide compared to those of five other thiazolides and three other agents against anaerobic species. Antimicrob Agents Chemother **50**:1112-1117.

126. **Paul, S., K. Gable, F. Beaudoin, E. Cahoon, J. Jaworski, J. A. Napier, and T. M. Dunn**. 2006. Members of the *Arabidopsis* FAE1-like 3-ketoacyl-CoA synthase gene family substitute for the Elop proteins of *Saccharomyces cerevisiae*. J. Biol. Chem. **281**:9018-9029.

127. **Pearson, R. D., A. A. Manian, D. Hall, J. L. Harcus, and E. L. Hewlett**. 1984. Antileishmanial activity of chlorpromazine. Antimicrob Agents Chemother **25**:571-574.

128. **Peiru, S., H. G. Menzella, E. Rodriguez, J. Carney, and H. Gramajo**. 2005. Production of the potent antibacterial polyketide erythromycin C in *Escherichia coli*. Appl Environ Microbiol **71**:2539-2547.

129. **Pereda, A., R. G. Summers, D. L. Stassi, X. Ruan, and L. Katz**. 1998. The loading domain of the erythromycin polyketide synthase is not essential for erythromycin biosynthesis in *Saccharopolyspora erythraea*. Microbiol **144(Pt 2)**:543-553.

130. **Perez-Arriaga, L., M. L. Mendoza-Magana, R. Cortes-Zarate, A. Corona-Rivera, L. Bobadilla-Morales, R. Troyo-Sanroman, and M. A. Ramirez-Herrera**. 2006. Cytotoxic effect of curcumin on *Giardia lamblia* trophozoites. Acta Trop **98**:152-161.

131. **Persson, B., and P. Argos**. 1994. Prediction of transmembrane segments in proteins utilising multiple sequence alignments. J Mol Biol **237**:182-192.

132. **Pfeifer, B. A., and C. Khosla**. 2001. Biosynthesis of polyketides in heterologous hosts. Microbiol. Mol. Biol. Rev. **65**:106-118.

133. **Prasitchoke, P., Y. Kaneko, T. Bamba, E. Fukusaki, A. Kobayashi, and S. Harashima**. 2007. Identification and characterization of a very long-chain fatty acid elongase gene in the methylotrophic yeast, *Hansenula polymorpha*. Gene **391**:16-25.

134. **Pukrittayakamee, S., S. Prakongpan, S. Wanwimolruk, R. Clemens, S. Looareesuwan, and N. J. White**. 2003. Adverse effect of rifampin on quinine efficacy in uncomplicated falciparum malaria. Antimicrob Agents Chemother **47**:1509-1513.

135. **Pukrittayakamee, S., C. Viravan, P. Charoenlarp, C. Yeamput, R. J. Wilson, and N. J. White**. 1994. Antimalarial effects of rifampin in *Plasmodium vivax* malaria. Antimicrob Agents Chemother **38**:511-514.

136. **Rasmussen, J. T., T. Borchers, and J. Knudsen**. 1990. Comparison of the binding affinities of acyl-CoA-binding protein and fatty-acid-binding protein for long-chain acyl-CoA esters. Biochem J **265**:849-855.

137. **Rasmussen, J. T., N. J. Faergeman, K. Kristiansen, and J. Knudsen**. 1994. Acyl-CoA-binding protein (ACBP) can mediate intermembrane acyl-CoA transport and donate acyl-CoA for beta-oxidation and glycerolipid synthesis. Biochem J **299 (Pt 1)**:165-170.

138. **Rautenbach, M., N. M. Vlok, M. Stander, and H. C. Hoppe**. 2007. Inhibition of malaria parasite blood stages by tyrocidines, membrane-active cyclic peptide antibiotics from *Bacillus brevis*. Biochim Biophys Acta **1768**:1488-1497.

139. **Rawlings, B. J.** 1997. Biosynthesis of polyketides. Nat. Prod. Rep. **14**:523-556.

140. **Reddy, R. C., P. G. Vatsala, V. G. Keshamouni, G. Padmanaban, and P. N. Rangarajan**. 2005. Curcumin for malaria therapy. Biochem Biophys Res Commun **326**:472-474.

141. **Reduker, D. W., C. A. Speer, and J. A. Blixt**. 1985. Ultrastructure of *Cryptosporidium parvum* oocysts and excysting sporozoites as revealed by high resolution scanning electron microscopy. J Protozool **32**:708-711.

142. **Rein, K. S., and R. V. Snyder**. 2006. The biosynthesis of polyketide metabolites by dinoflagellates. Adv Appl Microbiol **59**:93-125.

143. **Reungprapavut, S., J. Krungkrai, and S. R. Krungkrai**. 2004. *Plasmodium falciparum* carbonic anhydrase is a possible target for malaria chemotherapy. J Enz Inhib Med Chem **19**:249-256.

144. **Rider, S. D., Jr., X. Cai, W. J. Sullivan, Jr., A. T. Smith, J. Radke, M. White, and G. Zhu**. 2005. The protozoan parasite *Cryptosporidium parvum* possesses two functionally and evolutionarily divergent replication protein A large subunits. J Biol Chem **280**:31460-31469.

145. **Robertson, L. J., A. T. Campbell, and H. V. Smith**. 1993. In vitro excystation of *Cryptosporidium parvum*. Parasitology **106 (Pt 1)**:13-19.

146. **Romero Cabello, R., L. R. Guerrero, M. R. Munoz Garcia, and A. Geyne Cruz**. 1997. Nitazoxanide for the treatment of intestinal protozoan and helminthic infections in Mexico. Trans R Soc Trop Med Hyg **91**:701-703.

147. **Rosales, M. J., G. P. Cordon, M. S. Moreno, and C. M. Sanchez**. 2005. Extracellular like-gregarine stages of *Cryptosporidium parvum*. Acta Trop **95**:74-78.

148. **Rosendal, J., P. Ertbjerg, and J. Knudsen**. 1993. Characterization of ligand binding to acyl-CoA-binding protein. Biochem J **290 (Pt 2)**:321-326.

149. **Rossignol, J. F.** 2006. Nitazoxanide in the treatment of acquired immune deficiency syndrome-related cryptosporidiosis: results of the United States compassionate use program in 365 patients. Aliment Pharmacol Ther **24**:887-894.

150. **Rossignol, J. F., A. Ayoub, and M. S. Ayers**. 2001. Treatment of diarrhea caused by *Cryptosporidium parvum*: a prospective randomized, double-blind, placebo-controlled study of Nitazoxanide. J Infect Dis **184**:103-106.

151. **Rossignol, J. F., and H. Maisonneuve**. 1984. Nitazoxanide in the treatment of *Taenia saginata* and *Hymenolepis nana* infections. Am J Trop Med Hyg **33**:511-512.

152. **Rotte, C., F. Stejskal, G. Zhu, J. S. Keithly, and W. Martin**. 2001. Pyruvate : NADP+ oxidoreductase from the mitochondrion of *Euglena gracilis* and from the apicomplexan *Cryptosporidium parvum*: a biochemical relic linking pyruvate metabolism in mitochondriate and amitochondriate protists. Mol Biol Evol **18**:710-720.

153. **Ryan, U. M., P. Monis, H. L. Enemark, I. Sulaiman, B. Samarasinghe, C. Read, R. Buddle, I. Robertson, L. Zhou, R. C. Thompson, and L. Xiao**. 2004. *Cryptosporidium suis* n. sp. (Apicomplexa: Cryptosporidiidae) in pigs (*Sus scrofa*). J Parasitol **90**:769-773.

154. **Ryan, U. M., L. Xiao, C. Read, I. M. Sulaiman, P. Monis, A. A. Lal, R. Fayer, and I. Pavlasek**. 2003. A redescription of *Cryptosporidium galli* Pavlasek, 1999 (Apicomplexa: Cryptosporidiidae) from birds. J Parasitol **89**:809-813.

155. **Salas, J. J., E. Martinez-Force, and R. Garces**. 2005. Very long chain fatty acid synthesis in sunflower kernels. J. Agric. Food Chem. **53**:2710-2716.

156. **Satayavivad, J., O. Wongsawatkul, D. Bunnag, P. Tan-ariya, and C. R. Brockelman**. 1987. Flunarizine and verapamil inhibit chloroquine-resistant *Plasmodium falciparum* growth in vitro. Southeast Asian J Trop Med Public Health **18**:253-258.

157. **Schroeder, F., C. A. Jolly, T. H. Cho, and A. Frolov**. 1998. Fatty acid binding protein isoforms: structure and function. Chem Phys Lipids **92**:1-25.

158. **Sitja-Bobadilla, A., F. Padros, C. Aguilera, and P. Alvarez-Pellitero**. 2005. Epidemiology of *Cryptosporidium molnari* in Spanish gilthead sea bream (*Sparus aurata* L.) and European sea bass (*Dicentrarchus labrax* L.) cultures: from hatchery to market size. Appl Environ Microbiol **71**:131-139.

159. **Slavin, D.** 1955. *Cryptosporidium meleagridis* (sp. nov.). J Comp Pathol **65**:262-266.

160. **Smith, N. H., S. Cron, L. M. Valdez, C. L. Chappell, and A. C. White, Jr.** 1998. Combination drug therapy for cryptosporidiosis in AIDS. J Infect Dis **178**:900-903.

161. **Smith, S.** 1994. The animal fatty acid synthase: one gene, one polypeptide, seven enzymes. FASEB J. **8**:1248-1259.

162. **Snyder, R. V., P. D. Gibbs, A. Palacios, L. Abiy, R. Dickey, J. V. Lopez, and K. S. Rein**. 2003. Polyketide synthase genes from marine dinoflagellates. Mar Biotechnol (NY) **5**:1-12.

163. **Snyder, R. V., M. A. Guerrero, C. D. Sinigalliano, J. Winshell, R. Perez, J. V. Lopez, and K. S. Rein**. 2005. Localization of polyketide synthase encoding genes to the toxic dinoflagellate *Karenia brevis*. Phytochemistry **66**:1767-1780.

164. **Spano, F., and A. Crisanti**. 2000. *Cryptosporidium parvum*: the many secrets of a small genome. Int J Parasitol **30**:553-565.

165. **Staunton, J., and K. J. Weissman**. 2001. Polyketide biosynthesis: a millennium review. Nat. Prod. Rep. **18**:380-416.

166. **Strong, W. B., and R. G. Nelson**. 2000. Gene discovery in *Cryptosporidium parvum*: expressed sequence tags and genome survey sequences. Contrib Microbiol **6**:92-115.

167. **Strong, W. B., and R. G. Nelson**. 2000. Preliminary profile of the *Cryptosporidium parvum* genome: an expressed sequence tag and genome survey sequence analysis. Mol Biochem Parasitol **107**:1-32.

168. **Takeuchi, T., S. Kobayashi, and H. Kawasaki**. 1984. *Entamoeba histolytica*: inhibition in vitro by bithionol of respiratory activity and growth. Exp Parasitol **58**:1-7.

169. **Takeuchi, T., S. Kobayashi, M. Tanabe, and T. Fujiwara**. 1985. In vitro inhibition of *Giardia lamblia* and *Trichomonas vaginalis* growth by bithionol, dichlorophene, and hexachlorophene. Antimicrob Agents Chemother **27**:65-70.

170. **Tang, L., Y. J. Yoon, C. Y. Choi, and C. R. Hutchinson**. 1998. Characterization of the enzymatic domains in the modular polyketide synthase involved in rifamycin B biosynthesis by *Amycolatopsis mediterranei*. Gene **216**:255-265.

171. **Tekos, A., E. Prodromaki, E. Papadimou, D. Pavlidou, D. Tsambaos, and D. Drainas**. 2003. Aminoglycosides suppress tRNA processing in human epidermal keratinocytes in vitro. Skin Pharmacol Appl Skin Physiol **16**:252-258.

172. **Tetley, L., S. M. Brown, V. McDonald, and G. H. Coombs**. 1998. Ultrastructural analysis of the sporozoite of *Cryptosporidium parvum*. Microbiology **144 (Pt 12)**:3249-3255.

173. **Thompson, R. C., M. E. Olson, G. Zhu, S. Enomoto, M. S. Abrahamsen, and N. S. Hijjawi**. 2005. *Cryptosporidium* and cryptosporidiosis. Adv Parasitol **59**:77-158.

174. **Triffitt, M. J.** 1925. Observations on two new species of coccidia parasitic in snakes. Protozoology **1**:19-26.

175. **Tyzzer, E. E.** 1907. A sporozoan found in the peptic glands of the common mouse. Proc Soc Exp Biol Med **5**:12-13.

176. **Tyzzer, E. E.** 1912. *Cryptosporidium parvum* (sp. nov.), a coccidium found in the small intestine of the common mouse. Arch Protisenkd **26**:394-412.

177. **Tzipori, S.** 1998. Cryptosporidiosis: laboratory investigations and chemotherapy. Adv Parasitol **40**:187-221.

178. **Tzipori, S., and J. K. Griffiths**. 1998. Natural history and biology of *Cryptosporidium parvum*. Adv Parasitol **40**:5-36.

179. **Tzipori, S., and H. Ward**. 2002. Cryptosporidiosis: biology, pathogenesis and disease. Microbes Infect **4**:1047-1058.

180. **Umemiya, R., M. Fukuda, K. Fujisaki, and T. Matsui**. 2005. Electron microscopic observation of the invasion process of *Cryptosporidium parvum* in severe combined immunodeficiency mice. J Parasitol **91**:1034-1039.

181. **Upton, S. J.** 2000. Suborder Eimeriorina Legar, 1911*In* J. J. Lee, G. F. Leedale, and P. Bradbury (eds.), The illustrated guide to the protozoa, 2nd ed. Society of Protozoologists. Allen Press, Lawrence, KS.

182. **van Aalten, D. M., K. G. Milne, J. Y. Zou, G. J. Kleywegt, T. Bergfors, M. A. Ferguson, J. Knudsen, and T. A. Jones**. 2001. Binding site differences revealed by crystal structures of *Plasmodium falciparum* and bovine acyl-CoA binding protein. J Mol Biol **309**:181-192.

183. **Vetterling, J. M., H. R. Jervis, T. G. Merrill, and H. Sprinz**. 1971. *Cryptosporidium wrairi* sp. n. from the guinea pig *Cavia porcellus*, with an emendation of the genus. J Protozool **18**:243-247.

184. **Wadum, M. C., J. K. Villadsen, S. Feddersen, R. S. Moller, T. B. Neergaard, B. B. Kragelund, P. Hojrup, N. J. Faergeman, and J. Knudsen**. 2002. Fluorescently labelled bovine acyl-CoA-binding protein acting as an acyl-CoA sensor: interaction with CoA and acyl-CoA esters and its use in measuring free acyl-CoA esters and non-esterified fatty acids. Biochem J **365**:165-172.

185. **Wang, Y., D. Botolin, B. Christian, J. Busik, J. Xu, and D. B. Jump**. 2005. Tissue-specific, nutritional, and developmental regulation of rat fatty acid elongases. J. Lipid Res. **46**:706-715.

186. **Werbovetz, K. A., E. K. Lehnert, T. L. Macdonald, and R. D. Pearson**. 1992. Cytotoxicity of acridine compounds for *Leishmania* promastigotes in vitro. Antimicrob Agents Chemother **36**:495-497.

187. **White, A. C., Jr.** 2003. Nitazoxanide: an important advance in anti-parasitic therapy. Am J Trop Med Hyg **68**:382-383.

188. **White, S. W., J. Zheng, Y. M. Zhang, and Rock**. 2005. The structural biology of type II fatty acid biosynthesis. Annu. Rev. Biochem. **74**:791-831.

189. **Widmer, G.** 2004. Population genetics of *Cryptosporidium parvum*. Trends Parasitol **20**:3-6; discussion 6.

190. **Woods, K. M., M. V. Nesterenko, and S. J. Upton**. 1996. Efficacy of 101 antimicrobials and other agents on the development of *Cryptosporidium parvum* in vitro. Ann Trop Med Parasitol **90**:603-615.

191. **Xiao, L., R. Fayer, U. Ryan, and S. J. Upton**. 2004. *Cryptosporidium* taxonomy: recent advances and implications for public health. Clin Microbiol Rev **17**:72-97.

192. **Xu, P., G. Widmer, Y. Wang, L. S. Ozaki, J. M. Alves, M. G. Serrano, D. Puiu, P. Manque, D. Akiyoshi, A. J. Mackey, W. R. Pearson, P. H. Dear, A. T. Bankier, D. L. Peterson, M. S. Abrahamsen, V. Kapur, S. Tzipori, and G. A. Buck**. 2004. The genome of *Cryptosporidium hominis*. Nature **431**:1107-1112.

193. **Zank, T. K., U. Zahringer, C. Beckmann, G. Pohnert, W. Boland, H. Holtorf, R. Reski, J. Lerchl, and E. Heinz**. 2002. Cloning and functional characterisation of an enzyme involved in the elongation of Delta6-polyunsaturated fatty acids from the moss *Physcomitrella patens*. Plant J. **31**:255-268.

194. **Zeng, B., X. Cai, and G. Zhu**. 2006. Functional characterization of a fatty acyl-CoA-binding protein (ACBP) from the apicomplexan *Cryptosporidium parvum*. Microbiol **152**:2355-2363.

195. **Zeng, B., and G. Zhu**. 2006. Two distinct oxysterol binding protein-related proteins in the parasitic protist *Cryptosporidium parvum* (Apicomplexa). Biochem. Biophys Res Commun. **346**:591-599.

196. **Zhu, G.** 2004. Current progress in the fatty acid metabolism in *Cryptosporidium parvum*. J Eukaryot Microbiol **51**:381-388.

197. **Zhu, G., J. S. Keithly, and H. Philippe**. 2000. What is the phylogenetic position of *Cryptosporidium*? Int J Syst Evol Microbiol. **50**:1673-1681.

198. **Zhu, G., M. J. LaGier, F. Stejskal, J. J. Millership, X. Cai, and J. S. Keithly**. 2002. *Cryptosporidium parvum*: the first protist known to encode a putative polyketide synthase. Gene **298**:79-89.

199. **Zhu, G., Y. Li, X. Cai, J. J. Millership, M. J. Marchewka, and J. S. Keithly**. 2004. Expression and functional characterization of a giant Type I fatty acid synthase (CpFAS1) gene from *Cryptosporidium parvum*. Mol. Biochem. Parasitol. **134**:127-135.

200. **Zhu, G., M. J. Marchewka, and J. S. Keithly**. 2000. *Cryptosporidium parvum* appears to lack a plastid genome. Microbiol **146 (Pt 2)**:315-321.

201. **Zhu, G., M. J. Marchewka, K. M. Woods, S. J. Upton, and J. S. Keithly**. 2000. Molecular analysis of a Type I fatty acid synthase in *Cryptosporidium parvum*. Mol. Biochem. Parasitol. **105**:253-260.

APPENDIX

FIG. A-1. The elongase maximum likelihood (ML) tree containing GenBank GI numbers and species names for all taxa. Posterior probability (PP) values at major nodes are indicated as either percent values, as 100% (solid diamonds), or 90 – 99% (solid circles). These PP values were derived from 3000 trees obtained after the ML values converged. GenBank GI numbers and species names for all taxa are provided. Additional ML analysis using PROML program yielded essentially the same topology shown here.

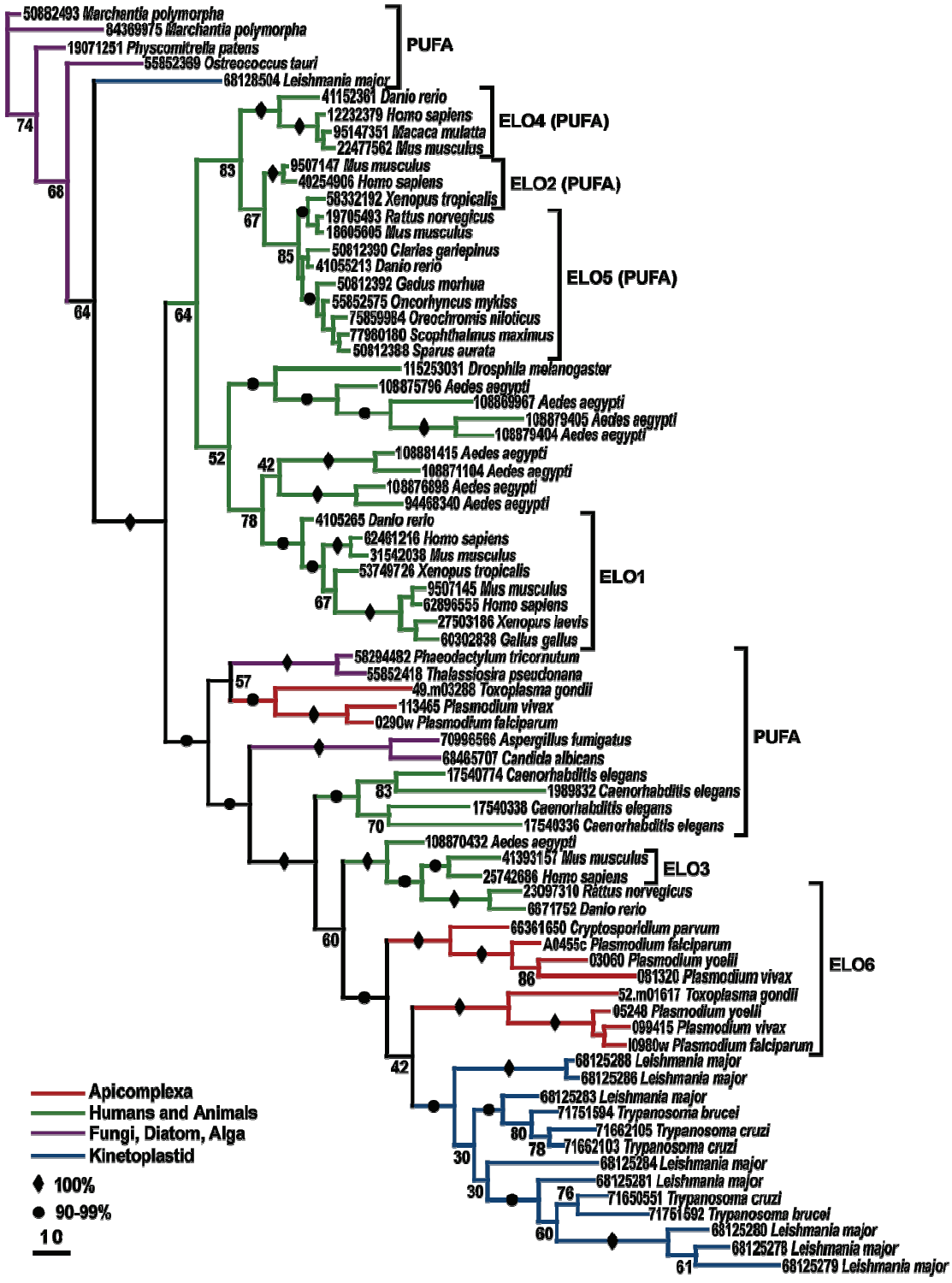
50682493 Marchantia polymorpha
84369975 Marchantia polymorpha
19071251 Physcomitrella patens
55852369 Ostreococcus tauri
68128504 Leishmania major
PUFA
41152361 Danio rerio
12232379 Homo sapiens
95147351 Macaca mulatta
22477562 Mus musculus
ELO4 (PUFA)
9507147 Mus musculus
40254906 Homo sapiens
58332192 Xenopus tropicalis
19705493 Rattus norvegicus
18605605 Mus musculus
ELO2 (PUFA)
50812390 Clarias gariepinus
41055213 Danio rerio
50812392 Gadus morhua
55852575 Oncorhyncus mykiss
75059984 Oreochromis niloticus
77980180 Scophthalmus maximus
50812388 Sparus aurata
ELO5 (PUFA)
115253031 Drosphila melanogaster
108875796 Aedes aegypti
108869967 Aedes aegypti
108879405 Aedes aegypti
108879404 Aedes aegypti
108881415 Aedes aegypti
108871104 Aedes aegypti
108876898 Aedes aegypti
94468340 Aedes aegypti
4105265 Danio rerio
62461216 Homo sapiens
31542038 Mus musculus
53749726 Xenopus tropicalis
9507145 Mus musculus
62896555 Homo sapiens
27503186 Xenopus laevis
60302838 Gallus gallus
ELO1
58294482 Phaeodactylum tricornutum
55852418 Thalassiosira pseudonana
49.m03288 Toxoplasma gondii
113465 Plasmodium vivax
0290w Plasmodium falciparum
70996586 Aspergillus fumigatus
68465707 Candida albicans
17540714 Caenorhabditis elegans
1989832 Caenorhabditis elegans
17540338 Caenorhabditis elegans
17540336 Caenorhabditis elegans
PUFA
108870432 Aedes aegypti
41393157 Mus musculus
25742686 Homo sapiens
23097310 Rattus norvegicus
6871752 Danio rerio
ELO3
65361650 Cryptosporidium parvum
A0455c Plasmodium falciparum
03060 Plasmodium yoelii
081320 Plasmodium vivax
52.m01617 Toxoplasma gondii
05248 Plasmodium yoelii
099415 Plasmodium vivax
I0980w Plasmodium falciparum
ELO6
68125288 Leishmania major
68125286 Leishmania major
68125283 Leishmania major
71751594 Trypanosoma brucei
71662105 Trypanosoma cruzi
71662103 Trypanosoma cruzi
68125284 Leishmania major
68125281 Leishmania major
71650551 Trypanosoma cruzi
71751692 Trypanosoma brucei
68125280 Leishmania major
68125278 Leishmania major
68125279 Leishmania major
Apicomplexa
Humans and Animals
Fungi, Diatom, Alga
Kinetoplastid
100%
90-99%
10

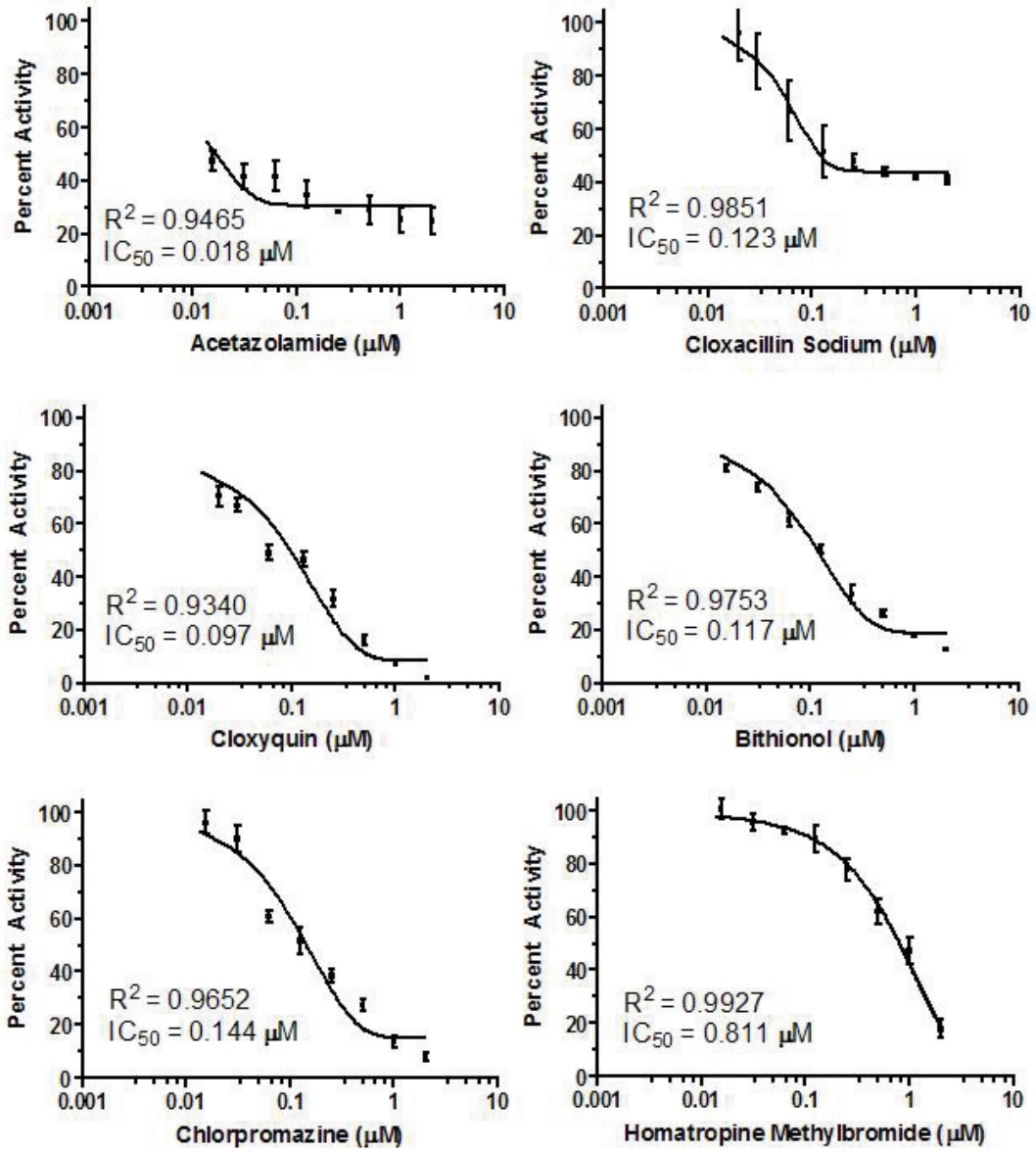

FIG. A-2. Inhibition curves of the CpACBP1 inhibitors. Values are represented as percent activity indicating the percent binding of NBD-C16:0-CoA to CpACBP1. The IC50 values displayed are defined as the compound concentration that displays a 50% inhibition of binding. Bars indicate the standard-error-of-the-mean of five experiments.

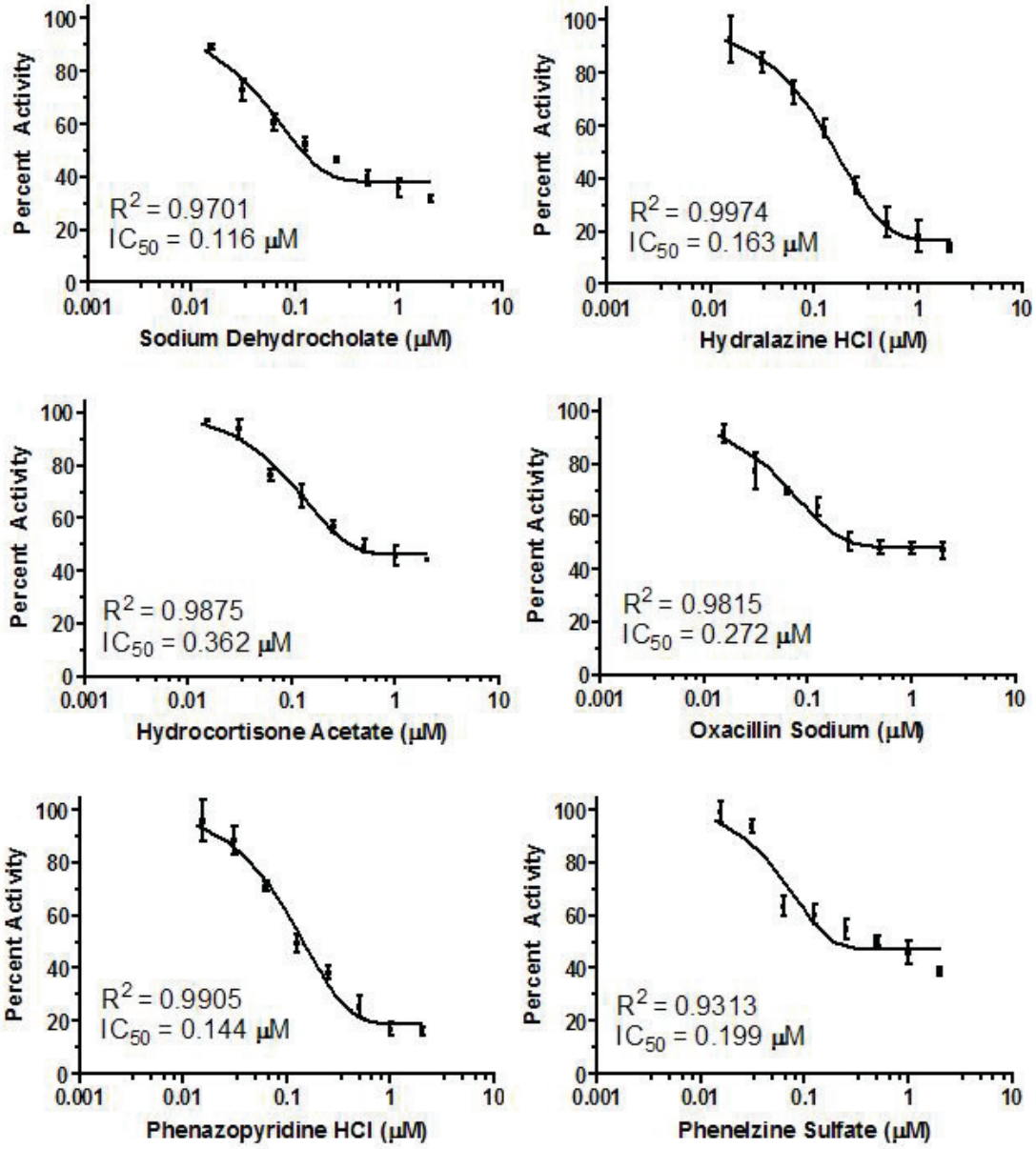

FIG. A-2 Continued

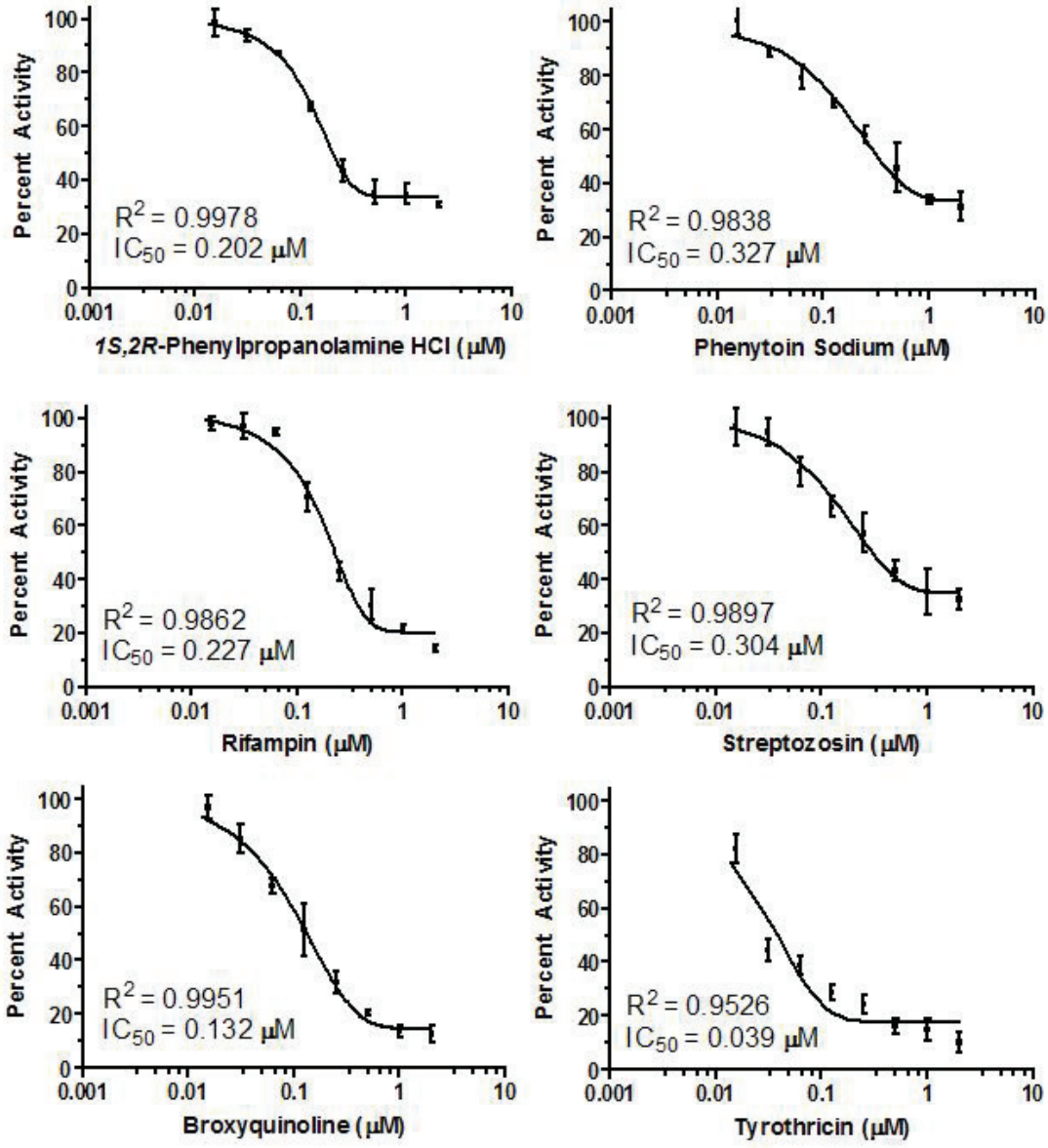

FIG. A-2 Continued

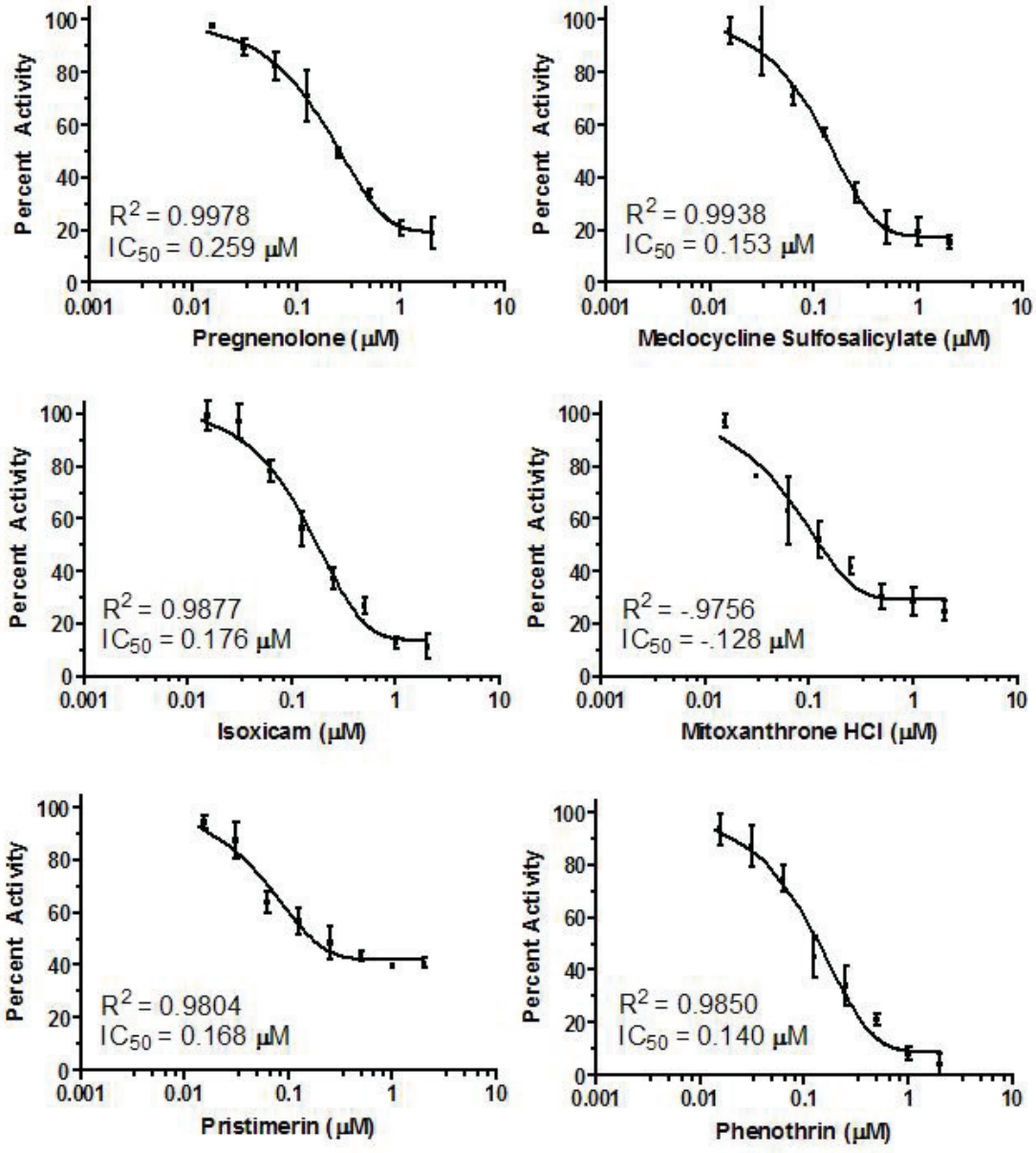

FIG. A-2 Continued

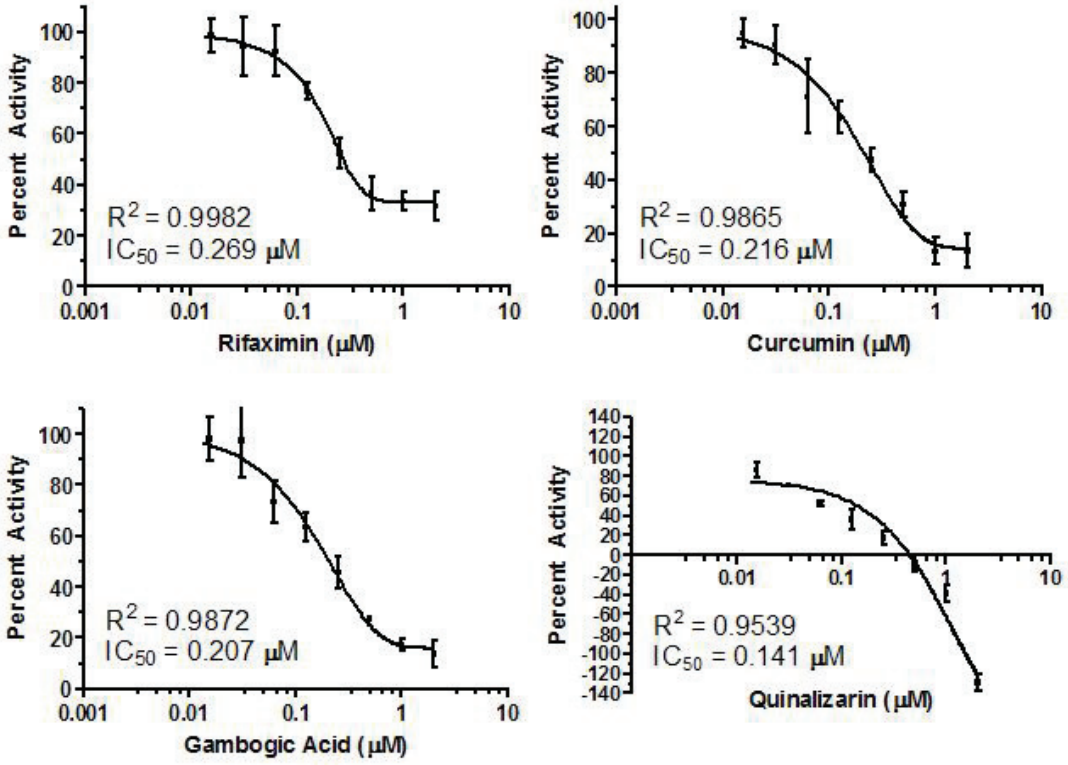

FIG. A-2 Continued

VITA

Name: Jason Michael Fritzler

Address: Department of Biology, Stephen F. Austin State University,
P.O. Box 13003, SFA Station, Nacogdoches, Texas 75962

Email Address: fritzlerjm@sfasu.edu

Education: B.S., Animal Science, Texas A&M University, 2003
Ph.D., Veterinary Microbiology, Texas A&M University, 2008

Professional Experience:

Graduate Research Assistant
Department of Veterinary Pathobiology, Texas A&M University, College Station, Texas

Undergraduate Research Assistant
Howard Hughes Medical Institute Undergraduate Research Intern Program, Departments of Honors Programs and Veterinary Integrative Biological Sciences, Texas A&M University, College Station, Texas

Publications:

Fritzler, J. M., J. J. Millership, and G. Zhu. 2007. *Cryptosporidium parvum* long-chain fatty acid elongase. Eukaryot. Cell **6:** 2018-2028.

Fritzler, J. M., and G. Zhu. 2007. Functional characterization of the acyl-[acyl carrier protein] ligase in the *Cryptosporidium parvum* giant polyketide synthase. Int. J. Parasitol. **37**: 307-316.

Zhu, G., S. Enomoto, J. M. Fritzler, M. S. Abrahamsen, and T. J. Templeton. 2008. *Cryptosporidium* and Cryptosporidiosis. In: Genome Mapping in Animals and Microbes. Vol. 8. (Eds.) Kole, C., and V. M. Nene. Springer. (In Press)